THE UNIVERSITY OF TENNESSEE
SPACE INSTITUTE

DOE/ET/10815-208
DIST. CATEGORY UC-112
UTSI-93-03

RECEIVED
NOV 22 1993
OSTI

SUPERHEATER/INTERMEDIATE TEMPERATURE AIRHEATER TUBE CORROSION TESTS IN THE MHD COAL FIRED FLOW FACILITY (EASTERN COAL PHASE)

TOPICAL REPORT

M. K. WHITE

The University of Tennessee Space Institute
Energy Conversion Research and Development Programs
Tullahoma, Tennessee 37388

November 1993

PREPARED FOR THE UNITED STATES
DEPARTMENT OF ENERGY

Under Contract No. DE-AC02-79ET10815

DISTRIBUTION OF THIS DOCUMENT IS UNLIMITED

TULLAHOMA, TENNESSEE 37388-8897

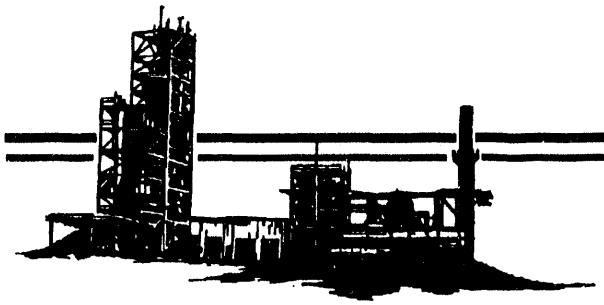

COAL FIRED FLOW FACILITY

"This report was prepared as an account of work sponsored by the United States Government. Neither the United States nor the United States DOE, nor any of their employees, nor any of their contractors, subcontractor, or their employees, makes any warranty, express or implied, or assumes any legal liability or responsibility for the accuracy, completeness, or usefulness of any information, apparatus, product or process disclosed, or represents that its use would not infringe privately owned rights."

TULLAHOMA, TENNESSEE 37388-8897

DOE/ET/10815-208
DIST. CATEGORY UC-112
UTSI-93-03

SUPERHEATER/INTERMEDIATE TEMPERATURE AIRHEATER TUBE CORROSION TESTS IN THE MHD COAL FIRED FLOW FACILITY (EASTERN COAL PHASE)

TOPICAL REPORT

M. K. WHITE

The University of Tennessee Space Institute
Energy Conversion Research and Development Programs
Tullahoma, Tennessee 37388

November 1993

PREPARED FOR THE UNITED STATES
DEPARTMENT OF ENERGY

Under Contract No. DE-AC02-79ET10815

MASTER

DISTRIBUTION OF THIS DOCUMENT IS UNLIMITED

TABLE OF CONTENTS

	Page
ABSTRACT	**1**
INTRODUCTION	**1**
BACKGROUND	**2**
TEST CONDITIONS	**6**
SAMPLING AND EVALUATION PROCEDURES	**21**
RESULTS	**25**
Corrosion Data Variability and Angular Variation	25
Stainless Steels: penetration kinetic data	25
Stainless Steels: scaling + penetration kinetic data	30
Stainless Steels: penetration versus average metal temperature data	30
Stainless Steels: scaling + penetration versus metal temperature data	30
Stainless Steels: leading versus trailing edge data	37
Stainless Steels: all data combined	37
Low Chromium Alloys: scaling kinetic data	43
Low Chromium Alloys: scaling versus metal temperature data	43
Tube Wall Recession Data	46
Corrosion Morphology and Scale Composition	46
DISCUSSION	**61**
SUMMARY AND CONCLUSIONS	**66**
ACKNOWLEDGMENTS	**68**
REFERENCES	**69**

LIST OF FIGURES

No.	Title	Page
1.	CFFF Integrated MHD Bottoming Cycle Schematic	7
2.	Average Element Profiles Through LMF4-N Frontal Deposits	11
3.	Typical TS1 Tube and Deposit Cross Section	11
4.	Typical TS1 Tube Deposits	12
5.	Typical Variation of Gas Temperature (Test LMF4-K)	13
6.	Locations of Tube Metal Thermocouples	14
7.	Average TS1 Tube Temperatures	18
8.	Average TS2 Tube Temperatures	19
9.	Average TS3 Tube Temperatures	20
10.	Tube Metal Temperatures at the Leading Edge of Tube 3 at the Vertical Middle of the First Pass	22
11.	Schematic Diagram of Measurements Made on Corroded Tube Samples	24
12.	Typical Corrosion Data at Bottom of Pass 1 Showing the Amount of Variation in Individual Samples	26
13.	Distribution of Penetration Depth Over Tube Leading Quadrant Derived from Summing and Normalizing Data from 32 TS1 and TS2 Samples	27
14.	Internal Penetration of TS1 and TS2 Alloys at the Bottom of the First Pass with Metal temperatures Near the Maximum for Superheater Service	28
15.	Internal Penetration of TS1 and TS2 Alloys at the Top of the First Pass with Metal Temperatures in the Range for ITAH Service	29
16.	Kinetic Corrosion Data (Scale Thickness + Penetration) for TS1 Alloys at the Bottom of the Front Pass	31
17.	Kinetic Corrosion Data (Scale Thickness + Penetration) for TS2 Alloys at the Bottom of the Front Pass	32

LIST OF FIGURES (Cont.)

No.	Title	Page
18.	Kinetic Corrosion Data (Scale Thickness + Penetration) for TS1 Alloys at the Top of the Front Pass	33
19.	Kinetic Corrosion Data (Scale Thickness + Penetration) for TS2 Alloys at the Top of the Front Pass	34
20.	Internal Penetration at the Leading Edge versus Average Metal Temperature for Stainless Steels in TS1 and TS2	35
21.	Scale Thickness + Penetration vs. Average Metal Temperature for Stainless Steels in TS1 and TS2	36
22.	Internal Penetration at the Trailing Edge versus Average Metal Temperature for Stainless Steels in TS1 and TS2	38
23a.	Linear Corrosion Rates of TS1 and TS2 Tube Alloys Exposed for 1500-2000 Hours During LMF4	39
23b.	Linear Corrosion Rate of Alloy 321H at TS2 Exposed for 2000 Hours During LMF4	40
24a.	Parabolic Corrosion Rates of TS1 and TS2 Tube Alloys Exposed for 1500-2000 Hours During LMF4	41
24b.	Parabolic Corrosion Rate of Alloy 321H at TS2 Exposed for 2000 Hours During LMF4	42
25.	Scale Thickness (Remaining) for TS3 Alloys at the Leading Edge and at the Maximum Average Exposure Temperatures	44
26.	Scale Thickness of Plain Carbon and Low Chromium Steels vs. Average Metal Temperature	45
27a.	Linear Recession Rates of TS1 and TS2 Alloys with 1500 Hour Exposures Based on Ultrasonic Initial Wall and Microscopic Remaining Wall and Penetration Measurements	47
27b.	Parabolic Recession Rates of TS1 and TS2 Alloys with 1500 Hour Exposures Based on Ultrasonic Initial Wall and Microscopic Remaining Wall and Penetration Measurements	48

LIST OF FIGURES (Cont.)

No.	Title	Page
28.	Linear Recession Rates of TS1 and TS2 Alloys with 2000 Hour Exposures Based on Nominal Initial Wall and Microscopic Remaining Wall and Penetration Measurements	49
29.	Linear Recession Rates of TS3 Alloys with 2000 Hour Exposures Based on Nominal Wall and Microscopic Remaining Wall and Penetration Measurements	50
30a.	SEM Micrograph and X-ray Dot Maps for Alloy 310 (TS2-2,P1,1')	51
30b.	SEM Micrograph and X-ray Dot Maps for Alloy 253MA (TS2-1-8,P1,1')	52
30c.	SEM Micrograph and X-ray Dot Maps for Alloy 304H (TS1-4,P1,1')	53
30d.	SEM Micrograph and X-ray Dot Maps for Alloy 316H (TS1-5,P1,1')	54
30e.	SEM Micrograph and X-ray Dot Maps for Alloy 321H (TS2-1,P1,1')	55
30f.	SEM Micrograph and X-ray Dot Maps for Alloy P5 (TS2-8,P2,7')	56
30g.	SEM Micrograph and X-ray Dot Maps for Alloy T22 (TS2-1,P2,4')	57
30h.	SEM Micrograph and X-ray Dot Maps for Alloy T11 (TS3-2,P2,7')	58
31.	Optical Micrograph Showing Iron Oxide Reprecipitation in Deposit	60
32.	Conventional Synthetic Coal-Ash Corrosion	63
33.	Effect of Chromium Content in Alloys on Conventional Synthetic Coal-Ash Corrosion	63

LIST OF TABLES

No.	Title	Page
1.	Test Alloys, Locations, and Sizes	8
2.	Deposit Compositions Inferred from Elemental and % Soluble Data, LMF4-K to LMF4-P	10
3.	Time Average Inlet Gas Temperatures to Test Sections for Each Run	12
4.	Time Average TS1 Metal Temperatures	15
5.	Time Average TS2 Metal Temperatures	16
6.	Time Average TS3 Metal Temperatures	17
7.	Conventional Coal Ash Corrosion Results from Various Superheater Probes	64
8.	Corrosion Probe Data from Philadelphia Electric's Eddystone Unit 1	65

SUPERHEATER/INTERMEDIATE TEMPERATURE AIRHEATER TUBE CORROSION TESTS IN THE MHD COAL FIRED FLOW FACILITY (EASTERN COAL PHASE)

ABSTRACT

Corrosion data have been obtained for tubes exposed for 1500-2000 hours in a proof-of-concept magnetohydrodynamics (MHD) power generation test facility to conditions representative of superheater and intermediate temperature air heater (ITAH) components. The tubes, coated with K_2SO_4-rich deposits, were corroded more than in most pulverized coal fired superheater service, but much less than the highly aggressive liquid phase attack encountered in conventional plants with certain coals and temperatures. The results indicated that, with parabolic corrosion kinetics, type 310 and 253MA stainless steels should be usable to 1400°F at the hot end of the ITAH. At final superheater temperatures, 2.25 and 5 Cr steels were indicated to have parabolic corrosion rates generally below a 0.5 mm/yr criterion, based on corrosion scale thickness. However, unknown amounts of scale loss from spallation made this determination uncertain. Stainless steels 304H, 316H, and 321H had parabolic rates variably above the criterion, but may be servicable under less cyclic conditions. Corrosion rates derived from scale thickness and intergranular corrosion depth measurements are reported, along with scale morphologies and compositions. The implications of the results on commercial MHD utilization of the alloys are discussed, as well as the indicated need for more corrosion resistant alloys or coatings under the most severe exposure conditions.

INTRODUCTION

The Energy Conversion Research and Development Programs (ECP) of the University of Tennessee Space Institute (UTSI) is pursuing the development of technology to generate electrical power directly from potassium seeded, coal fired plasmas expanding through open cycle magnetohydrodynamic (MHD) channels. Testing is conducted in the U.S. Department of Energy's Coal Fired Flow Facility (CFFF), located at UTSI. Testing has been devoted to establishing Proof of Concept (POC) for the design and operation of the "downstream" components of an MHD plant, including all aspects other than combustion, MHD power generation and conditioning, and seed regeneration. This report is of evaluations of the gas-side corrosion performance of selected tube alloys simulating superheater and intermediate temperature air heater surface during testing in the CFFF in the LMF4 POC test series, burning high sulfur Illinois #6 coal. The objectives of the testing were to determine the type and severity of tube corrosion occurring in this

environment with ferritic low chromium steels and austenitic stainless steels and to demonstrate the feasibility of operating a commercial MHD plant with existing and sufficiently economical tube materials.

BACKGROUND

An MHD bottoming plant will contain heat recovery surface similar to a PC-fired plant, including the boiler waterwall, superheater and reheater sections, economizer, and airheater. However, these components will have many design and operational differences from conventional plants. Combustion will be two-stage, with the lower or primary portion of the furnace being at 85-90% of stoichiometric. The waterwall in the primary zone will be refractory lined for corrosion protection. Instead of going to the primary combustor, air from the low temperature air heater will go to the secondary combustor, located in advance of the convective sections. Additional heat exchangers will be required for heating primary combustion air sufficiently to achieve the high gas temperatures required for MHD power generation. Various methods for doing this are contemplated. For early MHD retrofit plants, oxygen enrichment of the primary combustion air is planned so that the air need only be heated to 1100-1400°F, depending upon the design. This would be accomplished in a recuperative intermediate temperature air heater (ITAH) located in the furnace at the front of the convective banks, in some designs being situated in parallel with the secondary superheater. If no oxygen enrichment of the primary air is done, as would be the case in large commercial designs, it must be heated to near 2500°F or higher. This would be done in two stages, the first using the ITAH to heat the air to perhaps 1400°F, and the second using a high temperature air heater (HTAH) of ceramic construction. Some designs have the HTAH in the primary zone of the furnace and some as separately fired.

The requirement for the ITAH results in the necessity for higher gas temperatures at the secondary superheater/ITAH inlet, 2250°F or higher, than in PC-fired plants. At these temperatures, K_2SO_4 is molten in the gas stream and produces hard deposits on tubes, with a molten flow of sulfate over the outer surface of the deposit. The liquid surface results in a high sticking efficiency for deposition. At temperatures between 1956°F, the K_2SO_4 freezing point, and around 1700°F, sintering still produces hard tube deposits, whereas they are friable or powdery at lower temperatures. Possible modes of high temperature gas-side corrosion of recuperative tube metals are [1] gaseous oxidation or sulfidation via transport through pores and fissures in the deposit or by thermally driven diffusion through the solid sulfate salt lattice; [2] oxidation or sulfidation resulting from catalyzed decomposition of K_2SO_4 at or near the tube scale surface; [3] molten salt attack (hot corrosion) by a low melting phase formed adjacent to the tube surface by reaction or solution of the normal sulfate salt with other species derived from the gas, deposit, or tube metal; [4] at temperatures above 1193°F, the eutectic temperature of $Ni\text{-}Ni_3S_2$, a potential for catastrophic corrosion of high-nickel alloys lacking sufficient chromium to prevent nickel sulfidation; and [5] at temperatures above about 1530°F, the eutectic in the K_2SO_4 - Na_2SO_4 system, catastrophic corrosion by the liquid sulfate solution.

Hot corrosion by molten potassium iron trisulfate or other similar phases was the principal early concern with respect to MHD superheater and ITAH corrosion, owing to the very high alkali content of deposits. The corrosive attack of certain aggressive coal ashes on fireside surfaces of boiler and superheater tubes in conventional pulverized-coal-burning power plants has received much attention since it was first evident in 1942. This attack has been attributed to the occurrence within tube deposits of molten complex alkali-iron trisulfates which react with the tube metal or its oxide scale. The severity of corrosion has been shown to be influenced by the composition of the coal ash, the nature of the deposits, the flue gas composition, and the temperatures of the ash and the tubewall. In the complex sulfate molten range of approximately 1022-1400°F, corrosion is increased by high concentrations of alkalies, iron, or SO_3 in the deposit. Corrosion reaches a maximum between 1250°F and 1350°F, depending upon the alloy. No alloy has been found to be completely resistant to this attack under the severest conditions.[1] In contrast to conventional PC-fired boilers in which deposits generally contain no more than a few percent of alkali sulfates, MHD tube deposits in the vacinity of the tube surface may be 80% or more K_2SO_4. This high alkali content, however, has the effect of reducing the gaseous SO_2 and SO_3 concentrations to low levels, typically 350-400 ppm of SO_2 at the CFFF furnace exit and about 0.1 ppm SO_3, with the firing of Illinois #6 coal. While this probably accounts for the usual absence of alkali iron (or aluminum) trisulfate in MHD superheater and ITAH tube deposits, it is not inferred that these phases can not be formed. In fact, trace amounts of $K_3Fe(SO_4)_3$ have been detected by x-ray analysis of CFFF deposits on two occasions, and Bienstock et al[2] reported $K_3Al(SO_4)_3$ and $Na_3Fe(SO_4)_3$ in deposits resulting from potassium seeded coal firing. Catalytic oxidation of SO_2 in the outer deposit and decomposition of K_2SO_4 under reducing or borderline conditions beneath deposits are two possible sources of SO_3 which could enable complex trisulfate formation.

Testing of candidate MHD superheater materials dates from 1964 with the work of Hals et al [3], who fired natural gas with additives of synthetic coal ash, sulfur, and a potassium salt and evaluated the corrosive effects on alloys ranging from carbon steel, low and intermediate chromium steels, and 300 series stainless steels, to Inconel 600 and Incoloy 800. Tubes were in three test sections with maximum metal temperatures of 1760, 1720, and 980°F, respectively. Alloys 310, 600, and 800 at metal temperatures above about 1550°F were severely corroded by 100 hours and failed at about 200 hours. Inconel corrosion was less severe than for alloy 310, which had extensive sigma formation. The severe attack was attributed to the formation of molten K_2SO_4 - Na_2SO_4, which has a eutectic at about 1530°F.

Bienstock, et al[2] of the Bureau of Mines in 1970 presented the results of tests using a coal-fired combustor burning Pittsburgh seam coal. Results of two tests were reported, one for 100 hours with 4.4% K_2CO_3 seeding and the other for 83 hours without seeding. Corrosion was more severe with seeding than without. Haynes 25 was slightly attacked at 1500°F metal temperature but was judged satisfactory, while alloys 310, 600, and nickel were totally oxidized at that temperature. No corrosion of alloys 310, 316, or 446 was found at 1100°F, whereas 406 stainless steel was attacked with or without

seeding. Carbon steel and alloy T5 were attacked at 800°F metal temperature while alloy T22 showed little attack and was judged satisfactory. The most abundant compound in the deposits was Glaserite, $Na_2SO_4 - 3K_2SO_4$. Complex trisulfates were also present, as stated above.

Natesan[4] at Argonne National Laboratory reported in 1984 results of lab tests in which carbon steel and alloys T22, T9, 304, 310, and 800 were exposed for durations of 500-2000 hours to simulated MHD combustion gases with stoichiometric ratios from 1.01 to 1.30 and to metal temperatures from 1100°F to 1300°F. The alloys were exposed bare, coated with reagent K_2SO_4, coated with a 50:50 mixture of K_2SO_4 and flyash, and coated with ground-up deposits of ash/sulfated seed from ANL's MHD test facility. A factor of ~2 greater corrosion was indicated for K_2SO_4-coated samples as opposed to either uncoated or K_2SO_4 + ash-coated samples, although scale morphological features were similar in all cases. The low-chromium steels developed an iron oxide outer scale layer and iron-sulfide or iron-chromium sulfide inner layer and no internal penetration. High-chromium austenitic alloys developed relatively thin chromium-rich scales along with internal penetration. Based on the results, only high-chromium alloys such as 310 stainless steel and Incoloy 800 were judged suitable for steam heaters with tube temperatures above 900°F. The low chromium steels were judged applicable below 800°F. Tests at 1100 and 1300°F metal temperature with K_2SO_4-coated samples in an argon atmosphere showed almost identical scale morphological features and thicknesses as those obtained with simulated combustion gas, confirming K_2SO_4 as the principal corrodant.

A continuation of Natesan's work was reported in 1988[5] in which alloys 304H, 316, 321, 310, and 800H, coated with deposits from the CFFF test sections, were tested in simulated MHD combustion gas with a 1.05 stoichiometric ratio for durations to 2000 hours and a metal temperature of 1400°F to simulate the hot end of an ITAH. Alloy 310 showed the least attack, with all the others having 3 to 4 times the attack of alloy 310 in terms of scale thickness and penetration. When calculated by parabolic kinetics, all the alloys had metal recession rates less than 0.5 mm/yr, but only alloy 310 had less if calculated by linear kinetics. Samples of alloys T22, T5, T9, 304H, and 310 were also exposed for 2000 hours in the same gas and deposit environment but with a metal temperature of 1100°F to simulate either the hot end of steam heater tubes or the transition region in an ITAH from lower temperatures (with lower alloys) to higher temperatures. All of the low-chromium alloys had linear corrosion rates 2-3 times higher than the 0.5 mm/yr level viewed as acceptable. Furthermore, a T22 weldment exhibited 2-3 times greater corrosion than the normal sample. Since linear kinetics was judged to be applicable to these alloys, the tests indicated they would not be usable at this temperature, in agreement with the earlier work. Alloys 304H and 310 in those tests both had very low levels of corrosion (about 0.04 mm/yr parabolic or 0.08 mm/yr linear) at 1100°F.

Tubes of a variety of alloys including carbon steel, low chromium steels, 300-series stainless steels and alloys 330, 800H, and 600 were exposed to oxidizing coal-fired MHD

flue gas in three gas temperature zones at the CFFF during the LMF3 and LMF4 test series from 1984 to 1986[6,7,8]. Tubes in the highest gas temperature zone were exposed for 156 hours and those in the other two zones for 62 hours. Tube deposits averaged 63% K_2SO_4, and time-average metal temperatures ranged from 500°F to 1150°F. All of the alloys appeared to perform well with the exception of high-nickel alloys 800H and 600, which showed considerable attack even in this short time. No meaningful quantitative corrosion measurements were obtained due to the wide range of exposure conditions and large number of thermal cycles.

The LMF4 Proof-of-Concept (POC) series of tests was initiated at the CFFF in 1987 with an objective of exposing candidate superheater and ITAH tube materials for accumulated durations of 500, 1500, and 2000 hours in three gas temperature zones and with metal temperatures chosen to simulate expected retrofit plant conditions. Tested alloys consisted of 316H, 304H, 253MA, and 310 in the first two zones and carbon steel, T11, T22, and T5 in the third zone. The results from evaluation of tubes removed at 500 hours were given in an earlier report.[9] The principal conclusions reached were as follows:

1. The form of corrosion was oxidation/sulfidation beneath deposits composed mostly of potassium sulfate with the occurrence of primarily spinel scales and internal grain boundary oxidation of stainless steels and mixed oxide and sulfide scales of low chromium and carbon steels.

2. Maximum linear corrosion rates for all alloys tested exceeded a 0.5 mm/yr criterion at metal temperatures up to 1400°F at TS1 and TS2 and 1100°F at TS3.

3. Resistance to corrosion generally corresponded with alloy chromium content.

4. All of the alloys tested appeared to have adequate corrosion resistance at superheater tube temperatures. However, of the alloys tested, only 310 stainless steel was judged to have potential for use at metal temperatures approaching 1400°F.

5. CFFF tube corrosion appeared to be more severe at a given temperature than was corrosion in laboratory tests conducted at the Argonne National Laboratory.

6. Scales on stainless steels were often spalled and/or fractured as a result of thermal cycling and the oxidation/sulfidation process which produced porous, weak and nonadherent scales.

7. What appeared to be breakaway corrosion occurred on TS2 alloys 304H, 316H and 253MA in the form of deep localized intergranular penetration.

Tubes removed from CFFF testing at 500 hours were also analyzed by Babcock and Wilcox[10] and by Argonne National Laboratory. ANL's reporting of 500 hour sample evaluation will be combined with that from evaluation of 1500 and 2000 hour samples. B&W concluded from 500 hour samples that alloy 310 may be serviceable at metal temperatures up to at least 1300°F under MHD conditions, and that alloys 304H, 316H, and 253MA may be servicable to 1150°F.

TEST CONDITIONS

During this test series, Illinois #6, a high sulfur eastern bituminous coal, was burned in the combustor of the Low Mass Flow (LMF) test train. Potassium carbonate in powder form was mixed and fired with the coal to provide 1% potassium in the combustion gas. Primary combustion was at 85% of stoichiometric. In the secondary combustor portion of the furnace, combustion was completed with 10% excess air. The tested tube materials were located after the secondary combustor in three duct modules of rectangular cross section termed "test sections (TS)", as depicted in Figure 1. TS1, TS2 and TS3 were in successively lower gas temperature regimes, chosen to simulate critical service regimes expected in an MHD retrofit plant, and accomplished by the introduction of water-cooled tube bundles between the test sections.

The tubes tested in this study consisted of 2 sets, the "A" set with 2000 hours of accumulated on-coal exposure time from LMF4-K through LMF4-V and the "B" set with 1500 hours of exposure time during LMF4-O through LMF4-V. The dates and durations of those tests are given below.

LMF4-K	Aug.	1987	198.00 hours
LMF4-L	Dec.	1987	63.34
LMF4-M	Feb.	1988	56.93
LMF4-N	Apr.	1988	179.02
LMF4-O	Aug.	1988	252.28
LMF4-P	Nov.	1988	101.20
LMF4-Q	May	1989	40.85
LMF4-R	Aug.	1989	265.38
LMF4-S	Nov.	1989	134.63
LMF4-T	May	1990	216.88
LMF4-U	Jul.	1990	252.00
LMF4-V	Nov.	1990	240.48

Tube materials and sizes are given in Table 1. Note that in some cases in TS2 and TS3, tubes consisted of two different alloys. In those cases, the hotter pass or passes had a higher alloy capable of being exposed to a higher temperature than the lower alloy. In most such cases, the higher alloy was also present as another entire tube. In the table, the last character of the tube number denotes set "A" or set "B". The majority were

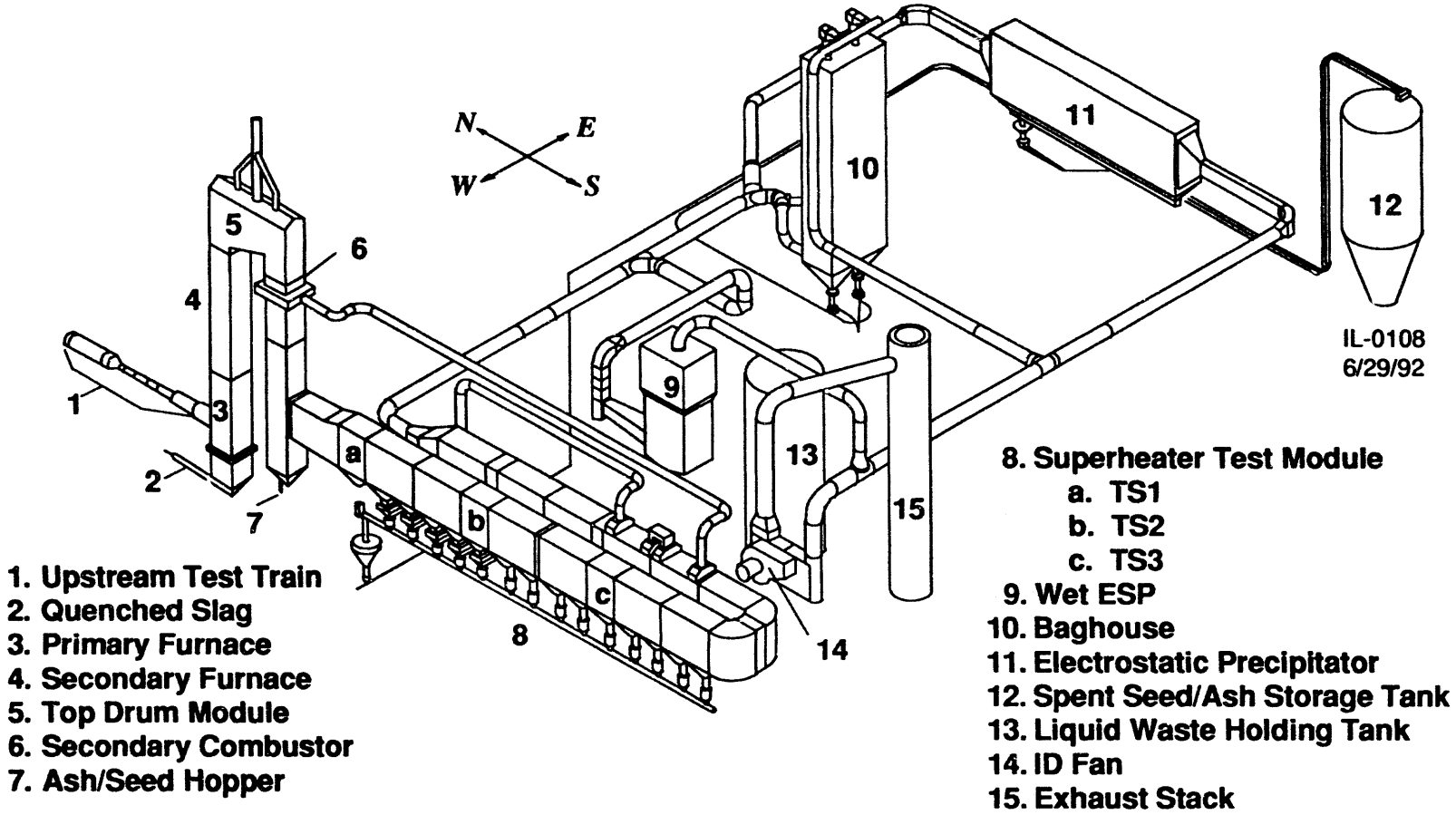

Figure 1. CFFF Integrated MHD Bottoming Cycle Schematic

Table 1. Test Alloys, Locations, and Sizes.

	Alloy 1				Alloy 2			
Tube	Pass	Alloy	Size	Nom. Wall (in)	Pass	Alloy	Size	Nom. Wall (in)
TS1-1A	1,2	310	1 " Pipe	0.140				
TS1-2B	1,2	316H	1 " Pipe	0.140				
TS1-3B	1,2	253MA	1" Pipe	0.133				
TS1-4A	1,2	304H	1 " Tube	0.148				
TS1-5A	1,2	316H	1 " Pipe	0.140				
TS1-6B	1,2	310	1 " Pipe	0.140				
TS1-7B	1,2	304H	1 " Pipe	0.140				
TS1-8A	1,2	253MA	1" Pipe	0.133				
TS2-1A	1	321H	1 " Tube	0.150	2	T22	1 " Tube	0.150
TS2-2A	1,2	310	1 " Pipe	0.140				
TS2-3B	1,2	253MA	1" Pipe	0.133				
TS2-4A	1,2	304H	1 " Tube	0.148				
TS2-5B	1,2	316H	1 " Pipe	0.140				
TS2-6B	1,2	310	1 " Pipe	0.140				
TS2-7B	1,2	304H	1 " Pipe	0.140				
TS2-8A	1	304H	1 " Tube	0.165	2	P5	1 " Pipe	0.140
TS3-1A	1,2	T22	1 " Tube	0.150	3,4	SA192	1 " Tube	0.165
TS3-2A	1	T22	1 " Tube	0.150	2,3,4	T11	1 " Tube	0.135
TS3-3B	1,2,3,4	P22	1 " Pipe	0.140				
TS3-4A	1,2,3,4	T22	1 " Tube	0.150				
TS3-5A	1,2,3,4	P5	1 " Pipe	0.140				
TS3-6B	1,2,3,4	P5	1 " Pipe	0.140				
TS3-7B	1	T22	1 " Tube	0.175	2,3,4	P11	1 " Pipe	0.140
TS3-8B	1,2	T5	1 " Tube	0.150	3,4	SA106B	1 " Pipe	0.140

actually pipe rather than tube, with attendant large variability of wall thickness. However, all are referred to genericly as tubes.

The three test sections were located in oxidizing flue gas having a typical molar composition of 59.4 % N_2, 26.3 % CO_2, 13.0 % H_2O, 1.26 % O_2, 0.040 % SO_2, 0.02 % CO, and 0.016 % NO_x. The gas particulate loading at the SHTM entrance was approximately 525 lb/hr, as estimated from the combustor inputs minus amounts removed at the slag tap and at the ash/seed hopper. No direct particulate loading measurements were done at the SHTM entrance, but the exit loading averaged 391 lbs/hr. Typical analyses of tube deposits are given in Table 2 for the three test sections. The deposits averaged about 20% flyash, 75% K_2SO_4, and 5% other salts, mostly sulfates. Deposits at the leading sides of tubes had a higher flyash content than those at trailing sides due to higher flyash content of large particles which deposited on leading edges by impingement. More importantly to the tube corrosion, the deposit composition varied through the thickness, as shown in Figure 2, having a higher salt content (>80% K_2SO_4) near to the tube surface than in the outer portion of the deposits. Thus, the material in contact with tubes was primarily K_2SO_4 with embedded ash spheres, which do not significantly affect corrosion. Figure 3 shows the cross-sectional structure of TS1 deposits. TS1 frontal deposits (Figure 4) grew fins as much as 8 inches long projecting into the flow because they were quite resistant to sootblowing. The bulk of that frontal deposit possessed a very porous, although strong, structure. At the leading edge, an intermediate zone extended from about 40 mils from the tube surface outward to as much as about 3/4 inch. This layer was relatively pore-free and hard. Toward the interior of this zone, deposit temperatures were too low for sintering of flyash. Within the innermost 40 mil (1 mm) zone, diffusion of iron from the tubes occurred, strengthening but also embrittling the deposit. The embritting effect was greatest very near the tube scale. Thus, during cooling after test shutdowns, separation of the outer bulk of the deposit from the innermost portion normally occurred at about the one millimeter distance, but sometimes the separation occurred adjacent to or very near the tube scale/deposit interface with attendent partial or total scale spalling. At times the outer deposit would fracture sufficiently to fall off.

Average inlet gas temperatures to each of the test sections are given in Table 3 for each test run as well as overall averages for the 1500 and 2000 hour periods. TS1 gas temperatures averaged about 2080°F according to unaspirated thermocouples, or around 2250°F corrected for radiation loss. TS2 and TS3 gas temperatures averaged near 1500°F and 1200°F, respectively. Measures were taken during the latter tests of the series to increase the TS2 and TS3 gas temperatures to make them more simulative of retrofit plant projections. Gas temperature variations during a typical run, LMF4-K, are given for each of the test sections in Figure 5.

Regulation of the cooling steam flow rate through the test section tubes was used to maintain the maximum tube metal temperature of TS1 at nominally 1400°F, and of TS3 at nominally 1100°F. TS2 maximum metal temperatures of 1400°F were also intended,

Table 2. Deposit Compositions Inferred from Elemental and % Soluble Data, LMF4-K to -P

Leading Edge, wt. %						
	TS1		TS2		TS3	
	Pass 1	Pass 2	Pass 1	Pass 2	Pass 1	Pass 2
Flyash	34.24	24.58	32.80	-	26.20	23.64
K_2SO_4	62.20	70.05	60.23	-	66.76	70.94
Na_2SO_4	0.63	1.03	0.92	-	1.08	0.95
$CaSO_4$	1.47	1.80	3.45	-	3.16	1.59
$MgSO_4$	0.08	-	0.18	-	0.32	0.13
$FeSO_4$	0.21	-	0.93	-	0.59	0.41
K_2CO_3	0.04	-	-	-	-	-
SO_3	1.85	2.80	4.73	-	4.89	2.46

Trailing Edge, wt. %						
	TS1		TS2		TS3	
	Pass 1	Pass 2	Pass 1	Pass 2	Pass 1	Pass 2
Flyash	17.29	17.90	18.39	15.83	19.84	-
K_2SO_4	78.46	77.78	74.33	79.49	76.75	-
Na_2SO_4	0.93	0.79	1.10	1.05	0.79	-
$CaSO_4$	1.88	1.40	2.32	0.95	1.13	-
$MgSO_4$	0.11	0.08	0.11	0.14	0.05	-
$FeSO_4$	-	-	0.44	0.51	0.33	-
K_2CO_3	0.03	-	-	-	-	-
SO_3	1.56	2.74	3.21	2.03	3.83	-

Combined Data, wt. %				
	All TS1	All TS2	All TS3	Overall
Flyash	23.5	22.34	23.36	23.11
K_2SO_4	72.12	71.35	71.48	71.70
Na_2SO_4	0.85	1.02	0.94	0.93
$CaSO_4$	1.64	2.24	1.96	1.92
$MgSO_4$	0.07	0.14	0.17	0.12
$FeSO_4$	0.05	0.63	0.44	0.35
K_2CO_3	0.02	0.0	0.0	0.0
SO_3	2.24	3.32	3.73	3.01

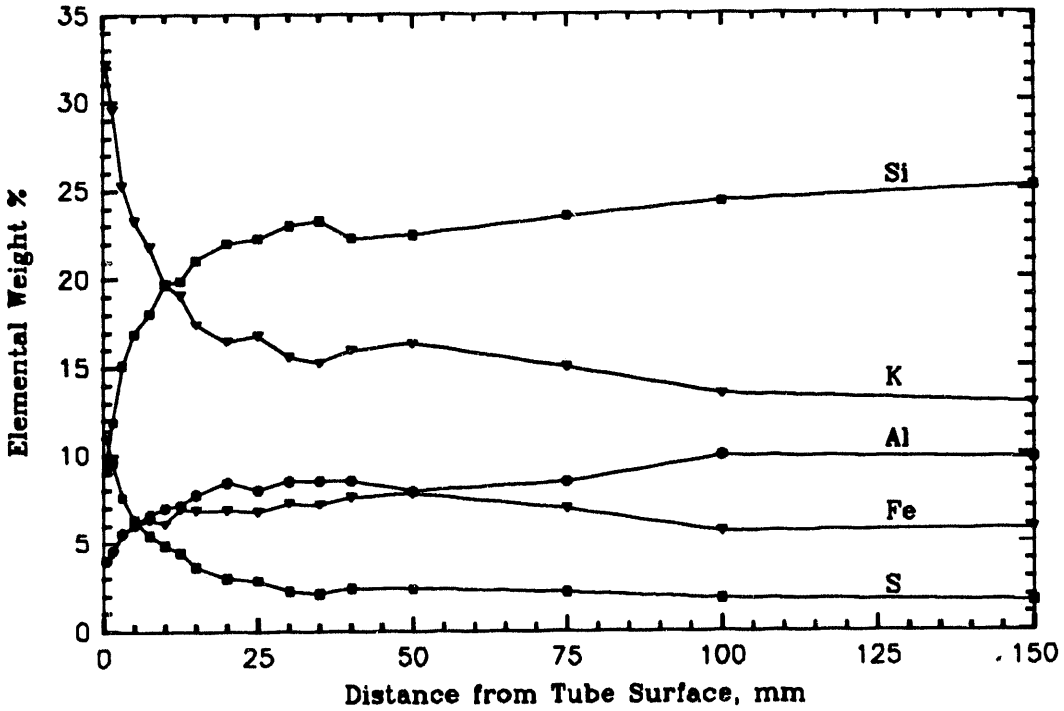

Figure 2. Average Element Profiles through LMF4-N Frontal Deposits

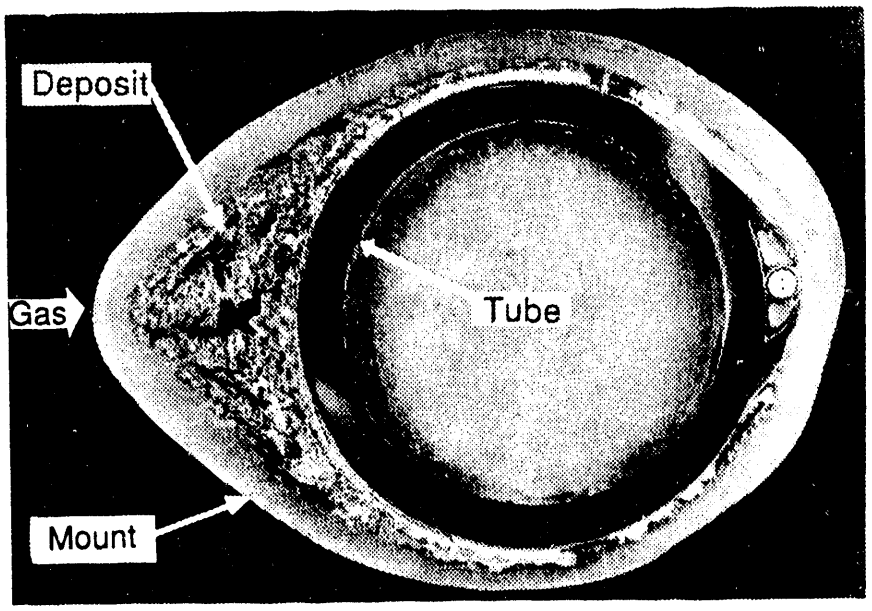

Figure 3. Typical TS1 Tube and Deposit Cross-Section

Figure 4. Typical TS1 Tube Deposits

Table 3. Time Average Inlet Gas Temperatures to Test Sections for Each Run (°F)

LMF4	K	L	M	N	O	P	Q	R	S	T	U	V	K-V Av.	O-V Av.
TS1	2046	2089	2049	2100	2065	2016	2031	2074	2078	2024	2113	2180	2079	2084
TS2	1421	1406	1328	1398	1333	1307	1483	1543	1594	1580	1570	1676	1493	1526
TS3	1183	1170	1070	1140	1087	1078	1061	1129	1179	1225	1276	1353	1184	1196

Note: Values are uncorrected for thermocouple radiation loss. Actual TS1 gas temperatures would be about 200°F higher.

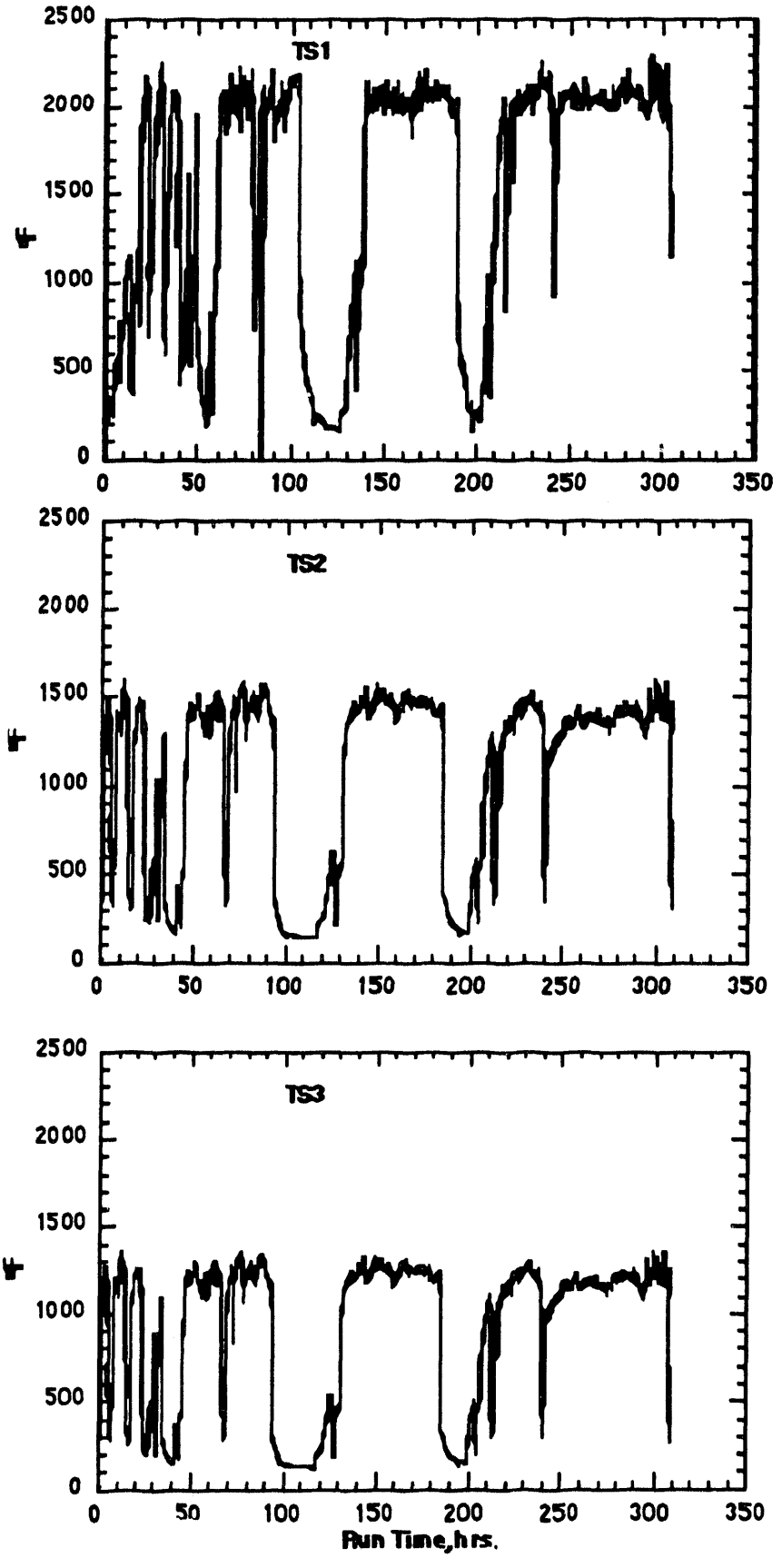

Figure 5. Typical Variation of Gas Temperature (Test LMF4-K)

but were not obtained until the later part of the test series due to too much water-cooled tube surface between TS1 and TS2. Thermocouples were distributed over the outer surface of tube in each of the test sections. These were metal sheathed thermocouples mounted on tubes by means of 1 inch x 1 inch x 0.125 inch thick weld pads, continuously welded on all sides. Their placement is depicted in Figure 6. In TS1 and TS2, tubes 1 and 4 had surface thermocouples on the leading edge at positions A-E in the figure. Tubes 5 and 8 had thermocouples at the same places, but at the trailing edge. Tubes 2 and 3 had a thermocouple at position D only, at the leading edge. In TS3, tube 4 had surface thermocouples on the leading edge at positions A-J. Tubes 1, 2, and 3 had thermocouples at positions B and I at the leading edge. There were no trailing edge thermocouples on TS3. Tables 4-6 give average tube metal temperatures at each of the thermocouple locations for each of the test runs, as well as overall averages for the 1500 hour and 2000 hour periods. The first column gives the thermocouple designation, the first digit of which is the tube number, and the last digit of which is the nth thermocouple for that tube from the cooler end. Shaded temperature values in the tables were more than two standard deviations from the overall mean, and were excluded from the overall mean reported, as being unrepresentative of the overall test series. These were generally not correct temperatures, but false indications caused by instrumentation malfunctions. The distribution of tube metal temperatures are shown in Figures 7-9 for the three test

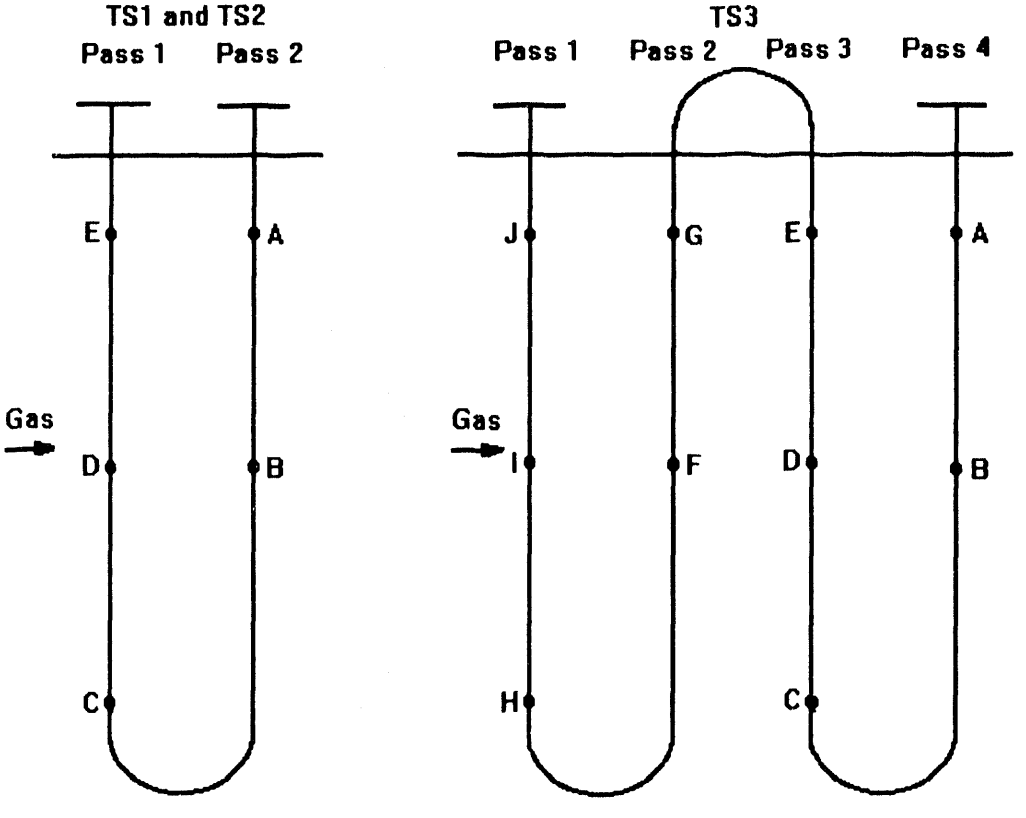

Figure 6. Locations of Tube Metal Thermocouples

Table 4. Time Average TS1 Metal Temperatures (°F)

LMF4-	K	L	M	N	O	P	Q	R	S	T	U	V	K-V Av.	O-V Av.
1M1	737	1094	906	891	831	940	665	597	694	798	838	772	780	767
1M2	694	987	1044	1027	932	1003	809	715	778	893	1003	850	879	875
1M3	921	983	1035	1209	1036	968	1075	847	1003	1077	1166	1074	1034	1030
1M4	1082	1239	1248	1248	1246	1260	1209	923	1091	1266	1303	1227	1184	1240
1M5	1055	1396	1351	1401	1227	1288	1120	1118	1155	1226	1288	1268	1229	1219
2M1	1094	1266	1307	1328	1475	1396	1221	1282	1231	1274	1411	1383	1346	1353
3M1	1205	1256	1239	1303	1284	1236	-	-	-	-	-	-	1259	1270
4M1	846	1002	1096	1076	1145	1184	894	887	917	934	-	887	975	975
4M2	736	992	1100	1090	1069	1024	928	886	906	964	1015	-	995	976
4M3	921	1112	1148	1196	1175	1316	1050	914	1051	1168	1266	-	1114	1132
4M4	1396	1300	1359	-	-	-	1188	-	1200	1253	1378	1297	1311	1289
4M5	938	1275	1338	1390	1369	1373	1381	1370	1378	1081	-	-	1320	1309
5M1	760	911	938	924	864	938	673	766	684	751	857	851	823	811
5M2	911	1037	1046	1005	977	1073	779	800	774	879	986	876	919	900
5M3	993	1099	1096	1236	1275	1283	953	964	991	1159	1225	1139	1131	1140
5M4	945	1192	1210	1256	1157	1298	1136	1188	1031	1145	1219	1219	1188	1179
5M5	972	1285	1295	1328	1256	1275	904	1011	967	1085	1217	1220	1151	1142
8M1	654	876	845	808	721	838	645	639	579	650	720	609	693	671
8M2	743	936	908	934	832	800	718	681	670	710	852	777	786	763
8M3	809	924	984	945	835	1009	801	758	810	902	1044	900	887	885
8M4	862	1058	1119	1102	1013	1038	821	838	808	906	1094	966	964	951
8M5	935	1080	1125	1103	1010	1038	819	838	808	903	1094	966	971	950

Table 5. Time Average TS2 Metal Temperatures (°F)

LMF4	K	L	M	N	O	P	Q	R	S	T	U	V	K-V Av	O-V Av
1M1	772	731	724	727	701	793	697	879	882	941	928	938	835	865
1M2	840	875	895	922	855	903	804	1009	1006	1058	1083	1110	975	1006
1M3	1033	999	1010	1078	1037	1022	960	1198	1216	1262	1287	1294	1156	1194
1M4	1085	1100	1071	1157	1053	1037	1050	1258	1259	1282	1318	1334	1200	1229
1M5	1148	1134	1099	1163	1086	1079	1094	1283	1320	1313	1340	1387	1235	1265
2M1	1074	1078	1076	1158	1043	1035	1141	1266	1237	1273	1316	1310	1194	1223
3M1	1101	1049	1065	1119	1116	1106	1171	1288	1279	1297	1324	1308	1214	1253
4M1	778	771	793	763	724	798	768	953	938	948	959	967	869	900
4M2	900	868	940	941	850	921	920	1072	1050	1080	1101	1096	1000	1028
4M3	1061	994	1115	1176	1085	1122	996	1191	1192	1229	1254	1220	1163	1184
4M4	987	1096	1125	1177	1107	1094	1194	1294	1288	1022	1328	1305	1182	1214
4M5	1168	1097	1125	1177	1099	1126	1184	1319	1337	1315	1350	1369	1249	1280
5M1	1177	1088	909	920	900	929	798	967	971	987	996	1007	962	963
5M2	917	936	918	920	911	929	932	1097	1096	1128	1142	1133	1031	1068
5M3	1071	1005	1107	1161	1071	1047	997	1189	1201	1230	1255	1224	1158	1178
5M4	1145	1065	1115	1161	1080	1050	1156	1269	1285	1294	1311	1289	1210	1235
5M5	1167	1143	1127	1171	1123	1119	1168	1297	1321	1302	1331	1331	1240	1266
8M1	765	767	761	728	725	778	746	910	902	957	957	955	853	887
8M2	820	791	811	888	821	893	903	1070	1071	1096	1110	1113	982	1029
8M3	994	934	967	1034	1000	1008	961	1177	1202	1230	1241	1234	1119	1160
8M4	1008	1005	995	1108	1036	1030	1097	1265	1287	1291	1308	1319	1182	1228
8M5	1092	1050	1072	1126	1063	1050	1113	1263	1308	1286	1314	1339	1204	1239

Table 6. Time Average TS3 Metal Temperatures (°F)

LMF4-	K	L	M	N	O	P	Q	R	S	T	U	V	K-V Av.	O-V Av.
1M1	731	729	677	716	684	696	648	745	710	689	685	679	702	697
1M2	1012	1048	928	989	956	941	928	1015	1010	1007	1033	1062	1005	1007
2M1	745	869	731	724	745	777	645	742	714	693	698	688	721	717
2M2	1028	1135	952	996	974	978	930	1019	1020	1012	1040	1060	1013	1015
3M1	760	866	749	737	769	787	691	761	737	743	758	745	757	754
3M2	1058	1137	978	1011	982	977	943	1023	1026	1034	1067	1086	1033	1030
4M1	621	708	626	614	624	668	534	603	593	586	870	862	677	692
4M2	737	873	744	733	731	763	650	731	713	700	707	694	720	715
4M3	823	906	809	864	836	853	735	836	814	785	811	796	824	817
4M4	897	1008	869	870	873	897	794	892	880	857	572	564	882	875
4M5	916	1011	891	887	890	911	801	903	891	859	863	866	883	879
4M6	883	968	857	856	859	878	802	886	865	848	837	844	859	856
4M7	965	1077	951	928	924	936	870	954	950	939	948	958	944	943
4M8	1025	1129	975	981	966	970	924	1016	1000	983	1033	1034	1001	1002
4M9	1035	1128	974	1005	992	991	946	1034	1041	1037	1067	1086	1035	1037
4M10	1063	1160	987	1019	998	996	940	1024	1042	1032	1046	1081	1032	1031

Note: In this and the two prior tables, the temperatures given were those measured by thermocouples whose designation is given in the first column. The locations of those thermocouples on the tubes were as shown in Figure 6. Data under column headings O through V were averages for those tests. Averages in the last two columns were obtained by weighting the individual run averages by the run duration. *These gave average temperatures for the 2000 and 1500 hour exposures, respectively. Shaded values were* more than two standard deviations from the mean and were excluded from the overall averages as unrepresentative.

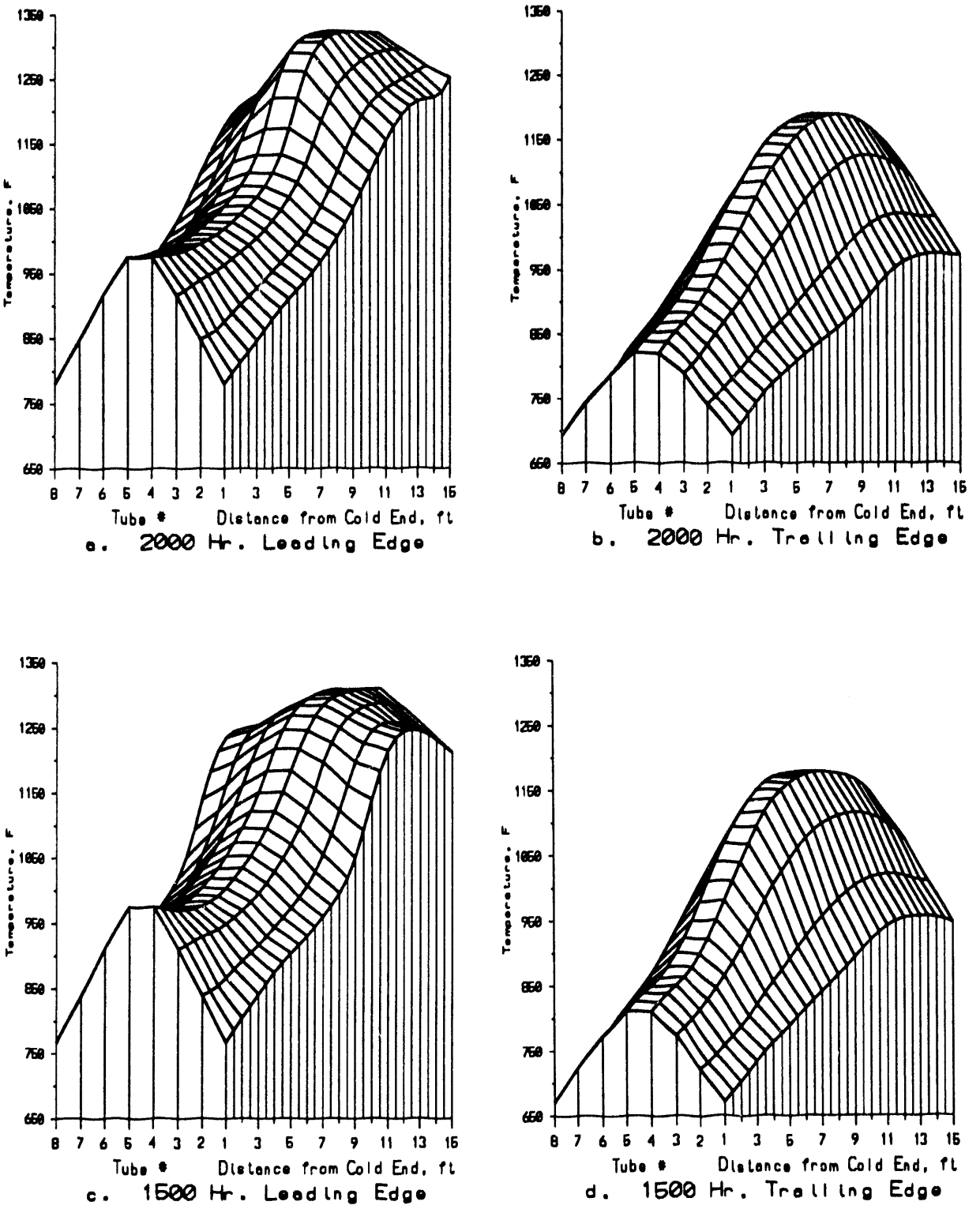

Figure 7. Average TS1 Tube Temperatures

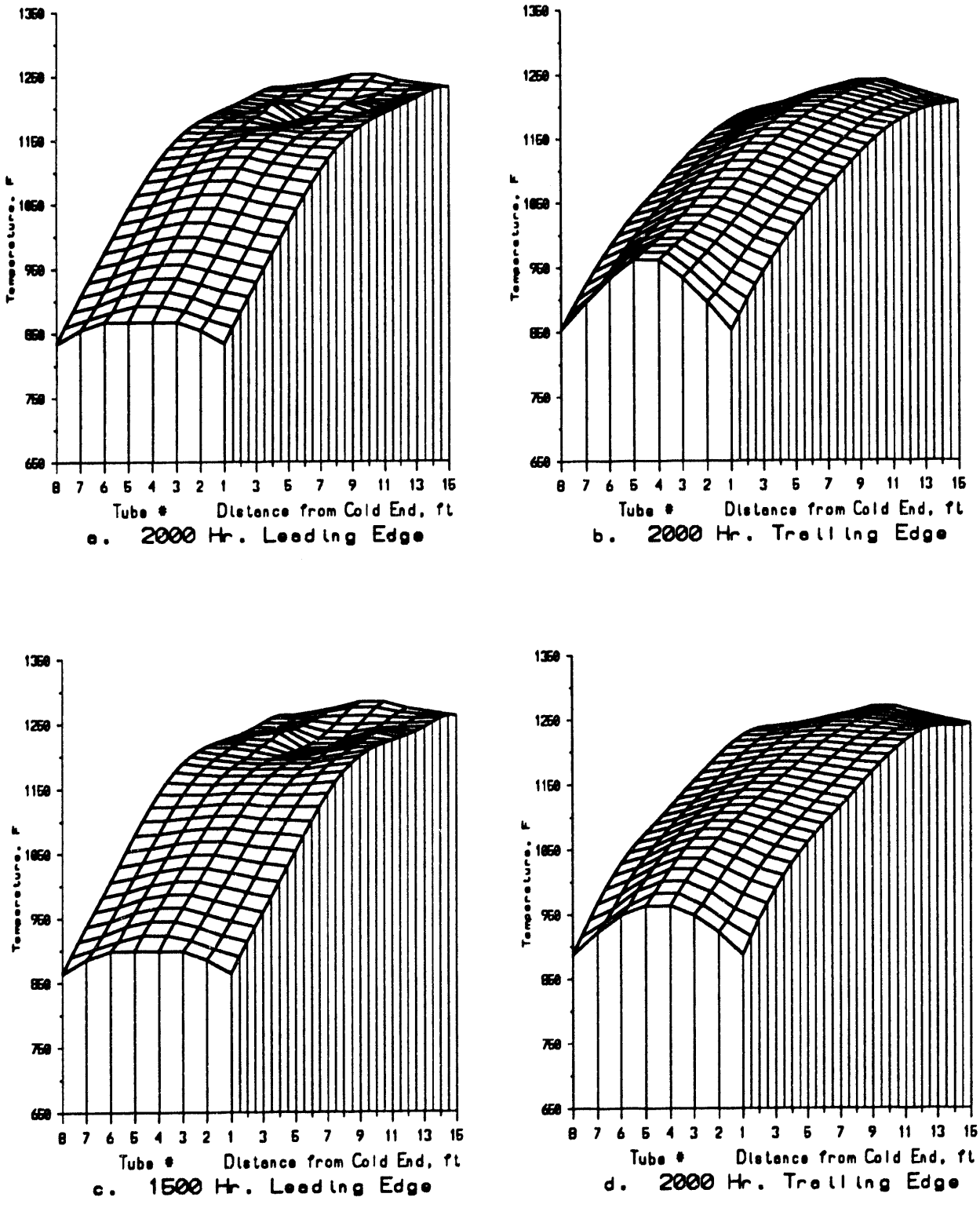

Figure 8. Average TS2 Tube Temperatures

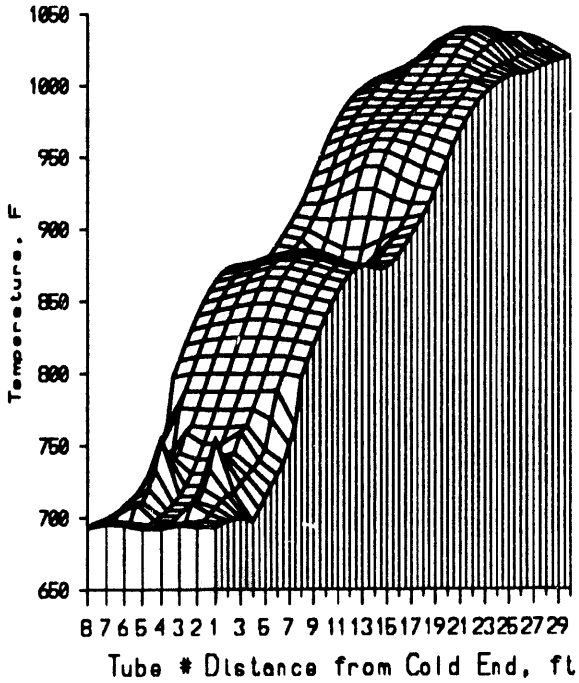

a. 2000 Hr.

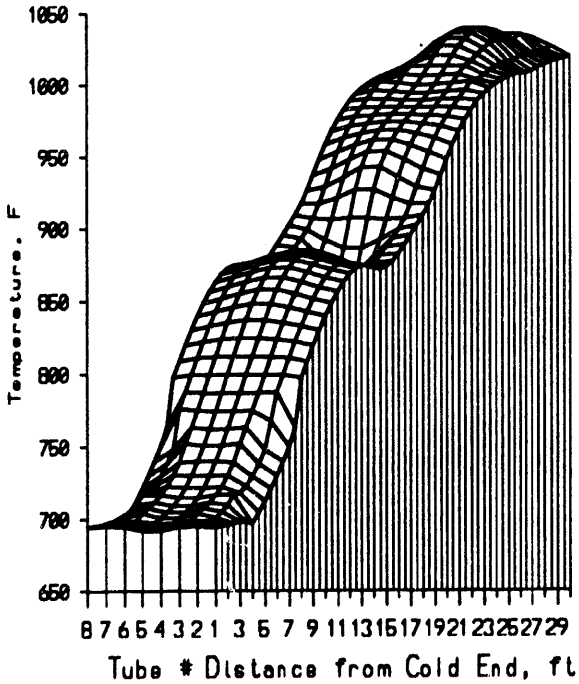

b. 1500 Hr.

Figure 9. Average TS3 Tube Temperatures

sections, respectively. These were obtained by interpolating data from the overall average columns of Tables 4-6. Lateral symmetry of tube temperatures about the center of the test section duct was assumed. Corrosion data was correlated to average exposure temperatures based on these interpolations. Figure 10 shows the metal temperature variations which occurred during tests LMF4-K to -N, as measured by one thermocouple at each of the three test sections, respectively. These variations were rather large as were the variations among the averages for the individual tests, and resulted from several factors, among which were the effect of sootblowing, process upsets or abnormalities, and imprecise control.

SAMPLING AND EVALUATION PROCEDURES

Following the last test of the series, LMF4-V, TS1 deposits were intact on the tubes, but very loosely adhered due to the thermal shock of cool-down. Since they would not have stayed in place during tube removal or cutting (that is, the thick outer portion of deposit; a thin inner layer often remained on the tubes), they were removed and tagged by location and stored. TS2 and TS3 deposits were thin and powdery or very friable. Small samples only were taken. Except for thin layers in some places, the remaining TS2 and TS3 deposits fell off during tube removal, handling, and cutting. The loss of spalled scale was also noted from many locations of all three test sections. Since it was not known what sort of examination would be done other than at the University of Tennessee, it was decided not to attempt to protect deposits and scales with a plastic coating as was done for the 500 hour tubes. Another factor in this decision was that deposit and scale spalling and loss had already occurred on many occasions as a result of test shutdowns, sootblowing, manual removal of oversize deposits, deposit sampling, removal of tubes for refractory repair, etc.

Tubes were initially cut with a band saw, with no coolant. For TS1 and TS2, half-inch long rings were cut by band saw from the top of each 1 foot length of tube. For TS3, the number of samples was lessened, samples being taken only from the top, middle, and bottom of each pass. Thus, 112 samples were obtained for each of TS1 and TS2, and 96 samples for TS3. A mark was placed with a chisel on the top side of each sample at approximately the center of the leading side. The leading quadrant of each of the samples was cut from the ring, encapsulated in plastic, sectioned by diamond cut-off saw, ground, and diamond polished, all with nonaqueous lubricant. Samples were also prepared of the trailing quadrant of TS1 and TS2 tubes at the 1, 3, 5 and 7 foot levels from the top of the first or hotter tube pass. Since the corrosion measurements were found to be quite time consuming, not all of the leading quadrant samples prepared were examined. For TS1 and TS2, these were at the 1, 3, 5, and 7 foot levels of the hotter pass, which included the highest exposure temperatures which are relevant to the intermediate temperature air heater as well as the upper end, where corrosion would be greatest, of the metal temperature range relevant to superheater service.

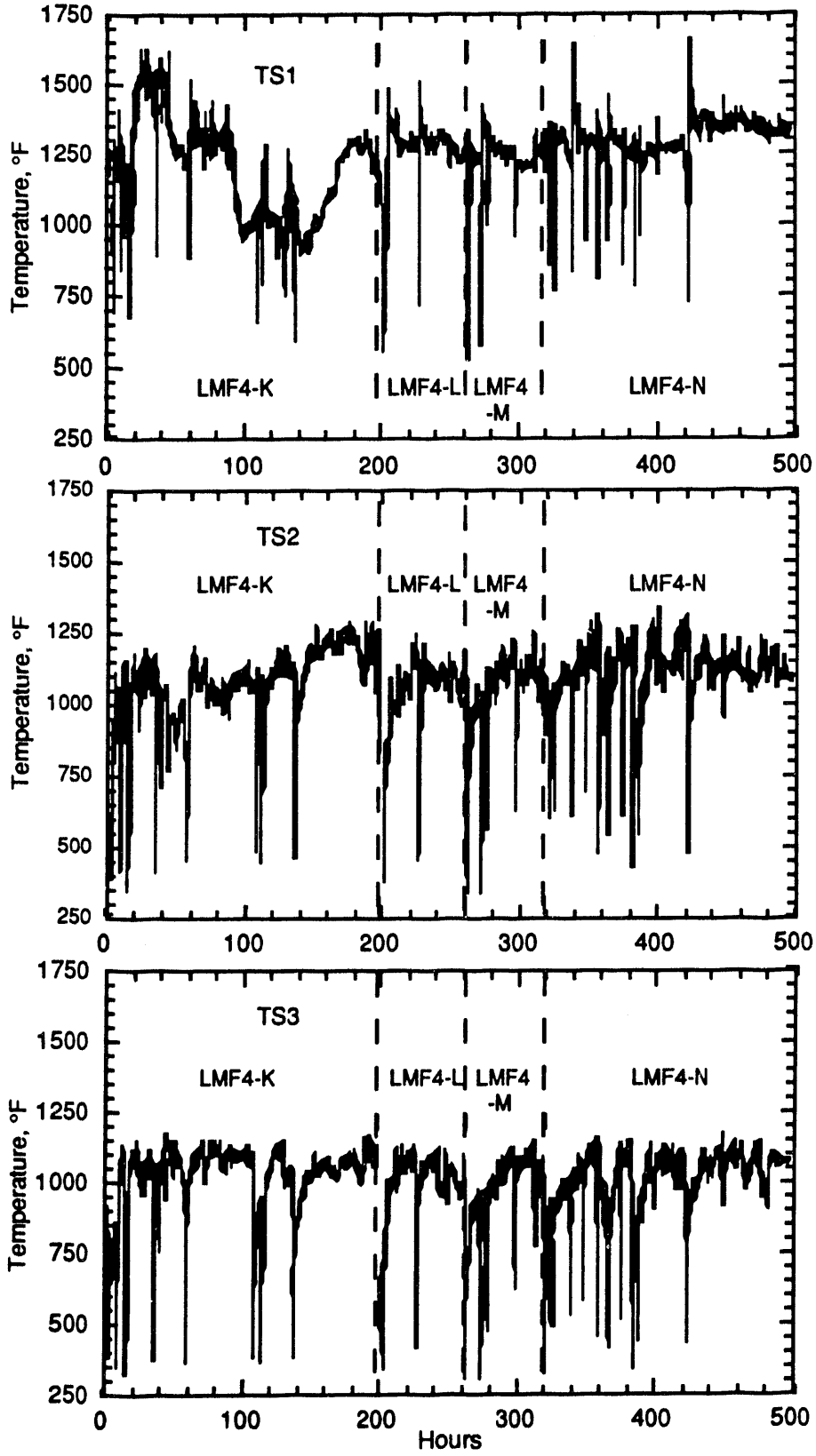

Figure 10. Tube Metal Temperatures at the Leading Edge of Tube 3 at the Vertical Middle of the First Pass.

The principal measure of the extent of corrosion was taken to be the sum of the corrosion scale thickness and the depth of internal penetration into the metal substrate, as depicted in Figure 11. These were measured using a light microscope and an image analysis system. One scale thickness and one penetration measurement were made from each image frame. Scale thickness was obtained as the area of corrosion scale in the image divided by the image width to give the equivalent or average scale thickness. Internal penetration was taken as the maximum extent of penetration in the image with respect to a straight line representing the average surface. This method was chosen as being more sensitive to the small extents of corrosion resulting from the relatively short exposure durations than the alternative method, ultrasonic wall thickness measurement. The ultrasonic method also possessed problems of necessitating corrosion scale removal from both the exterior and interior surfaces of the tube without significant metal removal, being unable to distinguish between metal loss at the exterior and the interior surfaces, and the difficulty of making measurements before and after exposure at precisely the same locations.

As a secondary measurement, the remaining wall thickness was measured at 5 locations on each sample examined and was compared to ultrasonic measurements made prior to exposure, or for tubes for which there was no pre-exposure measurements, to the original nominal wall thickness. Before and after measurements were within about an inch of each other, but not at the same exact spots. While this method was rather crude, it served to confirm the nonexistance of very large corrosion losses.

The microscopic method utilized, although sensitive, possessed several problems. Foremost was that scale thickness is not equal to metal thickness consumed to produce the scale. Thus, **SCALING RATES OR COMBINED SCALING AND PENETRATION RATES SUCH AS THOSE REPORTED HEREIN DO NOT EQUAL METAL RECESSION RATES AND SHOULD NOT BE USED DIRECTLY AS A BASIS FOR DESIGN.** This was compounded in the present case by the fact that an unknown amount of metal loss was unaccounted for as a result of scale spalling and the diffusion of metal into the deposit.

For TS1 and TS2, pass 1, at distances of 1 foot and 7 foot from the top plate, measurements were made at 5 degree increments over a 90 degree arc of tube centered on the leading edge. Because of the large variation in corrosion from spot to spot (the spot size being the area contained within each image frame), these 19 measurements were averaged to yield a single value for the sample. To reduce the task of making the measurements to a reasonable level, five measurements per sample were made at the other leading edge positions. Only a single measurement was made for each trailing edge sample. More measurements were done at the 1 foot level at the front of pass 1 because this was at or near the maximum tube temperature and therefore at the most severe service environment with respect to application in an intermediate temperature air heater. Likewise, more measurements were made at the 7 foot level at the front of pass 1 because the metal temperature there was generally closest to the maximum expected

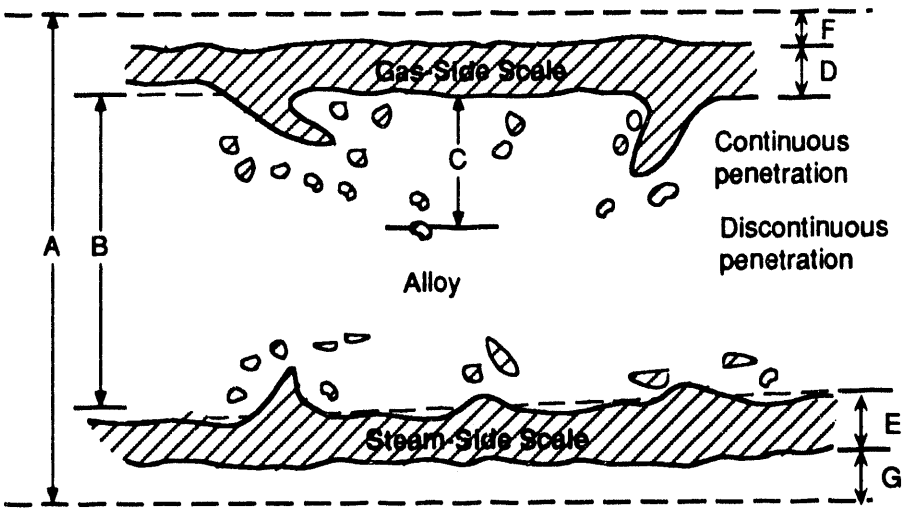

IL-1623

A = Original thickness (measured by ultrasonics)
B = Thickness of metal remaining after exposure (measured microscopically)
C= Depth of maximum penetration (measured microscopically)
D,E= Scale thickness of remaining
F,G= Thickness of spalled scale (unmeasured)
Gas-side metal recession

$= C + D + F \approx C + D$ for small F

$= A - B + C - E - G \approx A - B + C - E$ for small G

Figure 11. Schematic diagram of measurements made on corroded tube samples.

superheater metal temperature, where corrosion should be greatest. Five measurements per sample were done for each of the TS3 samples examined.

A scanning electron microscope with energy dispersive x-ray analyzer was used to make microphotographs of the corrosion morphology as well as to make x-ray dot maps for identification of the distribution of elemental constituents of tube scales, reacted subscale grain boundaries, and the deposit immediately adjacent to the tube.

RESULTS

Corrosion Data Variability and Angular Variation

Examples of the variation in the measured extent of corrosion for individual samples taken from the leading side of tubes are shown in Figure 12. The measurements were at different angular positions along a cross-sectioned 90° circular arc of tube. Large data scatter existed due to the inherently large spot-to-spot variability of the corrosion process under nominally constant conditions. Thus, inspection of data for individual samples did not show a discernable trend with respect to variation of corrosion over this arc. Internal penetration data from 32 TS1 and TS2 samples, for which measurements were made at 5 degree increments, were combined by summing them on an angular basis and then normalizing. The result, Figure 13, indicates little variation within ±30-35 degrees of the leading edge, but a sharp decrease at greater angles. Most of the remaining presentations of leading quadrant data are derived from averaging all the measurements for each sample. Inclusion of data beyond ±35 degrees may make the average for the quadrant somewhat lower than the average corrosion level within ±35 degrees. This was not considered of much importance since the measurements were really valid only for comparing alloys rather than for absolute corrosion rates.

Stainless Steels: penetration kinetic data

For the stainless steels, penetration was a more reliable measure of relative corrosion extent than scale thickness or combined scale thickness and penetration owing to errors introduced by scale spalling and the difficulties in accurately measuring scale thickness. Figure 14 shows leading edge data for TS1 and TS2, derived from tube samples taken from the bottom of the first pass where leading edge time-average temperatures were in the range of 831-915 K (1036-1188°F). These are the temperatures which would exist near the hot end of a secondary superheater or reheater and at which corrosion would be expected to be greatest for the component. Figure 15 presents the leading edge data for TS1 and TS2 at higher metal temperatures relevant to the intermediate temperature air heater. These data are from samples from the top of the first or hotter pass having leading edge time-average tube temperatures in the range of 889-995 K (1140-1332°F). Cubic spline interpolation lines through the data points are meant only to provide a visual linking of data for a given alloy and not to indicate the course of corrosion kinetics or as a basis for extrapolating the corrosion kinetics.

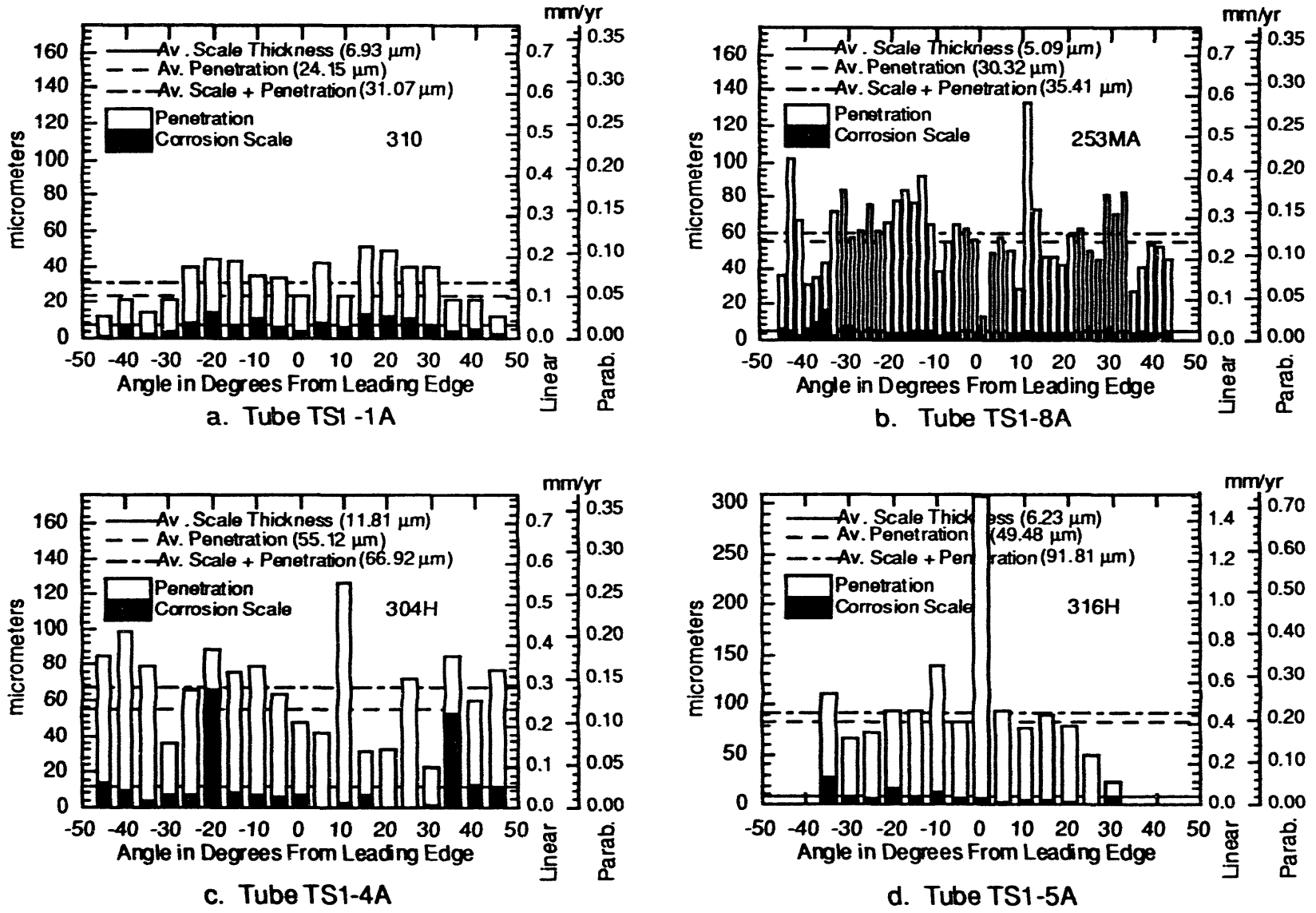

Figure 12. Typical Corrosion Data at Bottom of Pass 1 Showing the Amount of Variation in Individual Samples.

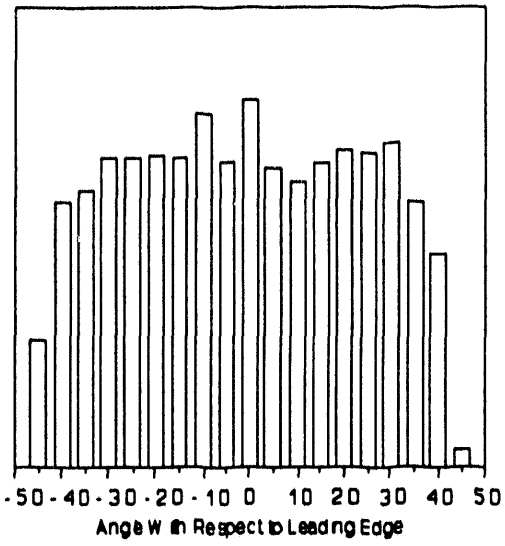

Figure 13. Distribution of Penetration Depth Over Tube Leading Quadrant Derived from Normalizing and Summing Data from 32 TS1 and TS2 Samples.

An anomalous behavior was seen with respect to corrosion at 1500 and 2000 hours as shown for several of the alloys in Figures 14 and 15. In these cases, the indicated corrosion at 2000 hours was substantially less than at 1500 hours. More scale spalling would be expected during longer exposure. But if scale spalling were to occur during the course of exposure, internal penetration should increase, not decrease. If scale spalled after exposure due to cutting, sample preparation, etc., then penetration would be unaffected. Thus, the apparently anomalous behavior must be attributed either to data scatter (very few measurements in a highly variable population) or to some difference in the test conditions for the two sets of tubes which resulted in more corrosion of the 1500 hour tubes. While many condition changes (such as changed coal seam) and fluctuations occurred during the course of the tests, it is unknown which one or ones may have produced this effect.

Given the amount of data scatter present and the relatively few measurements made, it was not possible to describe the corrosion kinetics of the test alloys. The usual possibilities are parabolic behavior with a decreasing rate with time as is normal if corrosion products are protective at limiting ionic transfer, or more or less linear as in the case where scales are unprotective and depletion has occurred of chromium or other alloying additions necessary for reformation of protective scales.

Generally increasing corrosion resistance with alloy chromium content was indicated, but with numerous deviations arising from the data scatter. For TS1, corrosion at the top of pass 1 was less than at the bottom, despite the higher temperatures. Since deposits were much thinner toward the top of the tubes owing to the downward deflection of the gas flow exiting the radiant furnace, a relationship between corrosion and deposit

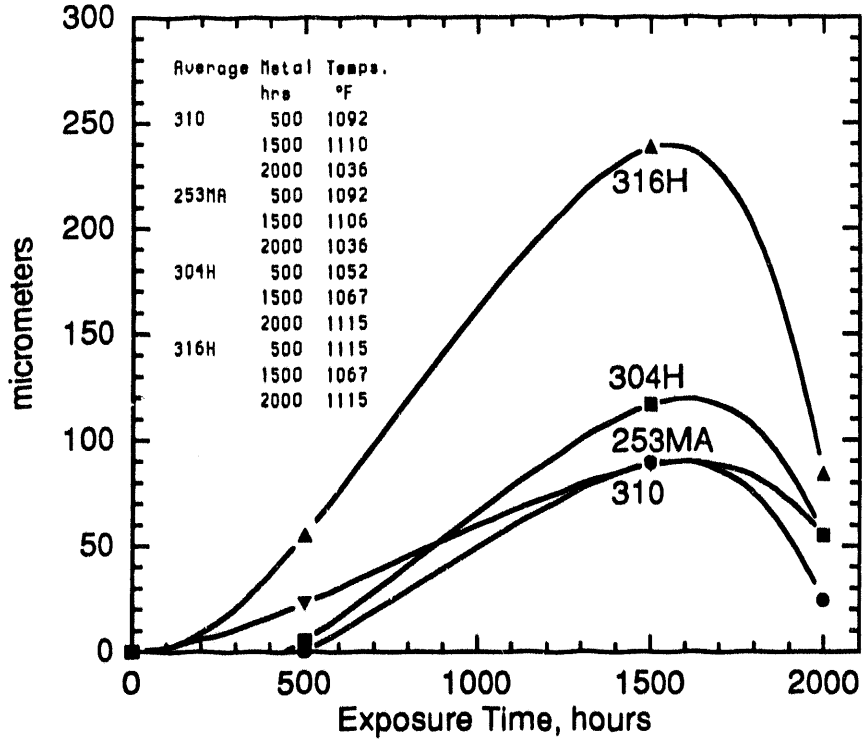

a. TS1

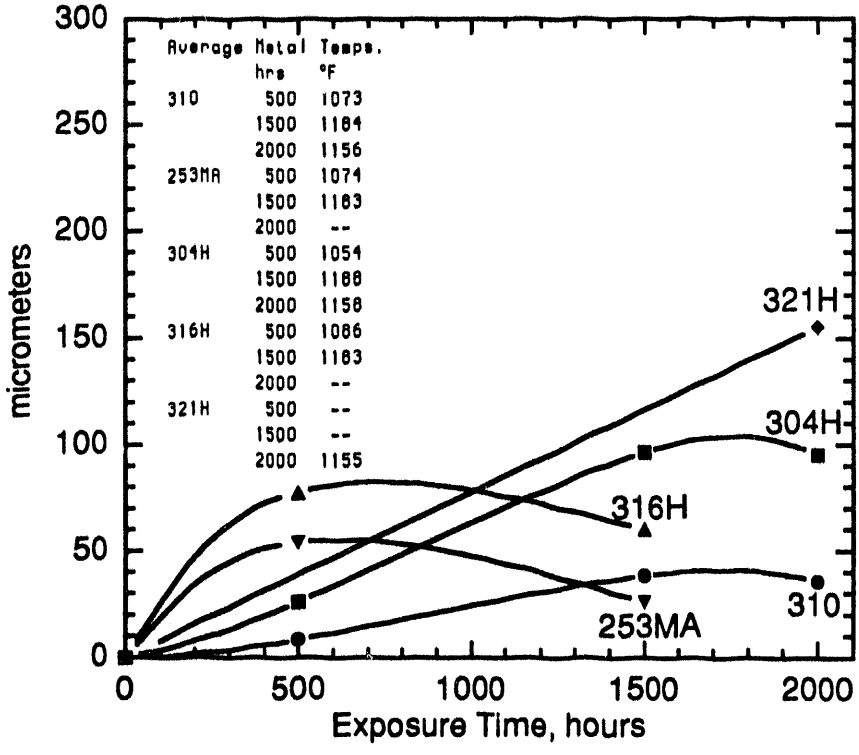

b. TS2

Figure 14. Internal Penetration of TS1 and TS2 Alloys at the Bottom of the First Pass with Metal Temperatures Near the Maximum for Superheater Service.

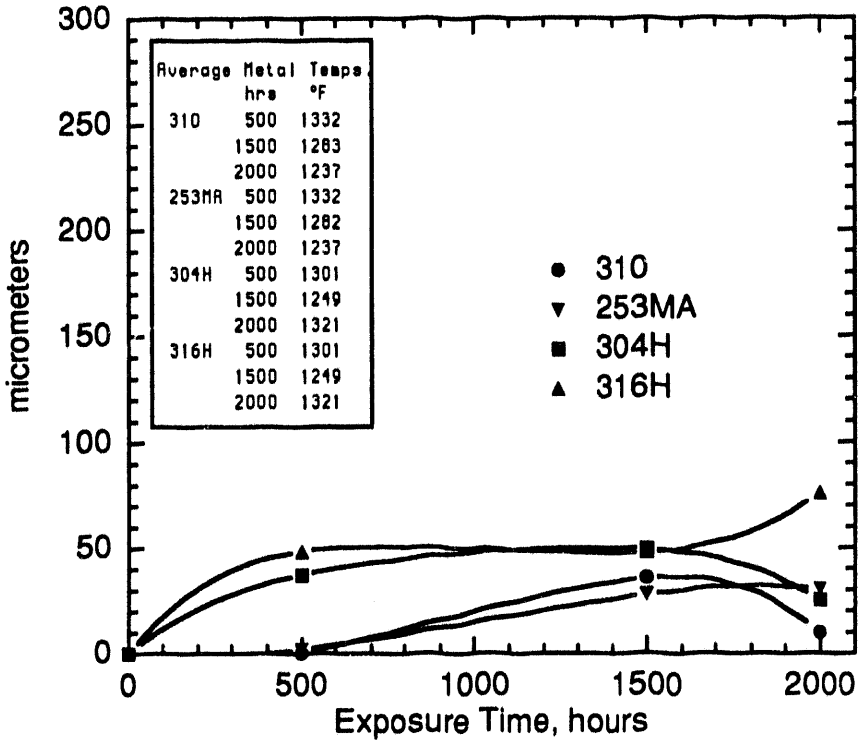

a. TS1

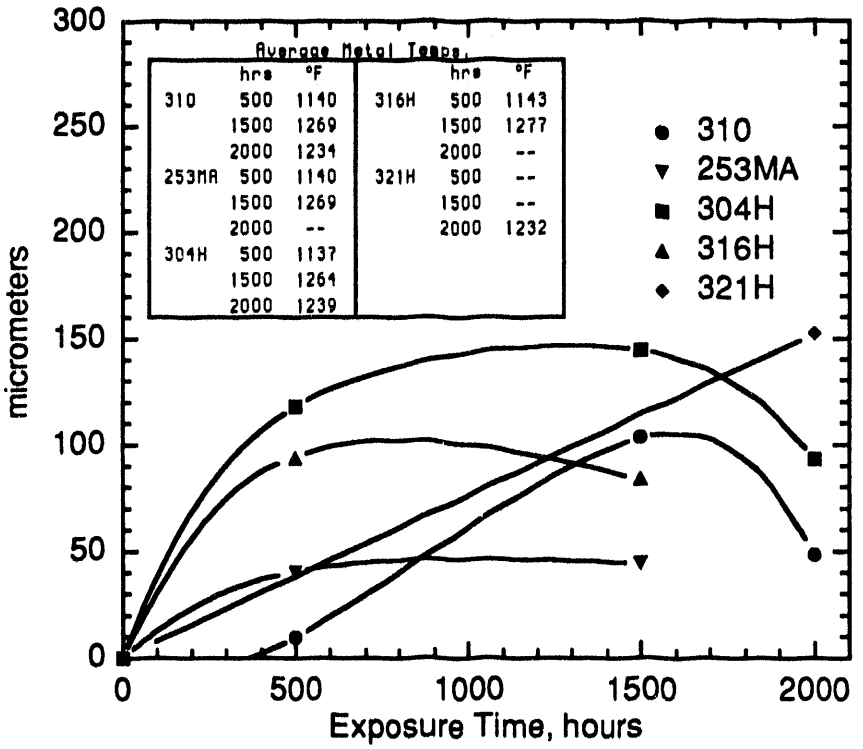

b. TS2

Figure 15. Internal Penetration of TS1 and TS2 Alloys at the Top of the First Pass with Metal Temperatures in the Range for ITAH Service.

thickness was suspected, agreeing with the indication of lower corrosion at greater than ±35 degrees angular position where deposits were thinner. For TS2, where deposits were of uniform thickness, there was little difference from the bottom to the top of pass 1.

Stainless Steels: scaling + penetration kinetic data

TS1 and TS2 data for scale thickness + penetration of the stainless steel alloys are given in Figures 16-17 for the bottom of pass 1 and Figures 18-19 for the top of pass 1. Again, the same anomalous behavior with regard to 1500 and 2000 hour exposures was seen. The scatter in the results precludes drawing too many conclusions. However, it would appear, that at both locations, only alloy 310 had corrosion generally less than 0.5 mm/yr if determined on a linear basis. The other alloys were variably below or above a 0.5 mm/yr parabolic rate. There was no discernable, consistant different between TS1 and TS2 or between the top and bottom of pass 1.

Stainless Steels: penetration versus average metal temperature data

Data for internal penetration of the stainless steels as a function of time-average metal exposure temperature is shown in Figure 20. Perhaps as a result of the scatter and the relatively narrow range in temperature over which measurements were made, no trend in corrosion with metal temperature could be discerned. The extent of penetration for 1500 hour and 2000 hour samples was indistinguishable. Also, no difference was seen between TS1 and TS2. Alloys 253MA, 304H, and 316H showed rather large variabilities in the extent of penetration, resulting from variable extents of disruption of the surface scale. Alloy 321H would likely have shown the same sort of variability if more samples had been examined. Error bars in the plots represent a 95% confidence interval.

Stainless Steels: scaling + penetration versus metal temperature data

Combined remaining scale thickness and penetration as a function of tube metal temperature for the leading side of stainless steel alloys in TS1 and TS2 are presented in Figure 21. Again, the temperature relationship was uncertain, given the amount of scatter and the relatively narrow range of temperatures. A hint of decline in the extent of remaining scale plus penetration with temperature for 304H and 316H could be attributed to increased scale disruption and exfoliation at higher temperatures. TS2 data was generally somewhat above that for TS1, but that was attributed to more scale loss at TS1 rather than more corrosion at TS1, since penetration data alone did not show the same trend. Limits for effective metal loss of 0.5 mm/yr (for the first year), calculated by both linear and parabolic kinetics, are shown on the plots. Scale plus penetration data for alloy 310 was mostly less than 0.5 mm/yr on a linear basis, the other alloys being either variably or totally above. Alloy 253MA data was definitely less than 0.5 mm/yr by parabolic kinetics. Alloy 304H average data was also less than 0.5 mm/yr parabolic. Alloys 316H and 321H were less adequate at meeting the criterion.

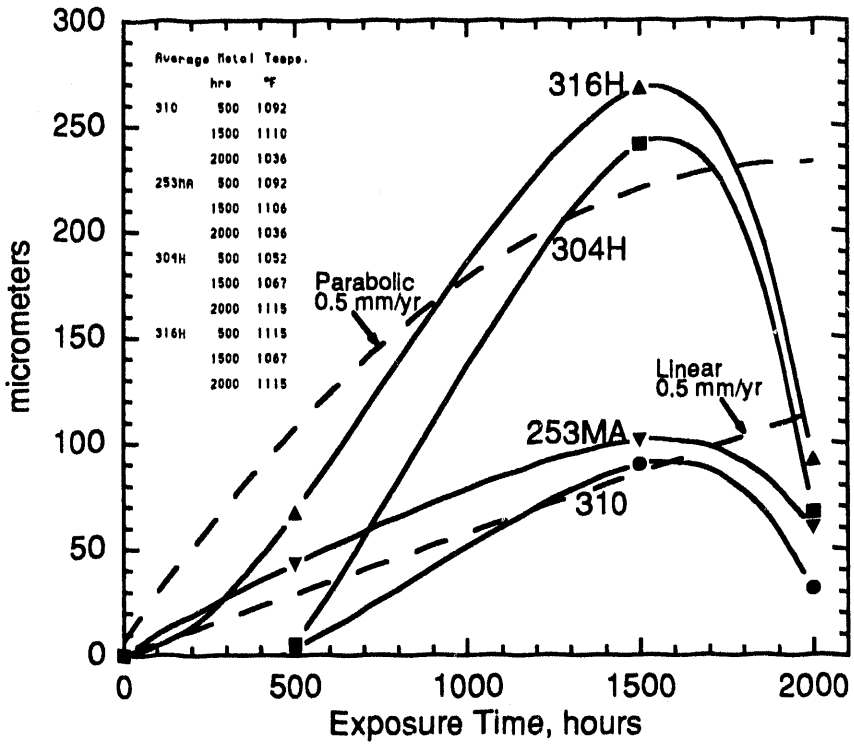

a. Leading Edge

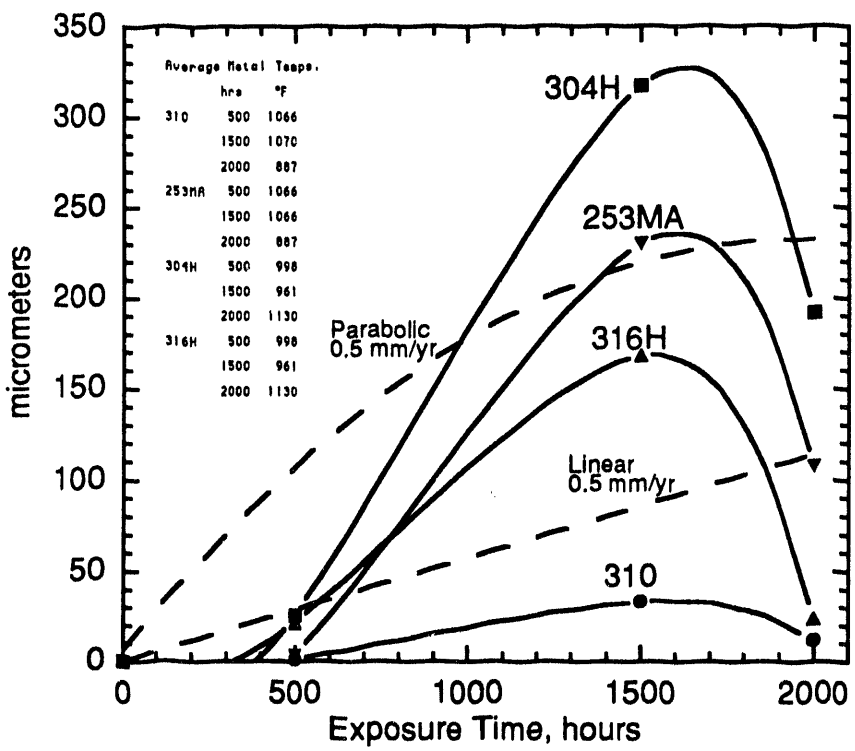

b. Trailing Edge

Figure 16. Kinetic Corrosion Data (Scale Thickness + Penetration) for TS1 Alloys at the Bottom of the Front Pass.

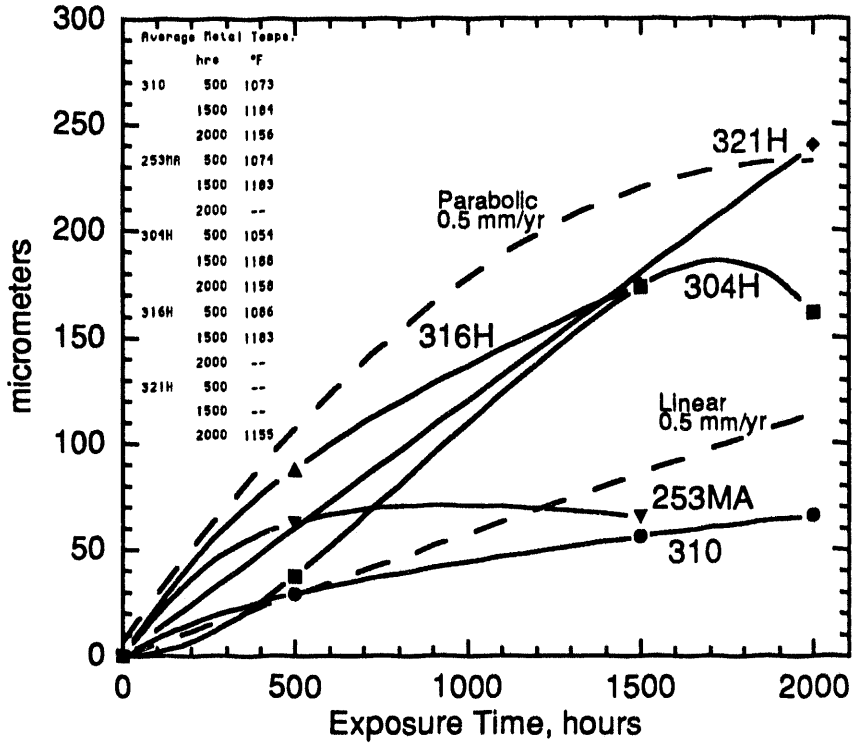

a. Leading Edge

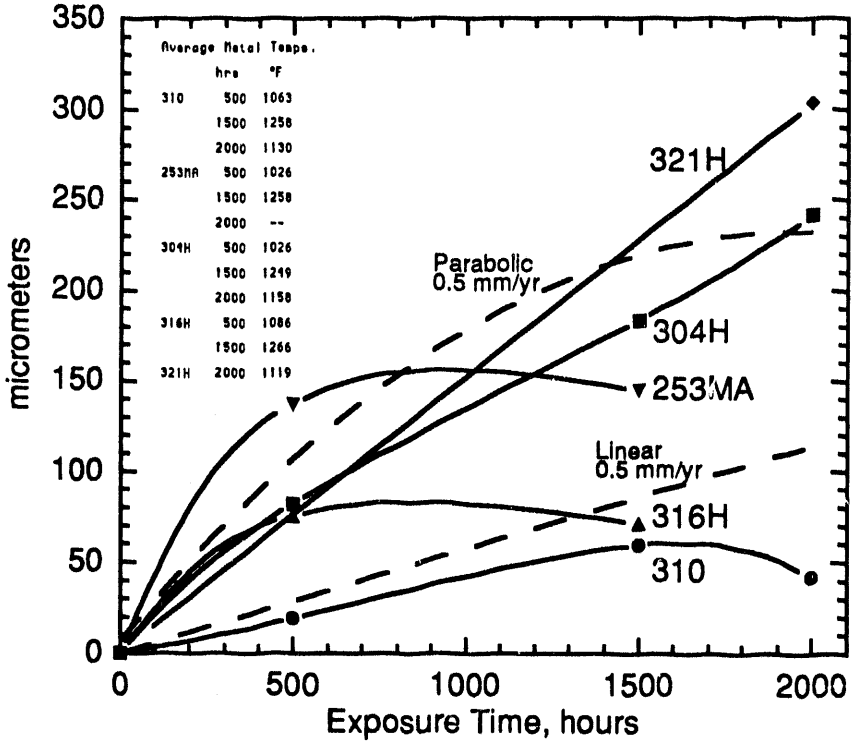

b. Trailing Edge

Figure 17. Kinetic Corrosion Data (Scale Thickness + Penetration) for TS2 Alloys at the Bottom of the Front Pass.

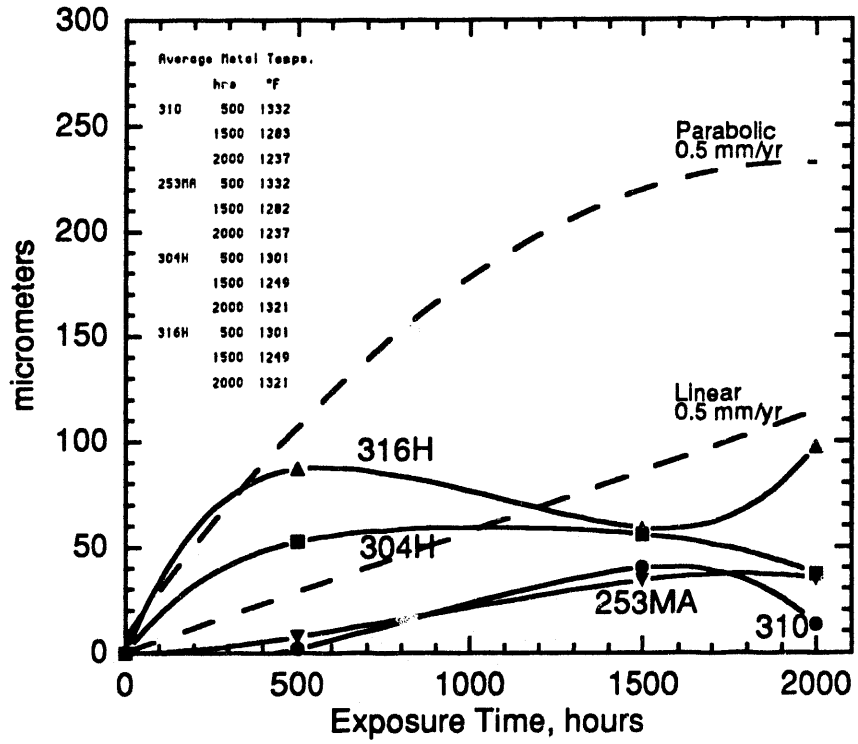

a. Leading Edge

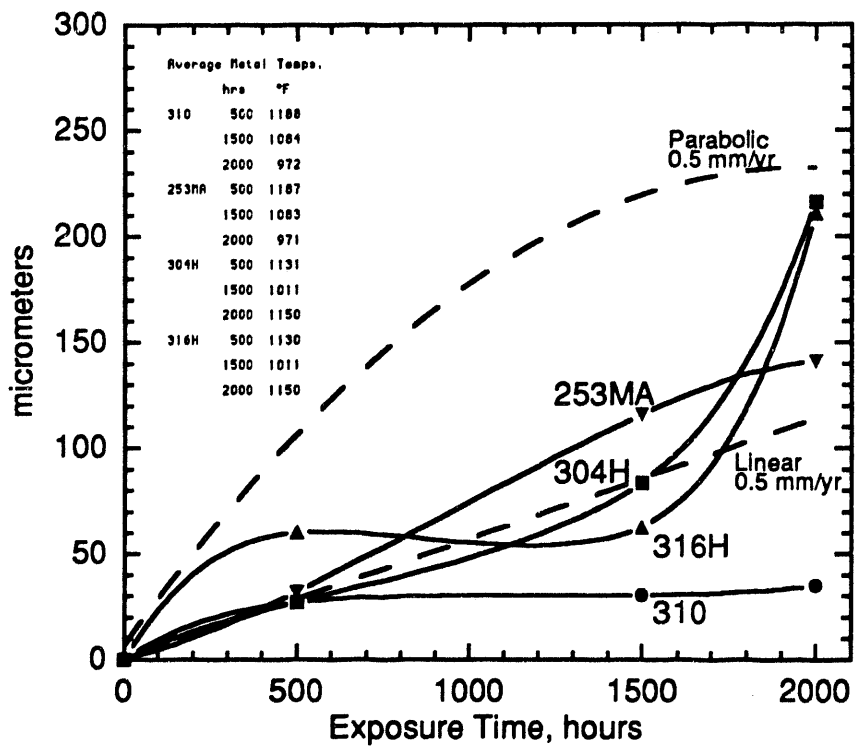

b. Trailing Edge

Figure 18. Kinetic Corrosion Data (Scale Thickness + Penetration) for TS1 Alloys at the Top of the Front Pass.

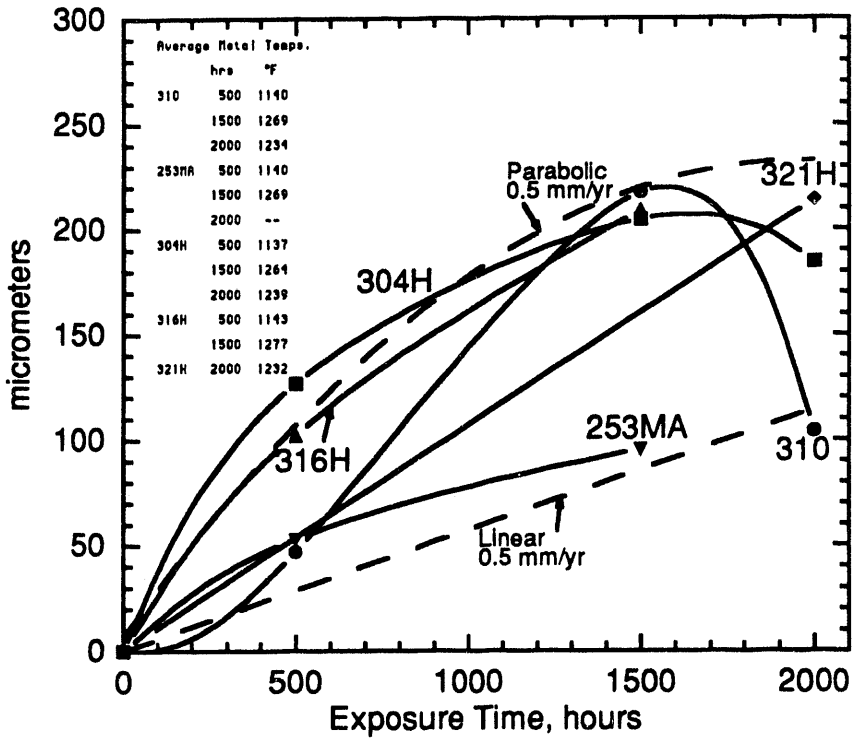

a. Leading Edge

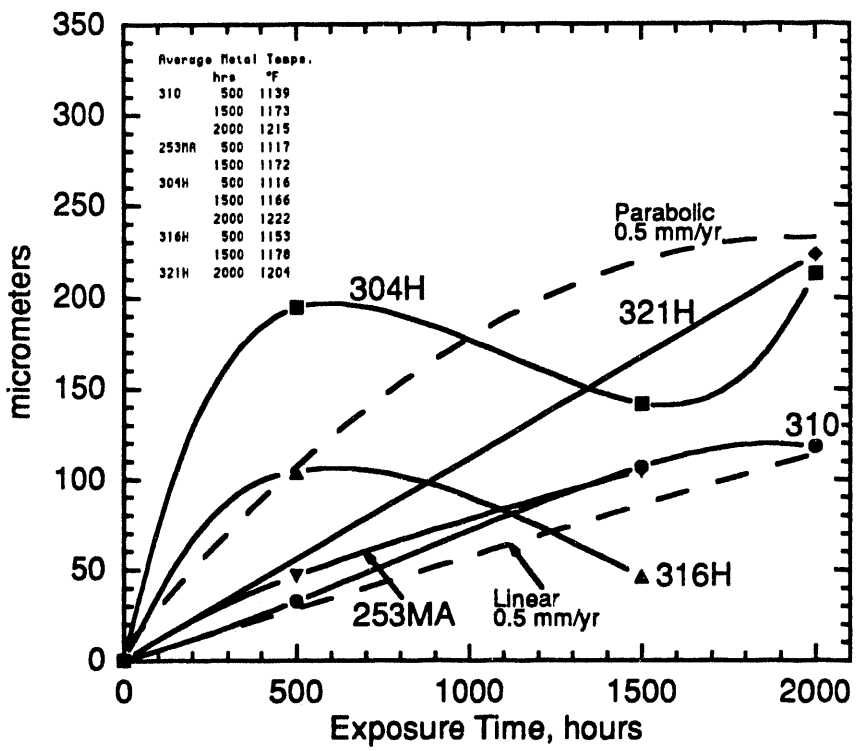

b. Trailing Edge

Figure 19. Kinetic Corrosion Data (Scale Thickness + Penetration) for TS2 Alloys at the Top of the Front Pass.

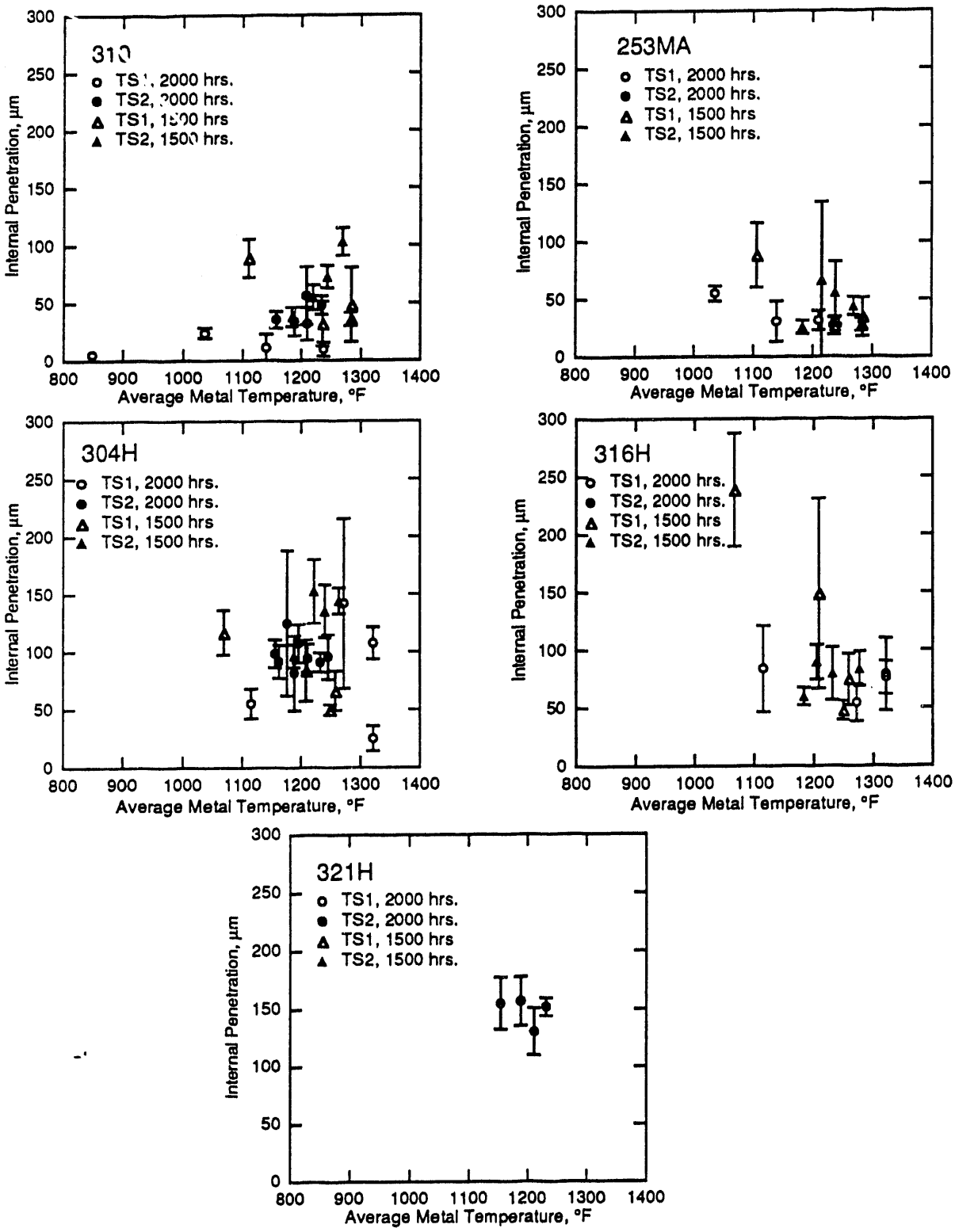

Figure 20. Internal Penetration versus Average Metal Temperature for Stainless Steels in TS1 and TS2.

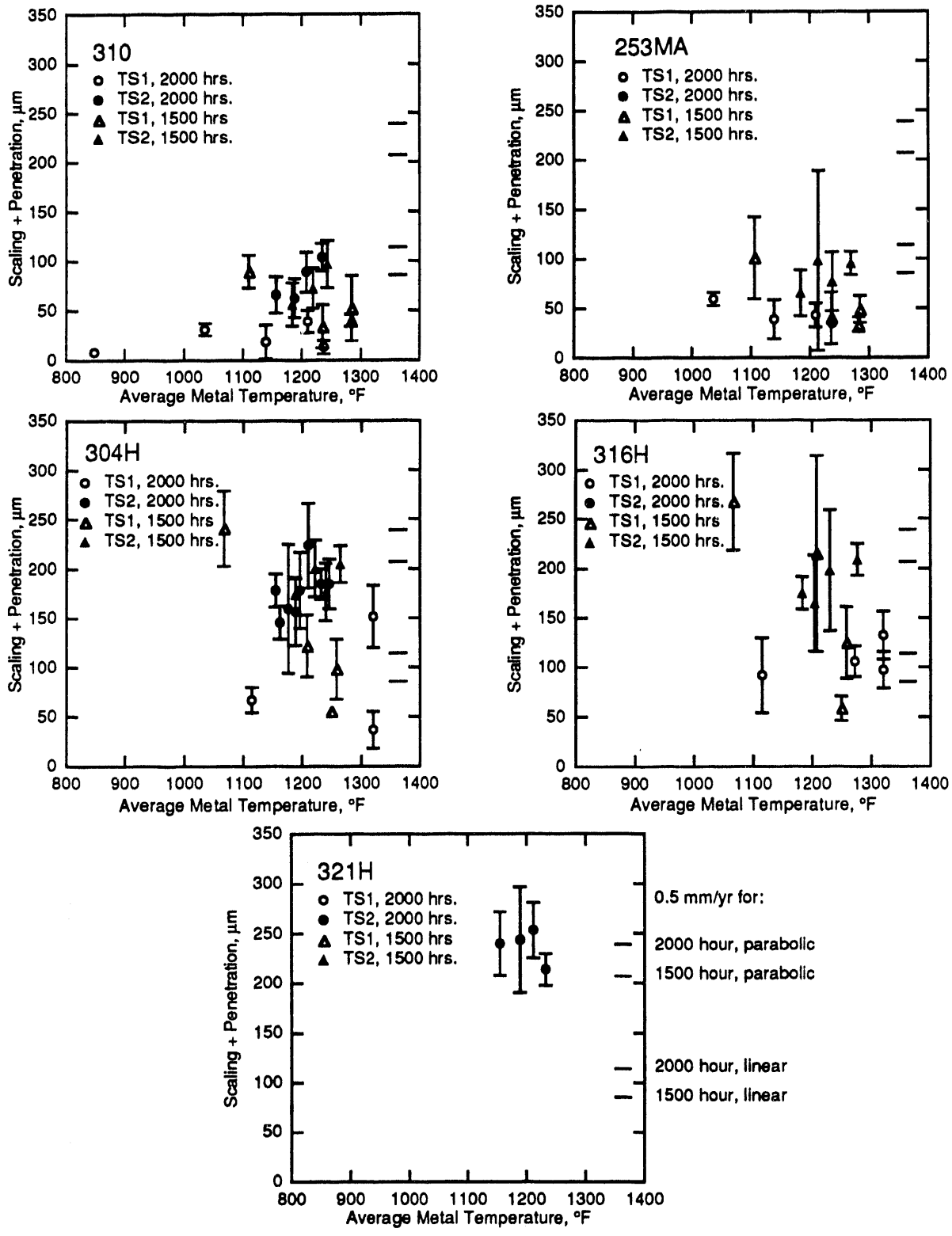

Figure 21. Scale Thickness + Penetration vs. Average Metal Temperature for the Leading Edge of Stainless Steel Tubes in TS1 and TS2.

Stainless Steels: leading versus trailing edge data

Results for internal penetration at the trailing edge of stainless steel tubes are presented in Figure 22 as a function of metal temperature. Comparison with leading edge data in Figure 20 indicates corrosion to have been approximately the same at the two locations.

Stainless Steels: all data combined

Measurement results with respect to metal temperature are next presented for the stainless steel alloys in TS1 and TS2, combining the two test sections so as to disregard differences in gas temperature, heat flux, deposit characteristics, and so forth. Results from both the 1500 hour and the 2000 hour exposures are also combined, as are data from both the leading and the trailing edges. Figure 23a and 23b show scaling and penetration rates for the alloys 310, 253MA, 304H, 316H, and 321H calculated in terms of linear rate kinetics. Figure 24a and 24b present the same data in terms of parabolic rate kinetics. Leading edge data values plotted were the average of several measurements, ranging from 5 to 46, while trailing edge values were from a single measurement. Previously made observations are reiterated with respect to the data of Figures 23 and 24:

1. A large amount of data scatter existed with the result that the temperature dependence was difficult to discern. Furthermore, variations within a relatively small temperature range appeared to be random. That is, they appeared to show little or no relation to whether the sample was from TS1 versus TS2, leading versus trailing edge, or 1500 hours versus 2000 hours. Such random variations were due partially to the actual spatial variability of corrosion over the tube surface as a result of variations in factors other than temperature affecting corrosion. The scatter in scaling data was also due partially to variable scale loss from spalling. Finally, measurement error contributed to the scatter in scaling data. This error arose mostly from the frequent difficulty in determining from images what was corrosion scale and what was not. Most of the difficulty was in determining whether voids, dark areas, or certain red areas (as seen in the eyepiece) were scale or in determining the area of scale fractured into many pieces or occurring as myriad fine precipitates in the deposit. A minor part of this difficulty was due to the inability of captured images to reveal sample features with the same clarity as looking through the eyepieces because of limited image resolution and a monochrome rather than color image.

2. Alloy 310 was the most corrosion resistant, overall, of those tested, as would be expected from its higher chromium content. Alloy 253MA was second best and about the same as 310 at the higher metal temperatures. This resulted from 253MA being unable at the lower temperatures to form the protective silica subscale which it forms at higher temperatures. There was not much difference between alloys 304H and 316H. While relatively little data was obtained for Alloy 321H, its performance was distinctly inferior to the other 18-8 alloys.

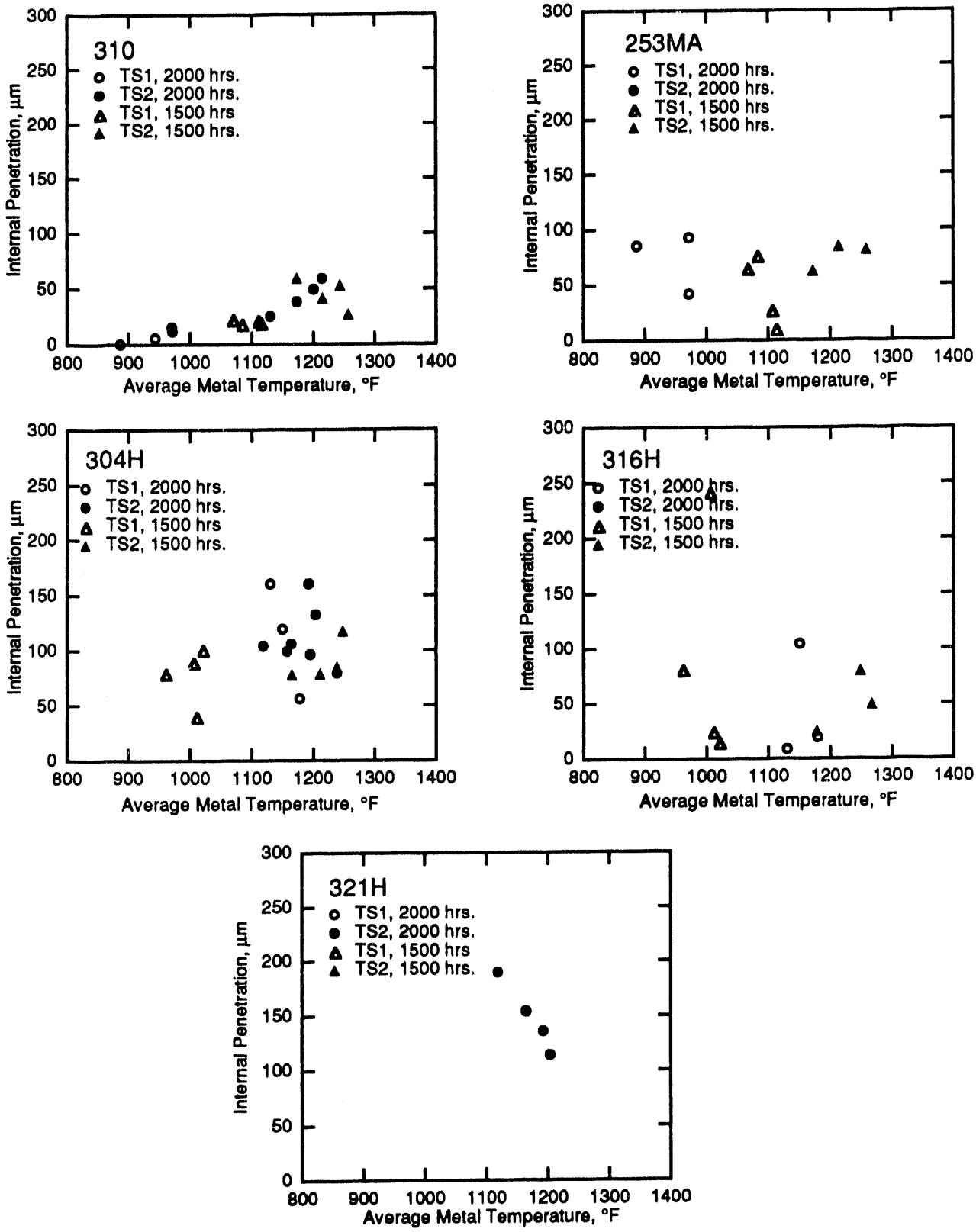

Figure 22. Internal Penetration at the Trailing Edge versus Average Metal Temperature for Stainless Steels in TS1 and TS2.

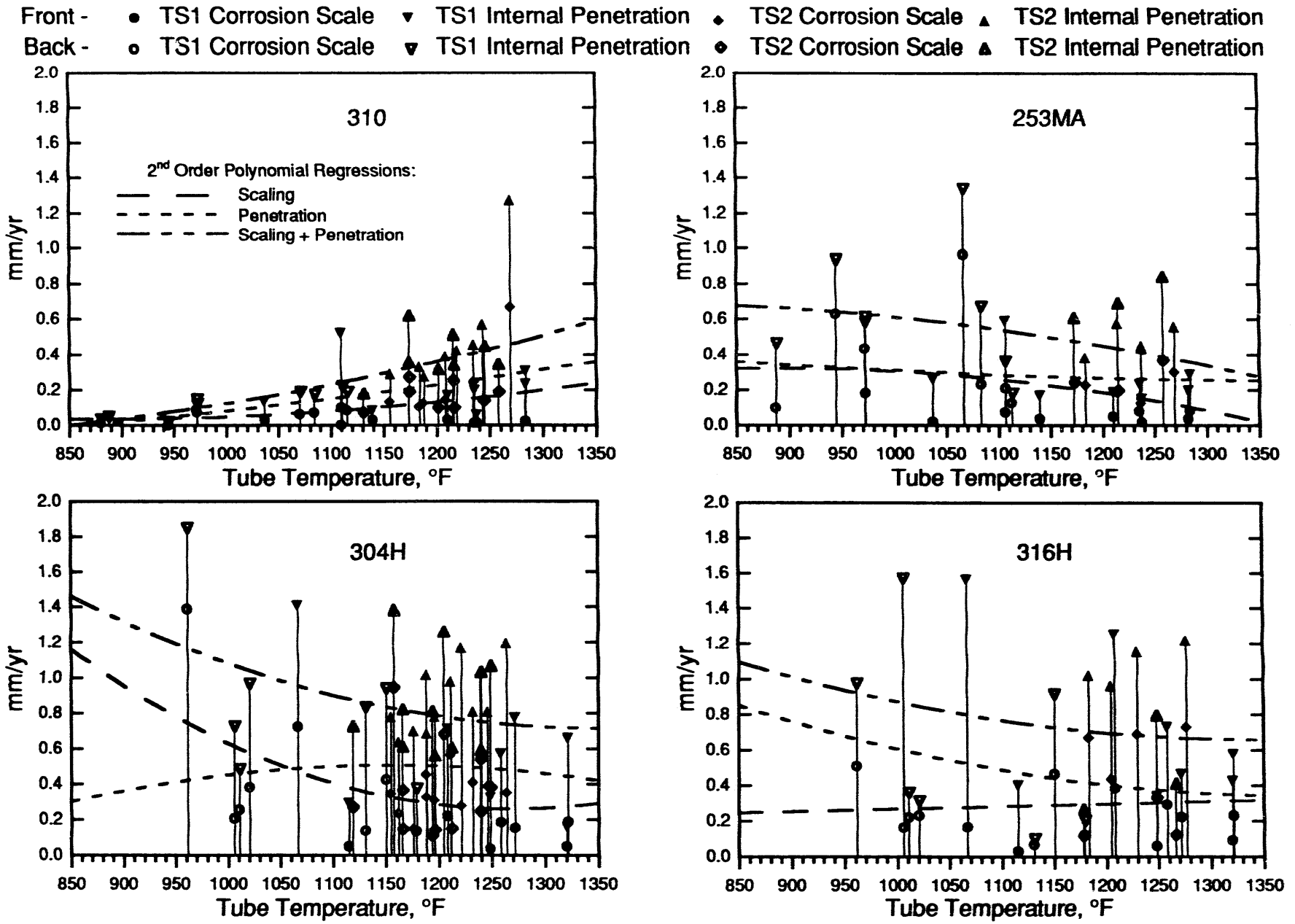

Figure 23a. Linear Corrosion Rates of TS1 and TS2 Tube Alloys Exposed for 1500-2000 Hours During LMF4

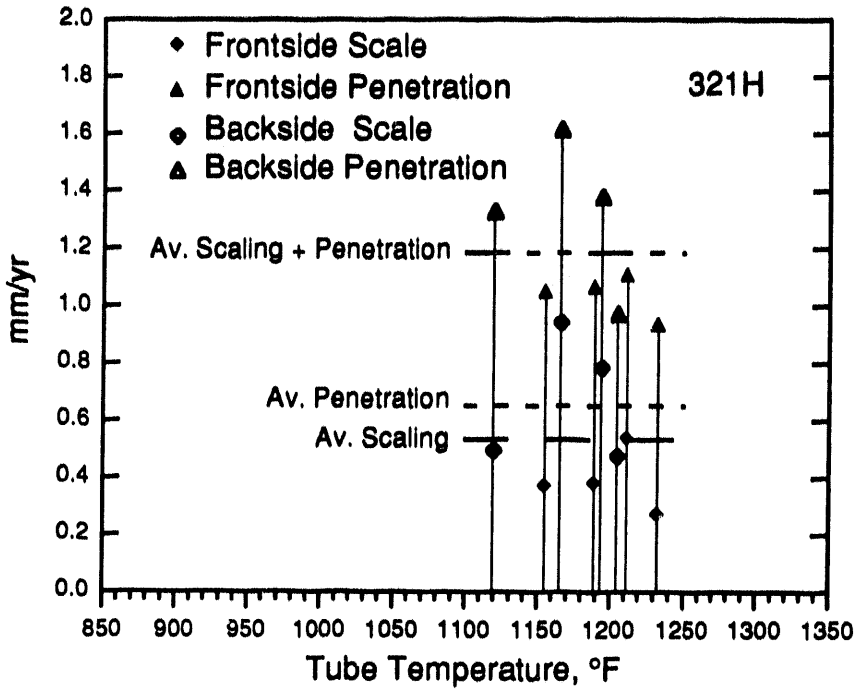

Figure 23b. Linear Corrosion Rate of Alloy 321H at TS2 Exposed for 2000 Hours During LMF4.

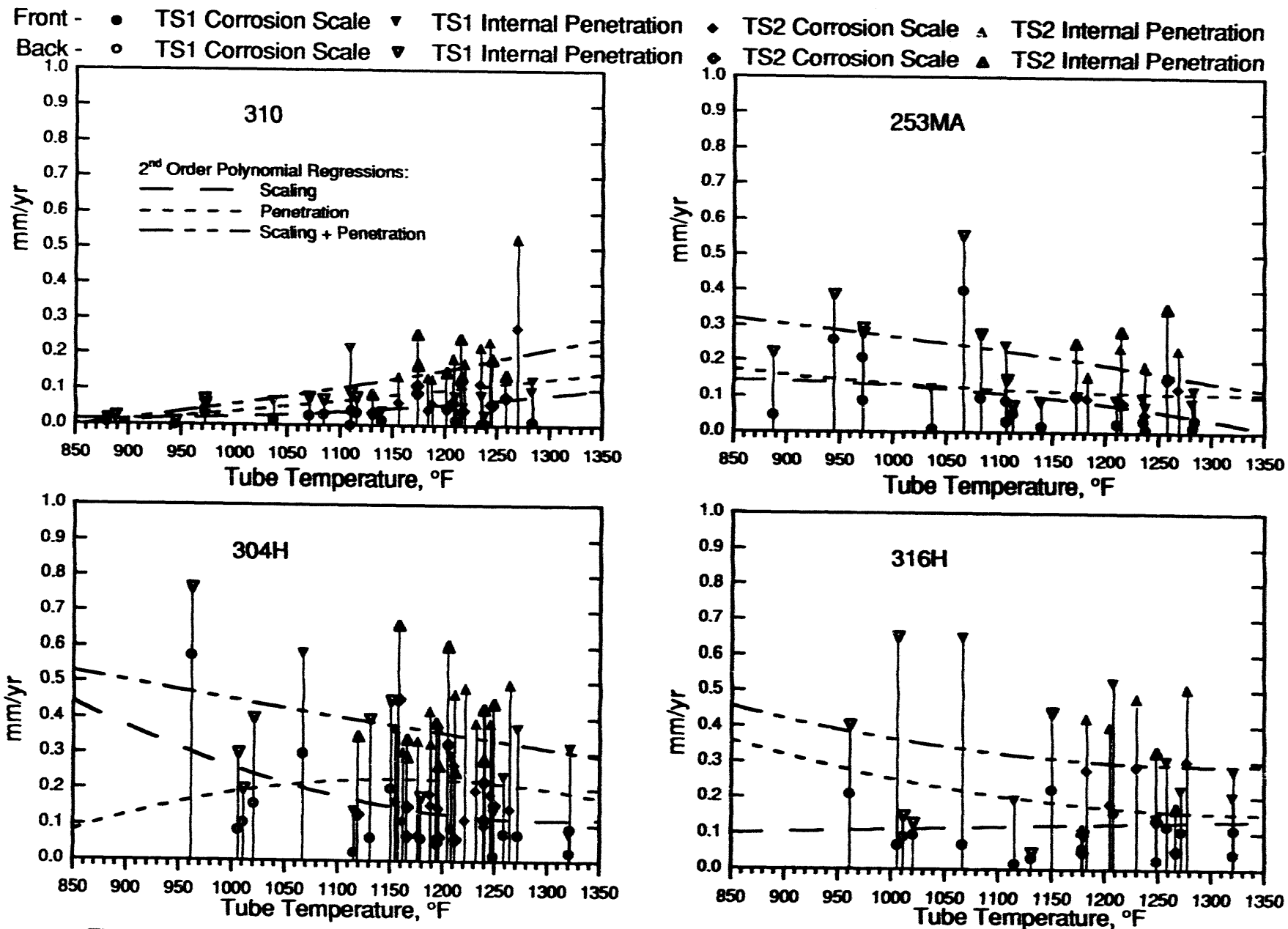

Figure 24a. Parabolic Corrosion Rates of TS1 and TS2 Tube Alloys Exposed for 1500-2000 Hours During LMF4

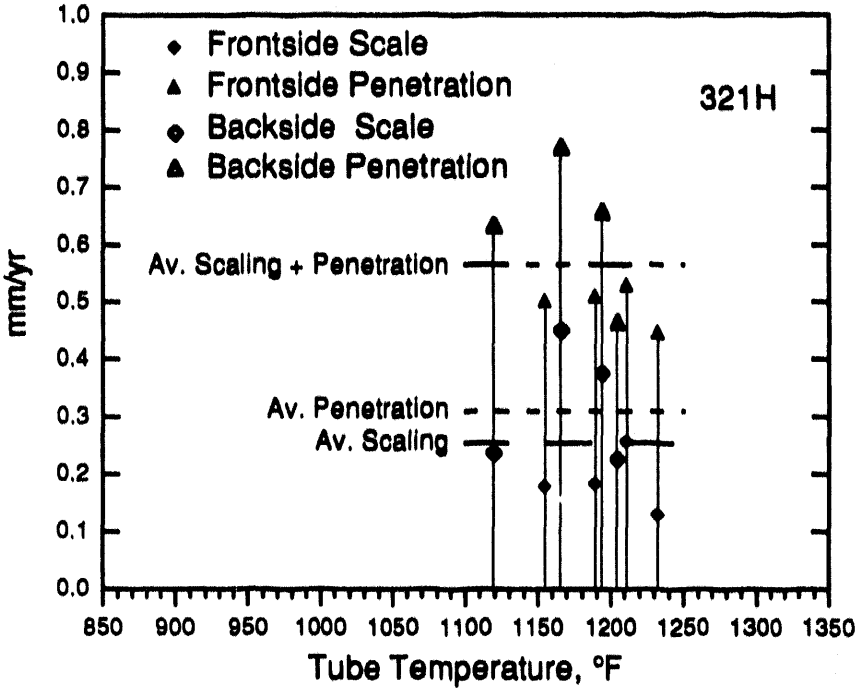

Figure 24b. Parabolic Corrosion Rate of Alloy 321H at TS2 Exposed for 2000 Hours During LMF4.

3. The extent of corrosion with respect to tube temperature for alloy 310 was seen to increase in the manner that would be expected of a strictly diffusion-controlled corrosion process. Data curvefits for alloy 253MA suggested a decreasing trend of corrosion with temperature. As mentioned above, this might be expected of 253MA due to its ability to form a more protective scale at higher temperatures. The curvefits for alloys 304H and 316H also suggested a generally decreasing trend with respect to temperature. If this was indeed the case, the most plausable explanation is that this actually resulted not from temperature effects but from changing deposit characteristics along TS1 tubes in this temperature range. Due to the gas flow pattern at TS1, tube deposits decreased in thickness from the bottom to the top of the first pass, as tube temperature increased. Heavier deposits may have made conditions more reducing at the scale-deposit interface such that the alloys were less able to form protective scales.

4. With respect to the magnitude of corrosion at 1100-1150°F superheater temperatures, all tested alloys except 310 displayed linear scaling plus penetration rates in excess of a 0.5 mm/yr criterion. If corrosion was parabolic with time, then 253MA would also meet the criterion at peak superheater temperatures, but the 18-8 stainless steels would not. At a peak ITAH temperature of 1400°F, it appeared by extrapolation of the data that none of the alloys would meet the 0.5 mm/yr criterion assuming linear kinetics. If corrosion proceeded parabolicly, then alloys 310 and 253MA would meet the criterion, but the 18-8 alloys would probably not.

5. For all alloys, metal loss from scaling and internal penetration were of similar magnitudes, with penetration being slightly greater.

Low Chromium Alloys: scaling kinetic data

Figure 25 shows TS3 corrosion data at the leading edge at the location of maximum tube temperature for each alloy. Only 500 and 2000 hour data are presented, since measurements have not yet been made on the 1500 hour samples. The graph would seem to indicate rather little difference among the alloys with respect to their corrosion performance. Since alloy T22 with 2.25% chromium was indicated to have somewhat more scaling than did SA192, plain carbon steel with no chromium, it was believed that more scale spalling and loss occurred for the SA192 and T11 samples than for T22 or P5, such that the actual amount of corrosion was more than the measurements indicated. None of these alloys had internal penetration.

Low Chromium Alloys: scaling versus metal temperature data

Plots of remaining scale thickness for the carbon steel, T11, T22 and P5 alloys as a function of metal temperature are given in Figure 26, to which the same remarks made above apply. The leading edge scale morphologies of SA192 and T11 indicated significantly more scale spalling and loss than did T22 and P5. The upward trend for T22 with temperature as opposed to the flatter trend or perhaps downward trend at higher temperatures for P5 may signify better scale retention by T22 than by P5. This is commonly found to be the case with these alloys in coal ash corrosion. None of the

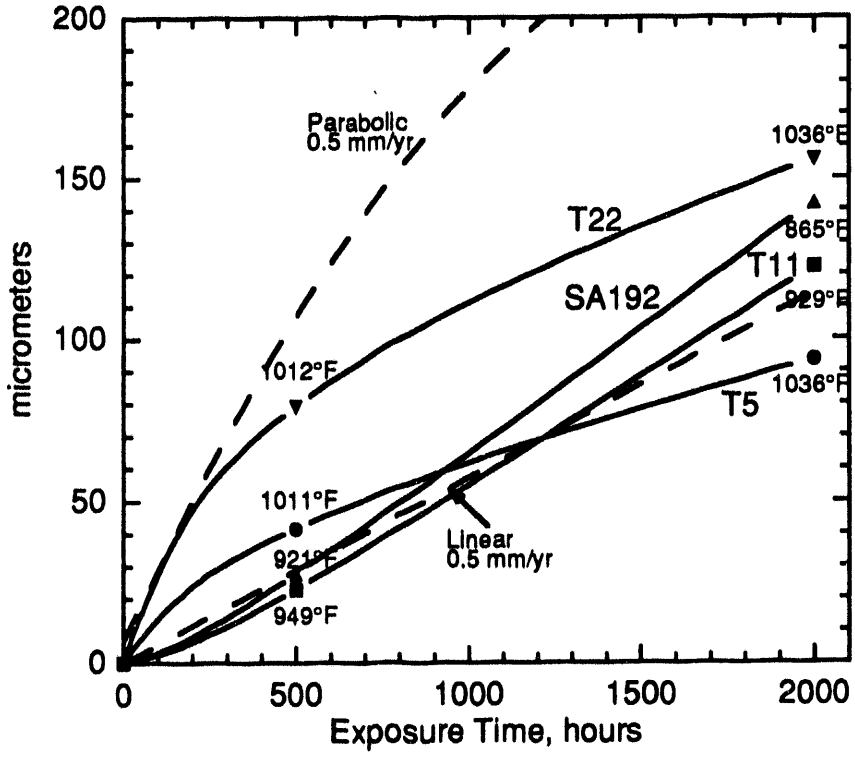

Figure 25. Scale Thickness (Remaining) for TS3 Alloys at the Leading Edge and at the Maximum Average Exposure Temperatures.

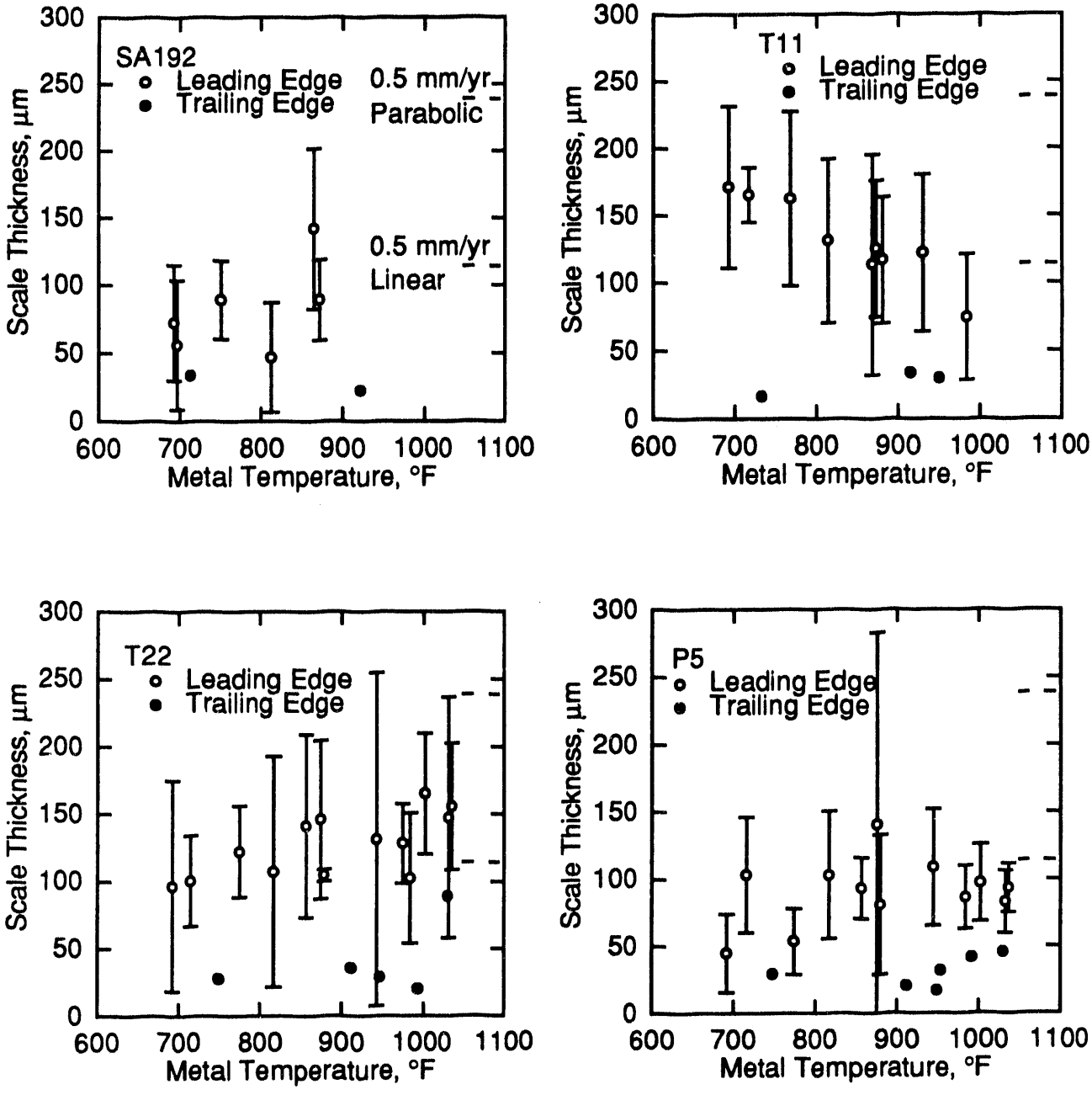

Figure 26. Scale Thickness of Plain Carbon and Low Chromium Steels after 2000 Hours versus Average Metal Temperature.

alloys had leading edge corrosion less than 0.5 mm/yr (for the first year) according to linear kinetics. T22 and P5 were generally within 0.5 mm/yr parabolic. And while the data show SA192 and T11 at the leading edge also below 0.5 mm/yr parabolic, they are suspected of being erroneously low due to spalling. In contrast to the stainless steels in TS1 and TS2, these alloys in TS3 showed distinctly less corrosion at the trailing edge than at the leading edge, being about the same for all alloys and well below a linear 0.5 mm/yr.

Tube Wall Recession Data

For the "B" set of tubes with 1500 accumulated test hours, ultrasonic tube wall thickness measurements were made prior to exposure at the leading edge at 1 foot intervals from the seal plate. Post-test remaining wall measurements were made with the optical microscope at the 1, 3, 5, and 7 foot levels. While the before and after measurement locations were nominally the same, they were not identical. The effect of this is seen in the results, Figure 27a&b, with false indications of increased wall thickness as well as a large amount of data scatter due to different before and after locations. This was particularly true of alloys 310, 253MA, and 316H, all of which were pipe, which has highly variable wall thickness. Less scatter was noted for 304H which was tube. The measured thinning also included metal loss due to scaling at the steam side. Although measurement of the steamside scale thickness was frequently prevented or made questionable by the presence of a burr from cutting, it was often a large fraction of the gas-side scale thickness. Thus, the wall thinning measurements were only a very rough indication of the gas-side corrosion recession. A comparison was also made between remaining wall thicknesses and nominal initial wall for the 2000 hour tubes for which no initial ultrasonic measurements were made. The results are shown for TS1 and TS2 in Figure 28 and for TS3 in Figure 29. Since the nominal initial wall values were generally minimum wall thicknesses, final wall thickesses were mostly greater than nominal initial values.

Corrosion Morphology and Scale Composition

SEM micrographs and x-ray dot maps for Fe, Cr, and S are presented in Figure 30a-h for each alloy. The following observations are made.

1. Oxide scales, with Fe and Cr as the principal cations, were produced on both the austenitic and ferritic alloys, as inferred from the oxidizing atmosphere of the tests and the absence of large amounts of sulfur in the scales. While energy dispersive x-ray dot maps were attempted for oxygen, self-absorption in the sample of characteristic x-rays for oxygen evidently prevented their detection. Some small amount of sulfur was also present, however, at most locations in all of the scales. In some cases, potassium was also present, leading to the suspicion that potassium sulfate from the deposit had been smeared into crevices and depressions in the scale during sample polishing. But where there was no potassium, some sulfur was still generally present. Tiny sulfide precipitates were sometimes observed in the scales as indicated under light microscopy

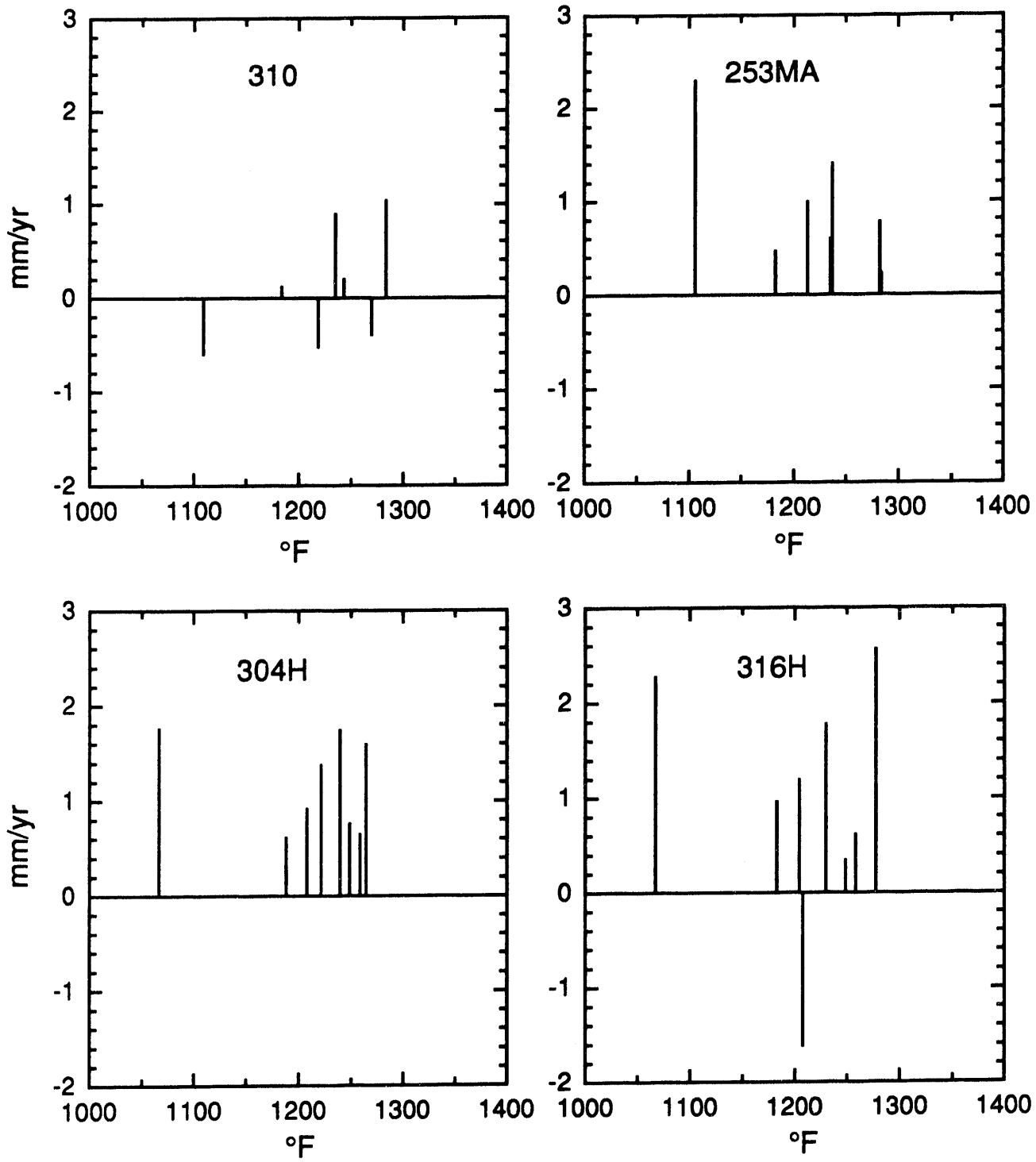

Figure 27a. Linear recession rates of TS1 and TS2 alloys with 1500 hour exposures based on ultrasonic initial wall and microscopic remaining wall and penetration measurements.

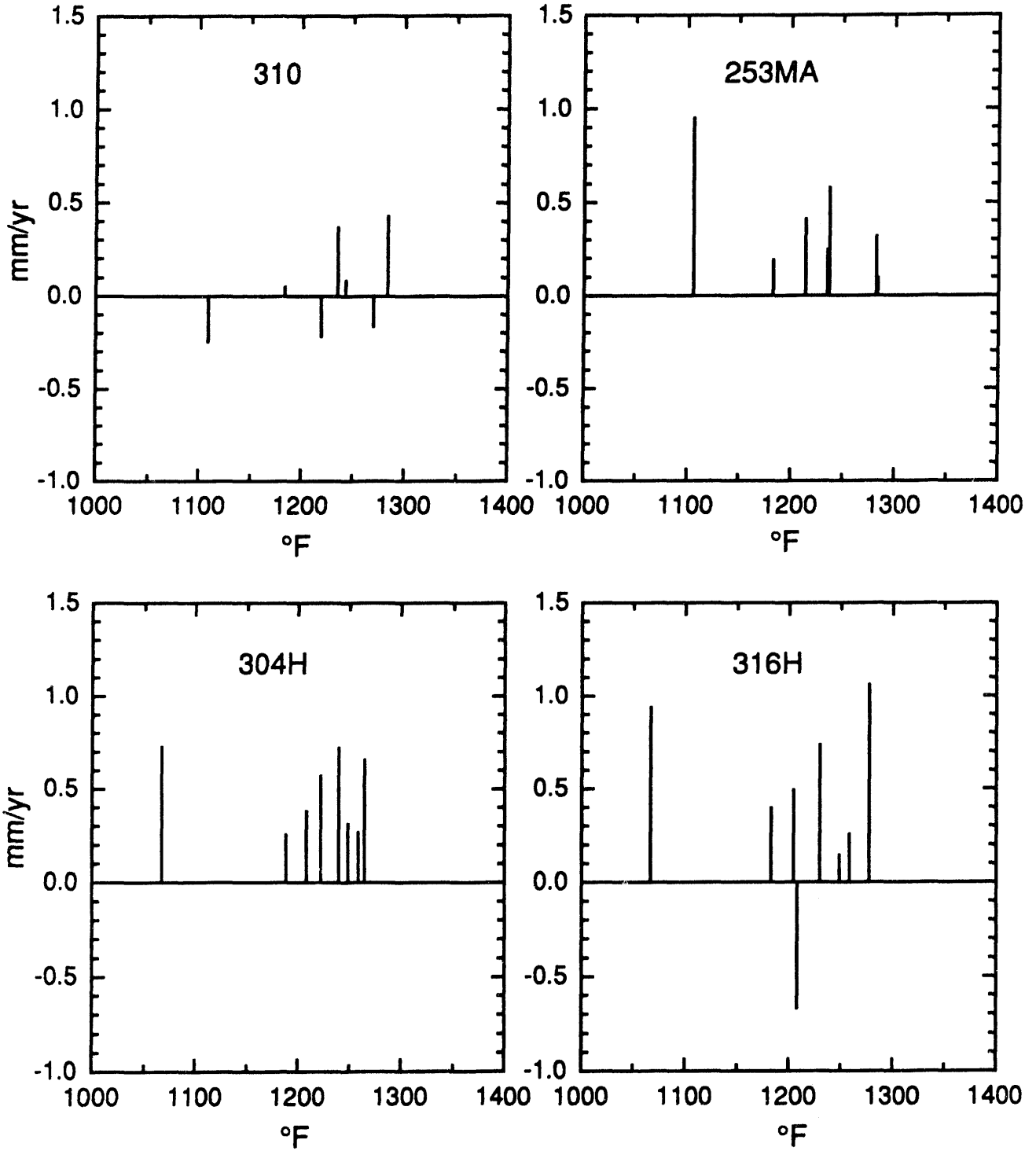

Figure 27b. Parabolic recession rates of TS1 and TS2 alloys with 1500 hour exposures based on ultrasonic initial wall and microscopic remaining wall and penetration measurements.

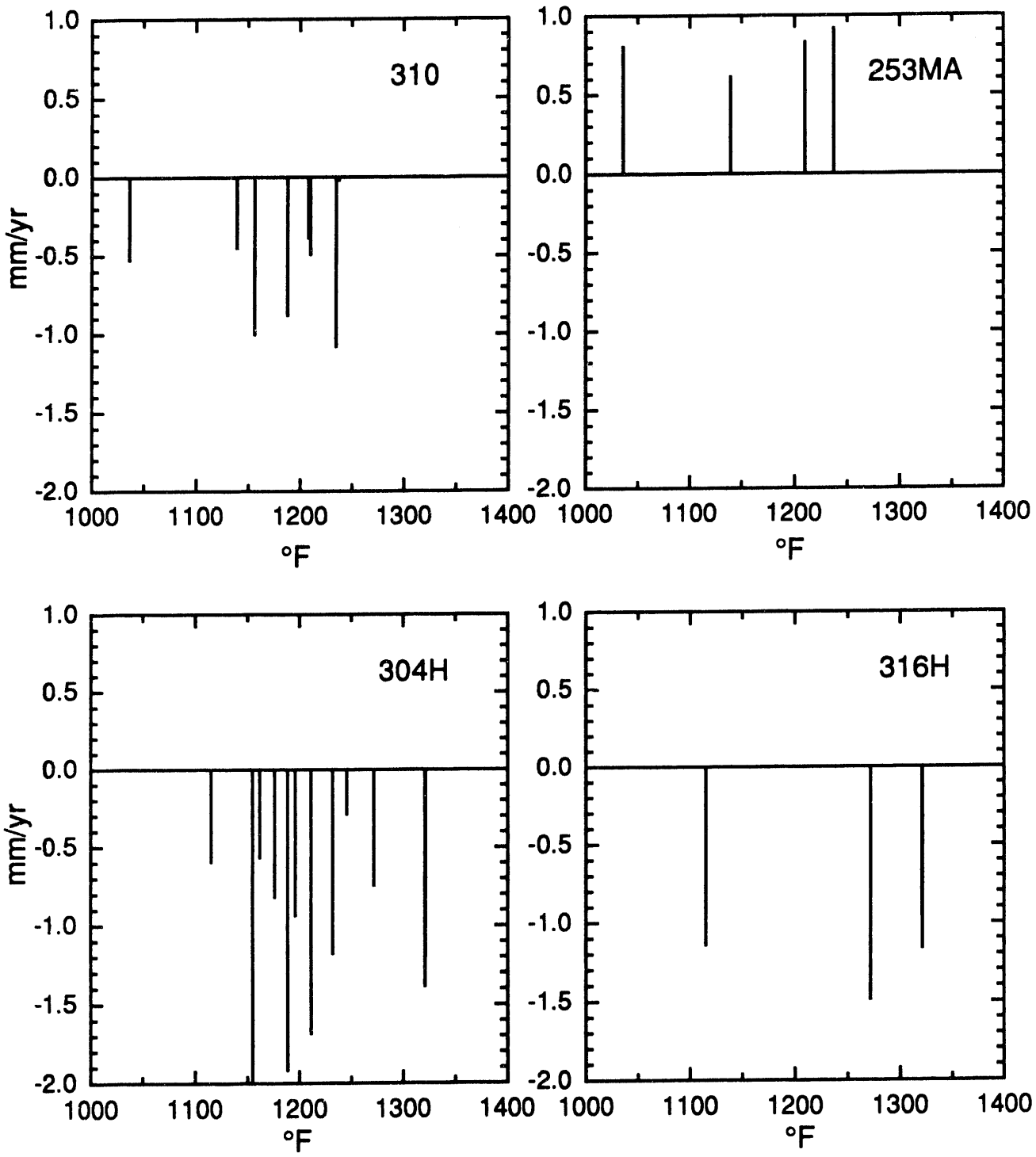

Figure 28. Linear recession rates of TS1 and TS2 alloys with 2000 hour exposures based on nominal initial wall and microscopic remaining wall and penetration measurements.

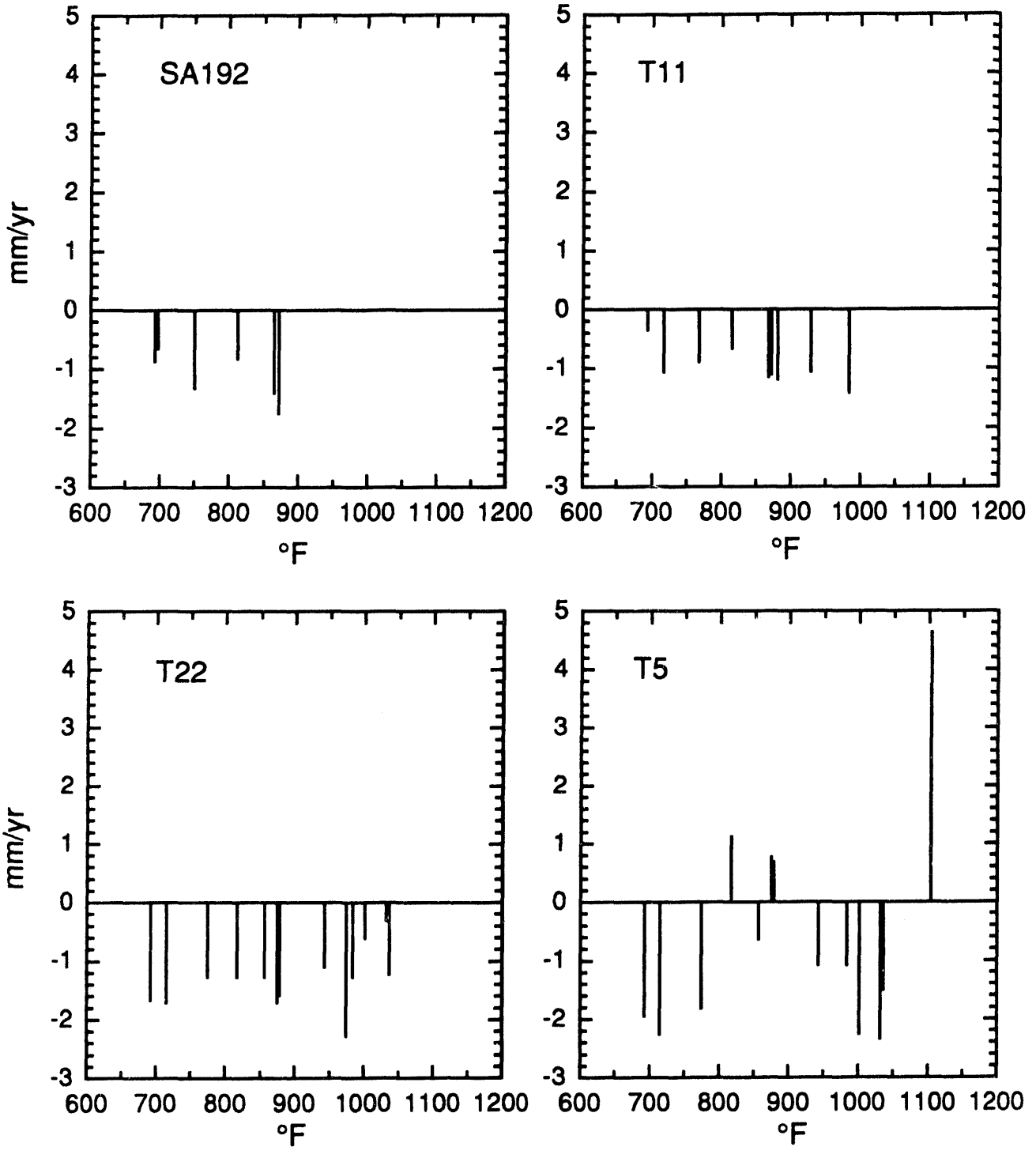

Figure 29. Linear recession rates of TS3 alloys with 2000 hour exposures based on nominal initial wall and microscopic remaining wall and penetration measurements.

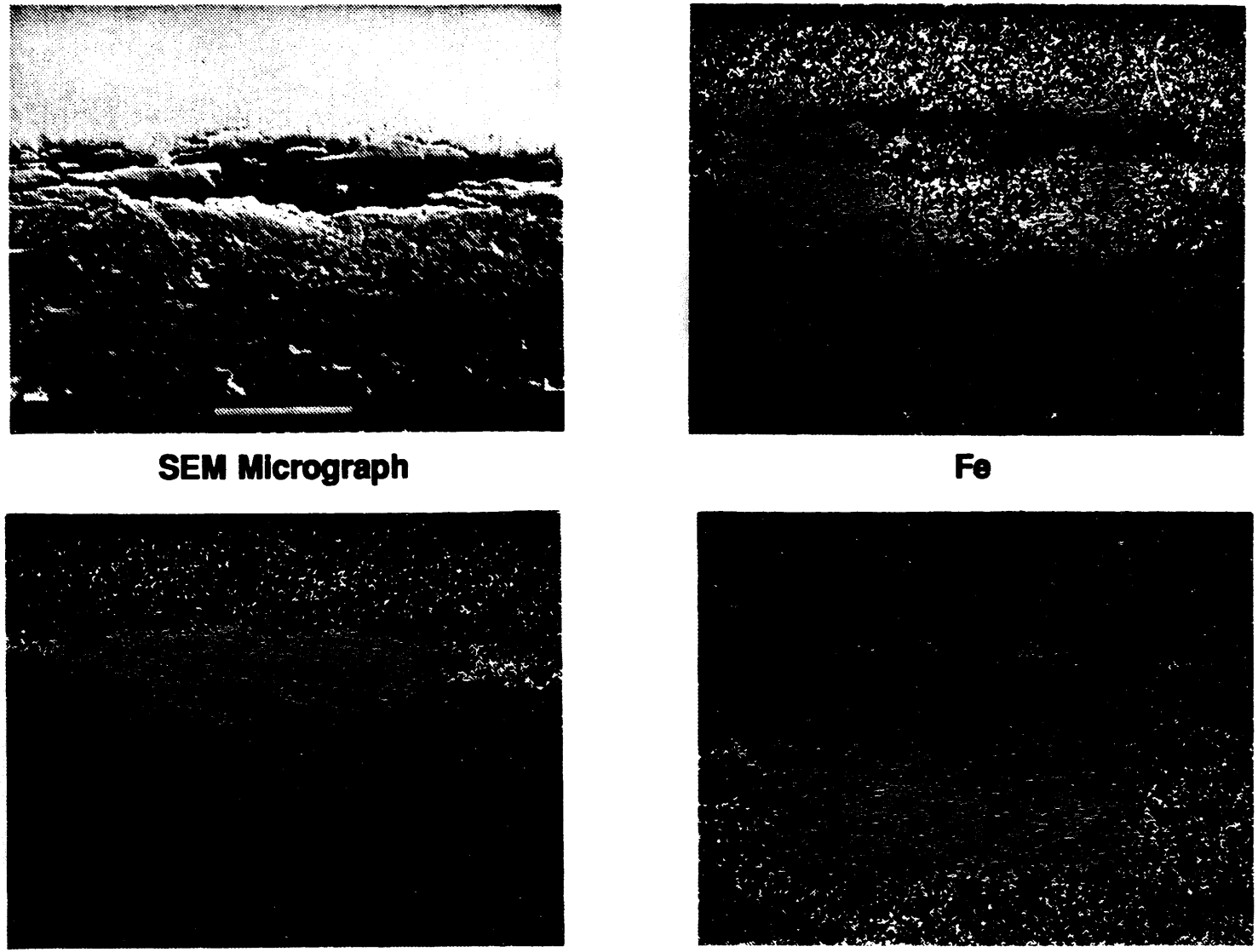

Figure 30a. SEM Micrograph and X-ray Dot Maps for Alloy 310 (TS2-2,P1,1')

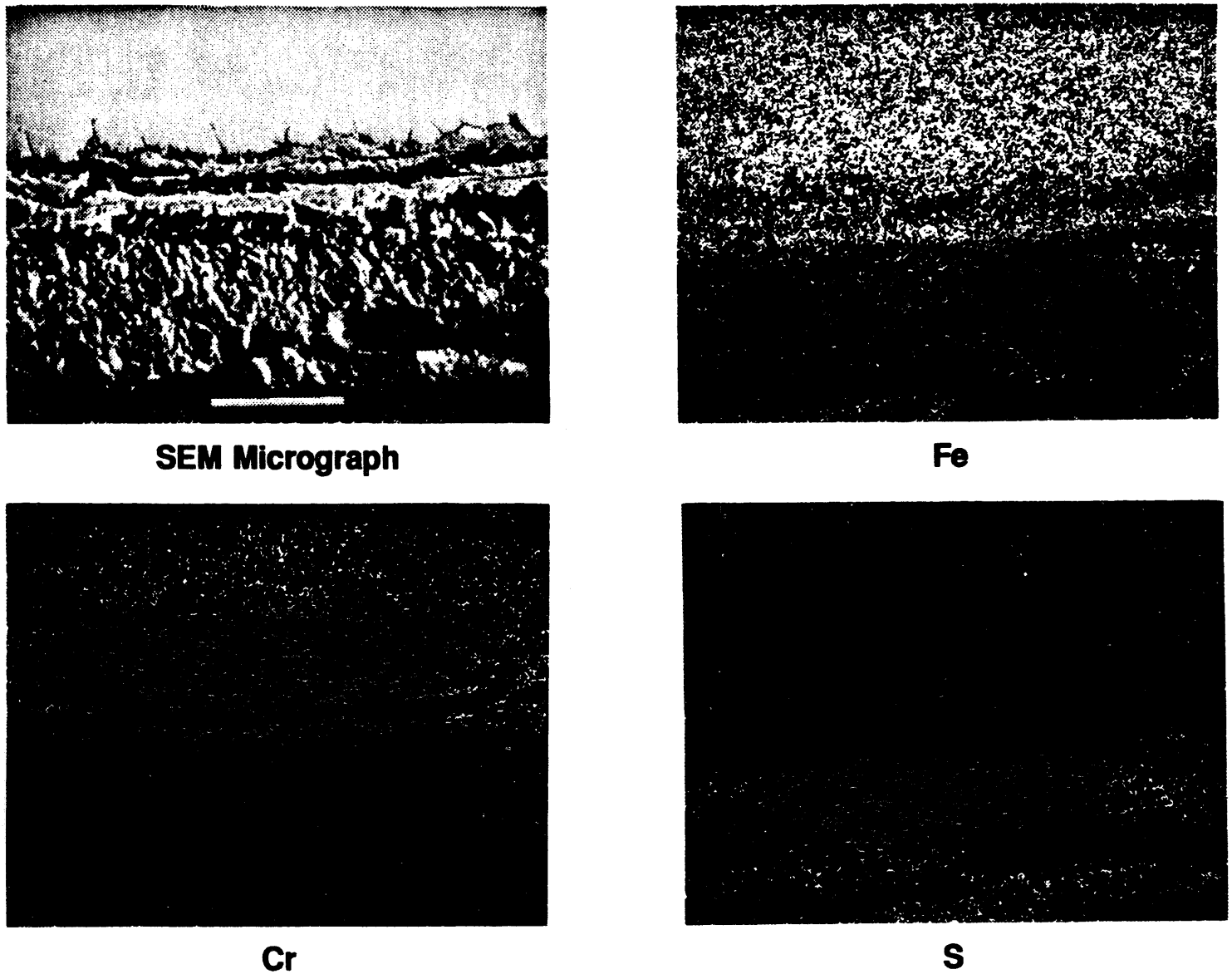

Figure 30b. SEM Micrograph and X-ray Dot Maps for Alloy 253MA (TS1-8,P1,1')

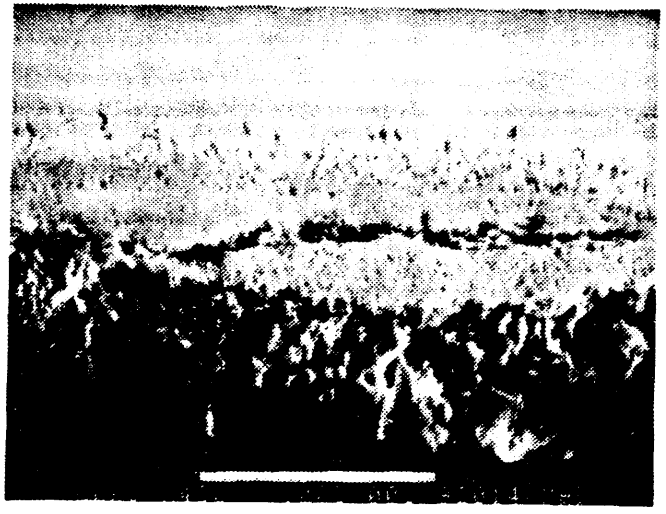

SEM Micrograph

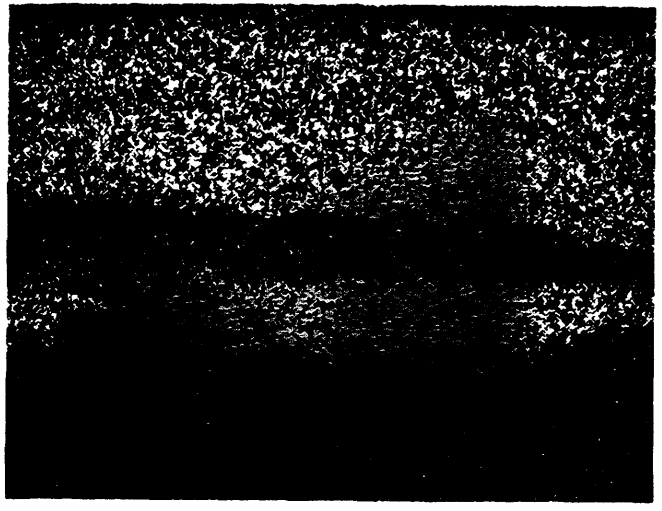

Fe

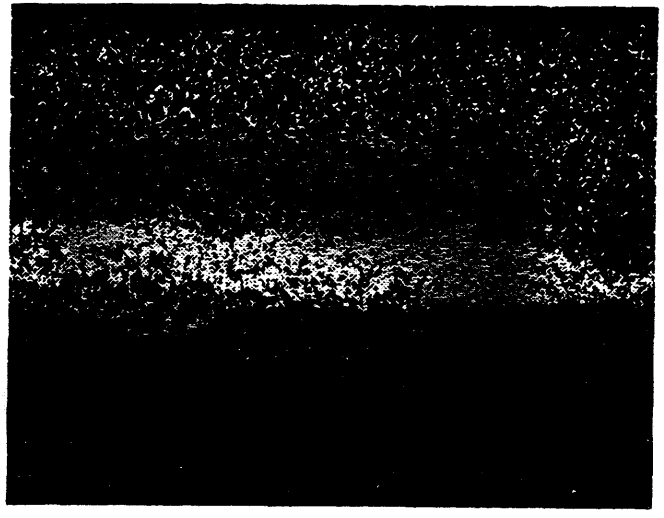

Cr

S

Figure 30c. SEM Micrograph and X-ray Dot Maps for Alloy 304H (TS1-4,P1,1')

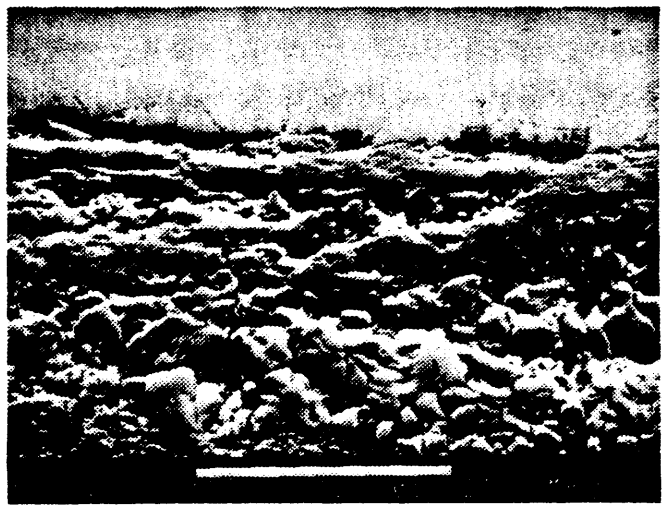

SEM Micrograph

Fe

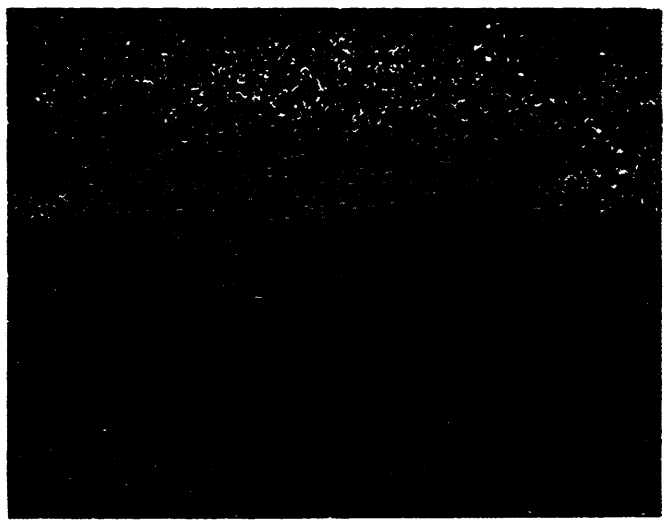

Cr

S

Figure 30d. SEM Micrograph and X-ray Dot Maps for Alloy 316H (TS1-5,P1,1')

SEM Micrograph

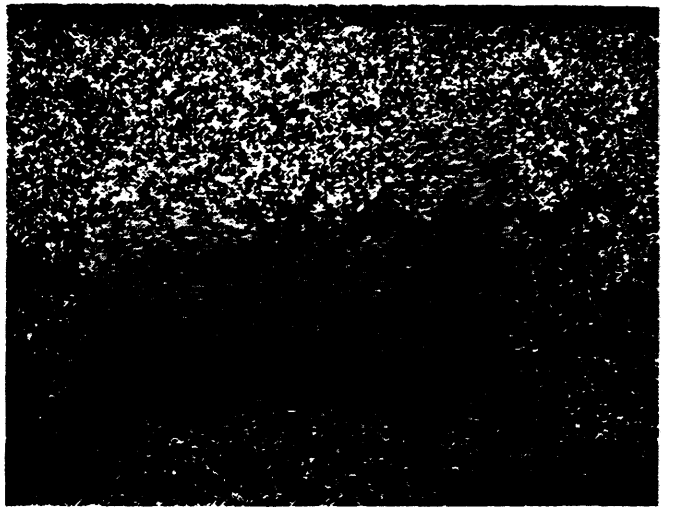

Fe

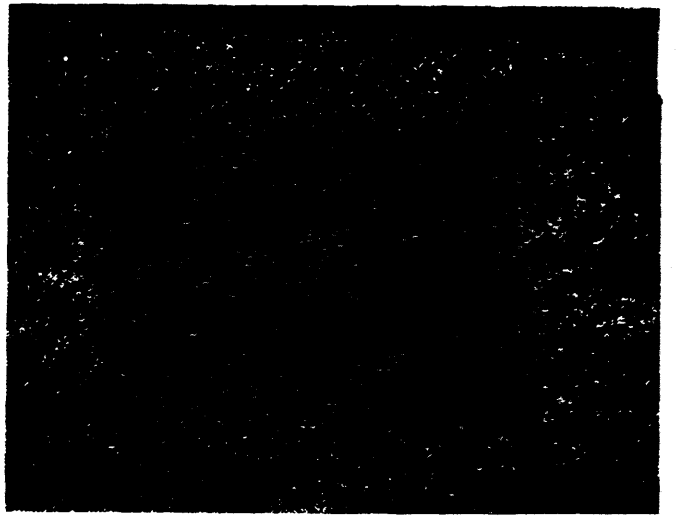

Cr

S

Figure 30e. SEM Micrograph and X-ray Dot Maps for Alloy 321H (TS2-1,P1,1')

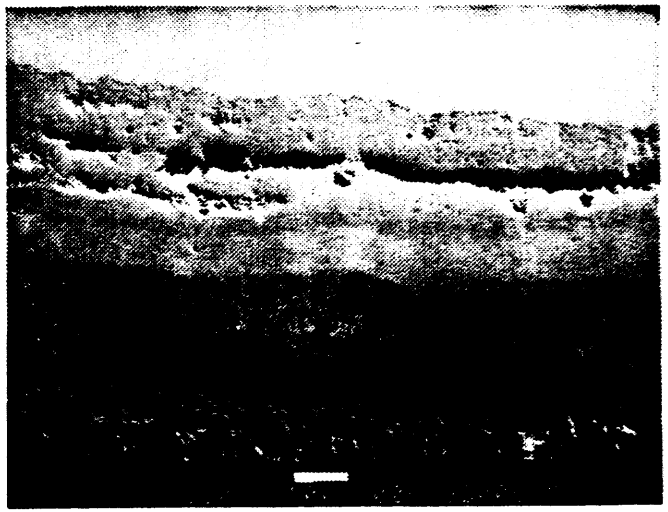

SEM Micrograph

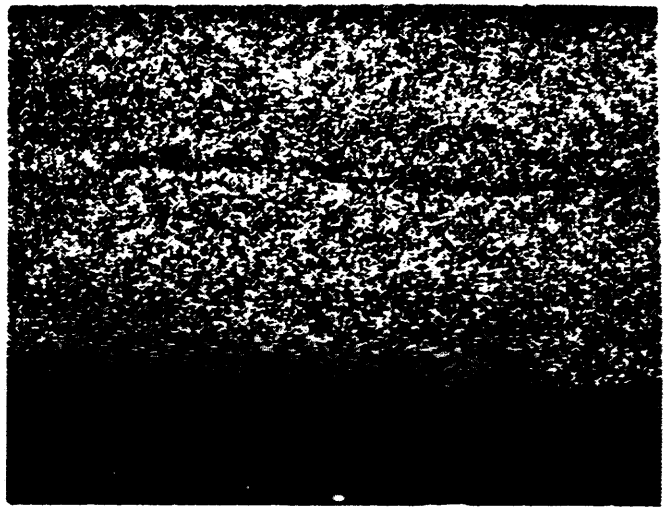

Fe

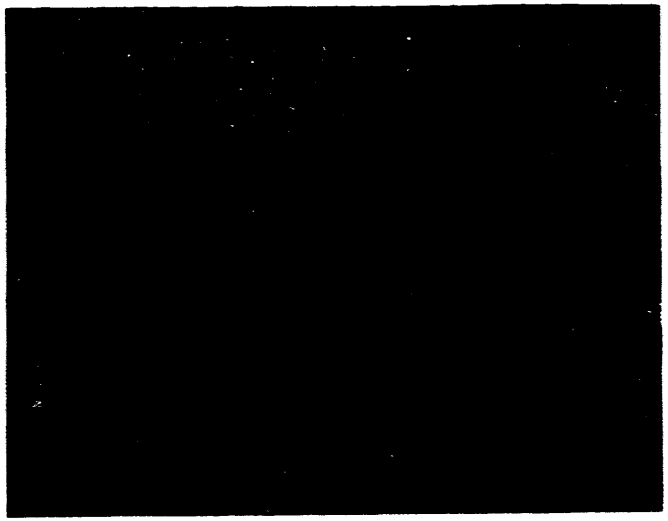

Cr

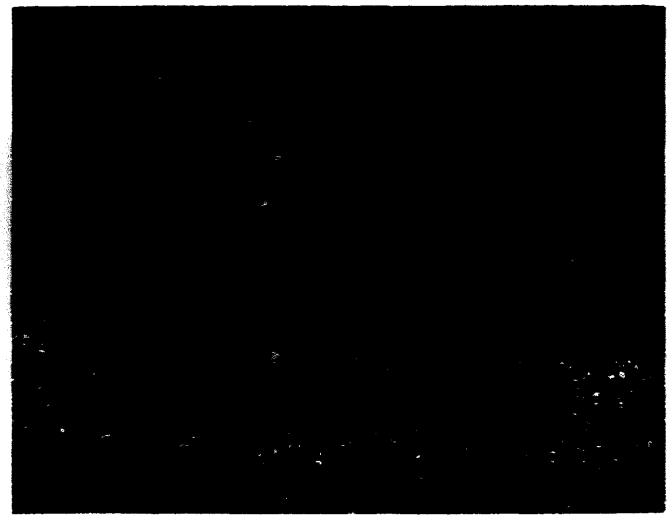

S

Figure 30f. SEM Micrograph and X-ray Dot Maps for Alloy P5 (TS2-8,P2,7')

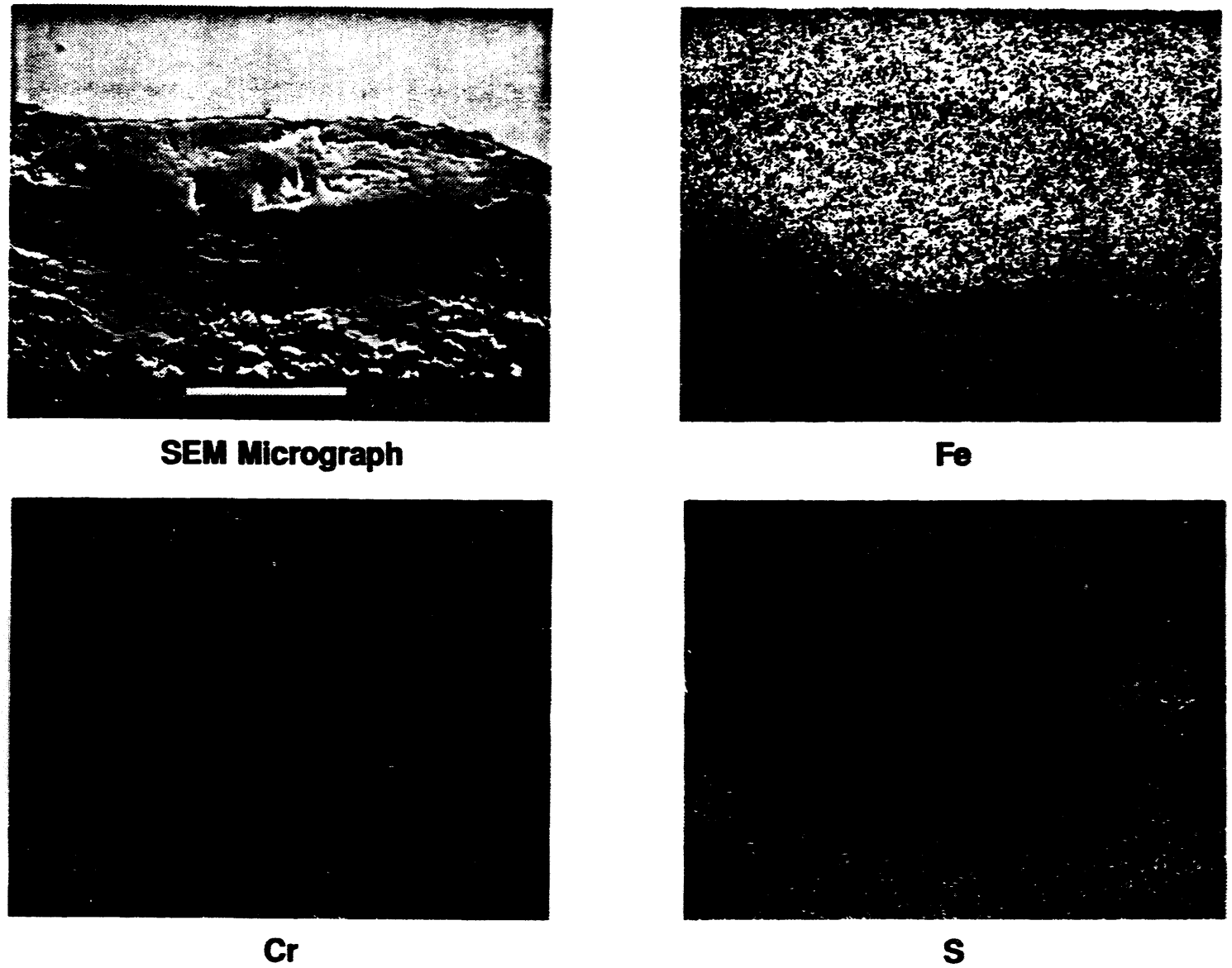

Figure 30g. SEM Micrograph and X-ray Dot Maps for Alloy T22 (TS2-1,P2,4')

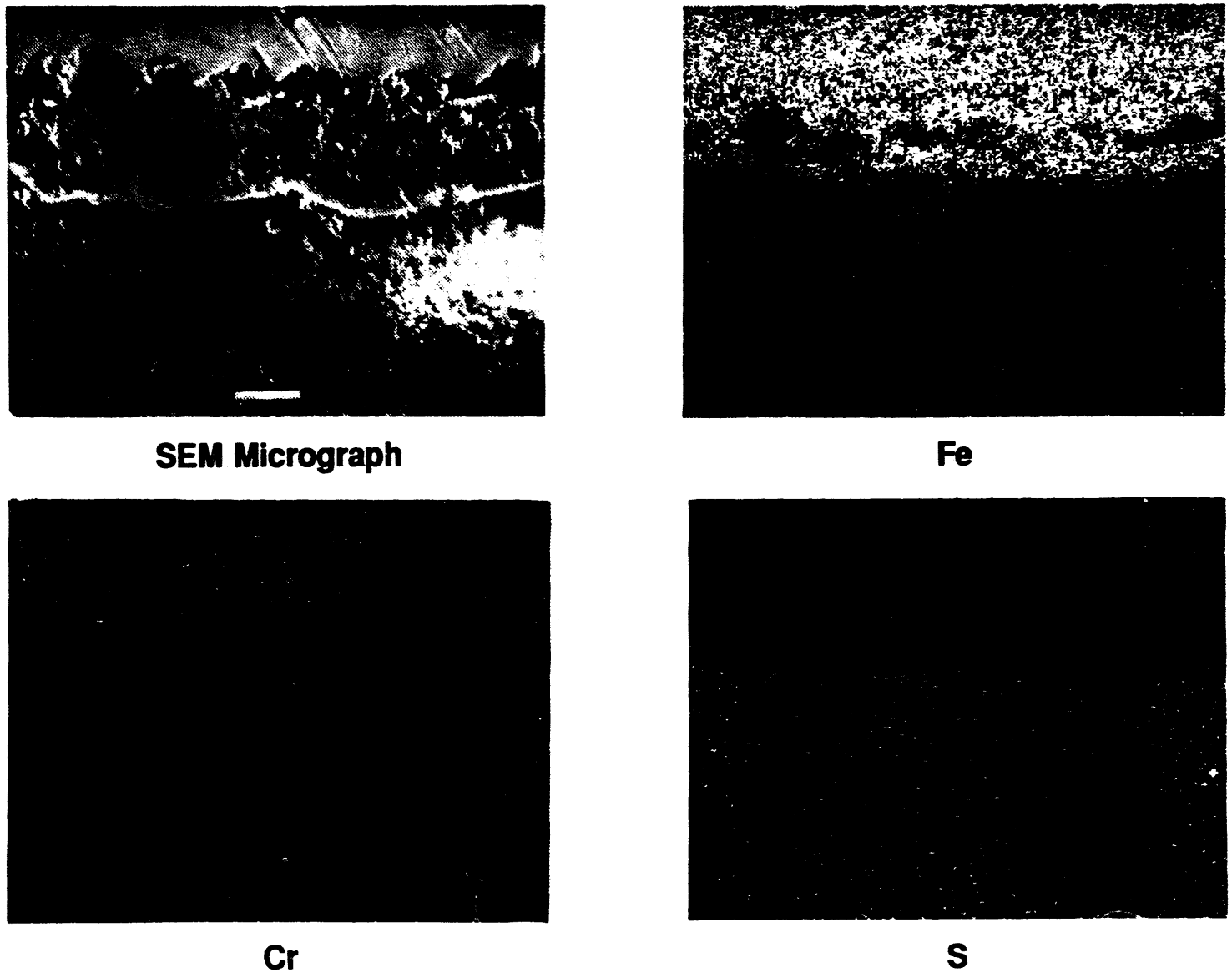

Figure 30h. SEM Micrograph and X-ray Dot Maps for Alloy T11 (TS3-2,P2,7')

by their characteristic high reflectivity. No attempt was made to quantify the scale compositions. Nor was there any identification of scale phases.

2. No differences were found in the corrosion morphologies or scale compositions with respect to gas temperature. That is, TS1 and TS2 appeared to be the same, and TS2 and TS3 appeared to be the same, for the cases where an alloy was present in both banks.

3. Scales generally exibited much spalling and fracturing. This often resulted in voids between scale layers, as in Figure 30b, or in areas where part or all of the scale was missing, as in Figure 30a. None of the alloys demonstrated any noticable superiority with regard to scale retention or resistance to fracturing.

4. Scales were quite non-uniform in thickness, on a microscopic level, aside from spalling. Alloy 310 and 253MA scale thicknesses were particularly variable, and at the lower metal temperatures showed indications of an early stage of oxidation prior to spreading of scale from nucleated sites over the entire surface.

5. Binary scale layers (i.e. Type B scales) were sometimes present for the 18-8 stainless steels with higher chromium content in the inner layer than in the outer layer, as seen for 304H in Figure 30c. This was often not the case, however, there either being only one layer or else two or more separated layers of the same composition. The absence of an outer low chromium layer in such cases was believed to be often attributable to spalling and loss of the outer layer rather than the existance of a single Type A scale.

6. Fine oxide precipitates which appeared to be of about the same composition as the scale were often found distributed in the K_2SO_4 deposit near to the scale, as seen in Figure 30a and in the optical micrograph Figure 31. Where these precipitates were present, the outer surface of the scale was very iregular and the outer region of the scale was discontinuous, consisting of islands and peninsulas of scale surrounded by deposit. This gave the appearance of the scale's outer surface having been dissolved in the deposit and reprecipitated. Whether or not these precipitates were formerly part of the scale, they represented in some cases a significant amount of metal loss. When the precipitates were at the polished plane, they had the same light grey appearance as polished scale oxide. In locations with a high fraction of precipitate, if the area was recessed below the polished plane due to crumbling of the brittle deposit, the color was dark grey with granular speckles, the same appearance as scale oxide recessed below the polished plane. This resulted in frequent difficulty in performing corrosion thickness measurements due to inability to visually distinguish between recessed areas which were all scale and areas which were precipitated scale in deposit. This behavior was true of all the alloys in all of the test sections.

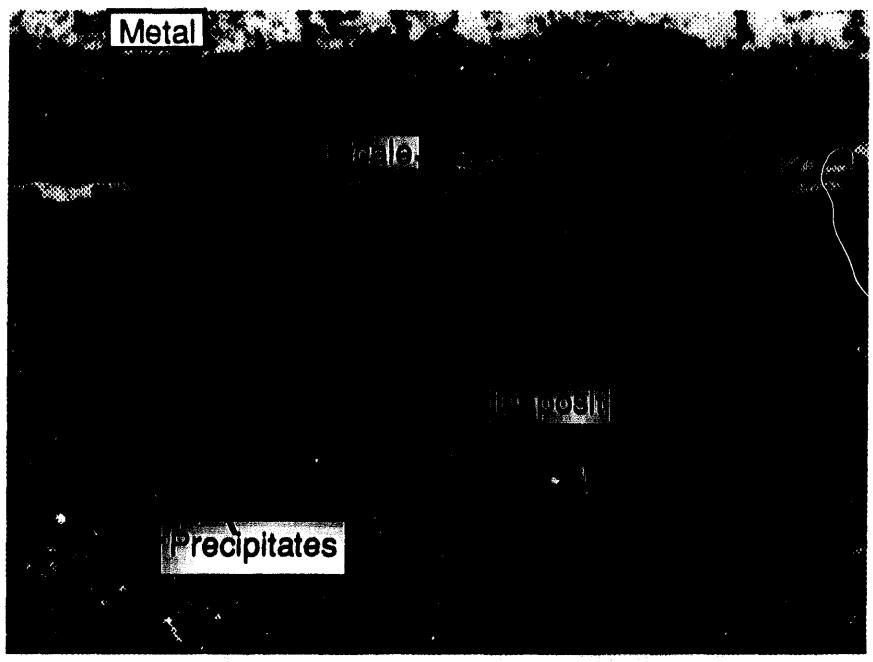

Figure 31. Optical Micrograph Showing Iron Oxide Reprecipitation in Deposit

7. Another morphological feature resulting from diffusion of tube metal elements into the deposit was a zone of deposit adjacent to the scale having a high iron content as determined by EDS and characterized by a red color under polarized light microscopy. No chromium was detectable in these deposit regions. The oxide precipitates described above were generally, but not always, surrounded by the red, high-iron deposit. However, precipitates were not always present in the red deposits.

8. In polished corrosion samples, a gap was commonly present either between the scale and the deposit, or within the deposit a short distance (up to a few hundred micrometers) from the scale. Where the gap existed between the scale and deposit, it was often apparent that some or all of the scale had also spalled. The prevalence of this gap and its location led to speculation that the deposit in this region was embrittled either by high iron content or by the presence of oxide precipitates, or both.

9. Internal penetration of the austenitic alloys occurred at most locations and temperatures. This occurred as intergranular or transgranular oxidation, or both. As with scaling, resistance to internal penetration in these alloys increased with chromium content. Transgranular oxidation was generally limited to surface metal grains, and for some grains, had proceeded until those grains were totally converted to oxide. Intergranular penetration, on the other hand, often extended several grain diameters from the surface. Thus, metal recession occurred partially by inward diffusion of oxygen through the scale and into the metal. This type of behavior occurs when scales are not very protective, either due to a high concentration of lattice defects such as cation vacancies, to a large compositional range such as with spinel oxide, or to physical defects such as cracks or voids. No difference could be seen from EDS spectra between the composition of intergranular oxide and the scale adjacent to the metal surface. A small amount of sulfur, generally just above the EDS detection limit, was present in the subsurface metal, as in the scales, and was suspected of playing a major role in reducing the protectiveness of scales and increasing the extent of internal penetration. There was no internal penetration of any of the ferritic alloys.

DISCUSSION

Most of the characteristics of MHD superheater/ITAH corrosion correspond to those of high temperature coal ash corrosion in the presence of liquid alkali iron trisulfates (AIT). Among these are the presence of the normal alkali sulfate, K_2SO_4 in the MHD case, in the tube deposit; increasing concentration of the normal alkali sulfate through the deposit toward the tube surface, at which there is a high sulfur partial pressure; initial formation of a thin, passive chromia scale on stainless steels; modification of the chromia scale and loss of passivity by one or a combination of mechanisms including dissolution, electrochemical dissolution arising from adjacent surface areas of differing reactivity, and diffusion of sulfur into the oxide to form a less protective oxide/sulfide scale; increased outward migration of iron and chromium through the scale to form a thicker, layered and

still less protective scale; increased inward migration of oxygen and sulfur through the scale resulting in subsurface oxidation and sulfidation and intergranular penetration; outward diffusion of iron into the sulfate salt to form iron sulfate; saturation of iron sulfate in the near tube deposit and reprecipitation of iron as Fe_2O_3 some distance from the tube in regions of high oxygen activity; and improved corrosion resistance with increasing alloy (or alloy coating) chromium content. For conventional coal ash corrosion, these features and mechanisms are described in articles by numerous researchers including Rapp [11], Hendry and Lees [12], and Lai [13]. Major differences include liquid AIT at temperatures of 1100-1400°F in the case of conventional coal ash corrosion and its general absence in the MHD case as a result of low SO_2; much lower MHD corrosion rates under otherwise similar conditions; and lack in the MHD case of the bell shaped relationship with temperature arising from the stability range for molten AIT. The similarities suggest the corrosion process to be basically the same whether the salt is liquid or solid, only the transport and reaction rates being different.

Figure 32 shows conventional coal ash corrosion rates of a number of alloys including 304H and 310S in a synthetic coal ash containing 34% Na_2SO_4, 41% K_2SO_4, and 25% Fe_2O_3 [14]. The total alkali content is about the same as in CFFF tube deposits. At 1300°F, the corrosion rate of 304H was near 17 mm/yr on a linear basis as compared to around 1 mm/yr for MHD in the present study. Alloy 310's corrosion in the conventional case was about 14 mm/yr compared to about 0.2 mm/yr for MHD. In similar simulated coal ash corrosion testing by Nakagawa[15], very similar results were obtained (Figure 33). Alloy 316 had a corrosion rate of 19 mm/yr and alloy 310 a rate of 12 mm/yr.

Comparison of MHD superheater/ITAH corrosion to corrosion of steam heaters in actual PC-fired boilers is difficult in that it is difficult to know to what PC boiler condition to compare. Most superheater tubes experience negligible or acceptably low corrosion because they operate at temperatures or with ash compositions that do not produce AIT or other complex alkali trisulfates. On the other hand, corrosion as high as 6 mm/yr has been observed on 18-8 stainless steel tubes near the outlet end of radiant superheaters or reheaters[16]. Table 7 gives data gathered from corrosion probes tested in power boilers in the U.S. and the U.K., all of which were burning corrosive coals[17]. Maximum measured corrosion of 347 stainless steel ranged from 0.3 to 0.6 mm/yr. This is compared to alloy 316H in the present study with maximum observed linear rates of scaling + penetration at near 1100°F of about 1.9 mm/yr. Maximum measured corrosion of alloy 310 in the conventional plants ranged from 0.1 to 1.1 mm/yr compared to about 0.6 mm/yr at the CFFF. Data[18] from probe tests in Philadelphia Electric's Eddystone Unit 1 are shown in Table 8. The loss rate from an 8000 hour exposure of 347H at near 1100°F was 0.06 mm/yr according to thickness loss measurements and 0.01 mm/yr from weight loss measurements. Considering that CFFF exposure conditions were highly fluctuating, including many large thermal cycles, compared to typical power boiler operation, the corrosion experienced would be expected to be more severe than in actual MHD plant service. Laboratory probe tests by Natesan[5] under constant simulated MHD final

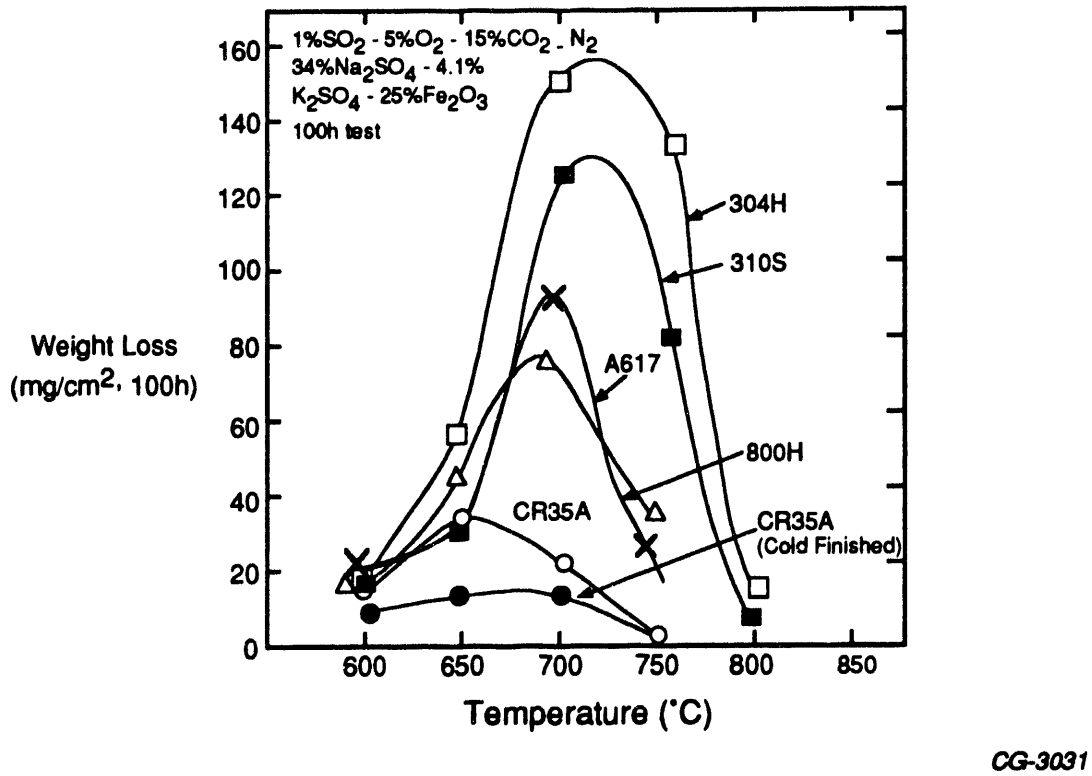

Figure 32. Conventional Synthetic Coal-Ash Corrosion

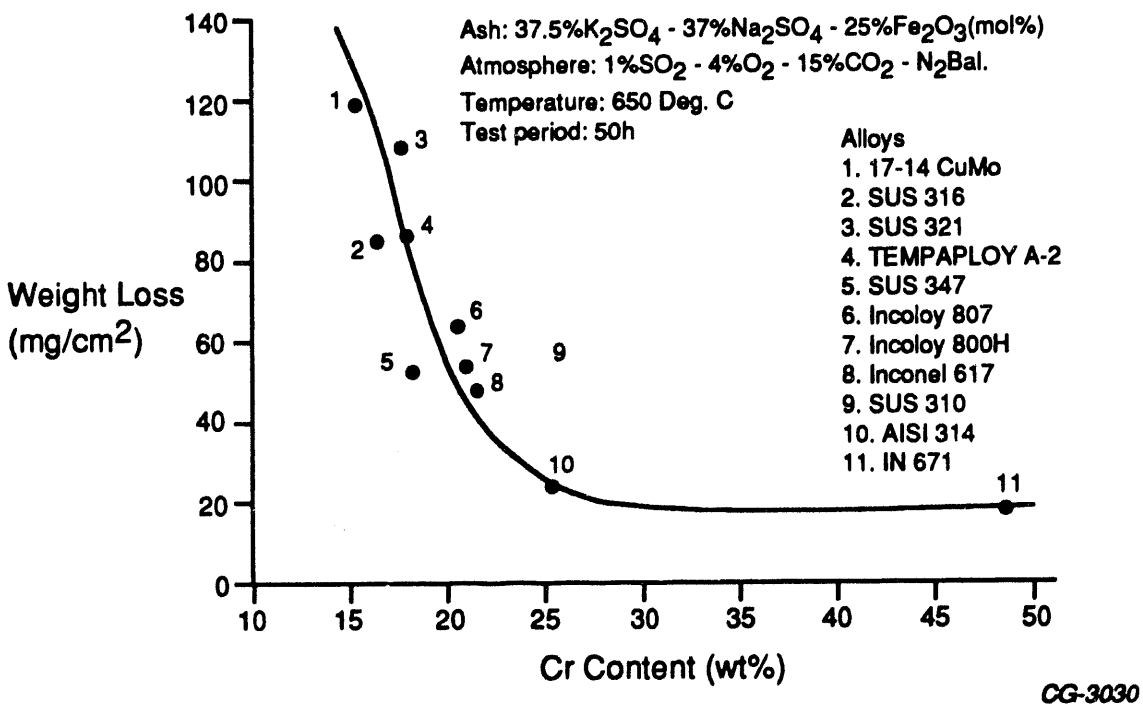

Figure 33. Effect of Chromium Content in Alloys on Conventional Synthetic Coal-Ash

Table 7. Conventional Coal Ash Corrosion Data from Various Superheater Probes [16]

Materials	Maximum Metal Loss, μm			
	Gallatin TVA 4000h	Crist Gulf Power 4000 h	Baldwin Illinois Power 3700h	Drax NP 2000h
T91	-	-	575* (HCM12)	300 (600) **
E1250	-	-	350 *	200 (200) **
17-14Cu-Mo	250 (600) **	825 *	-	-
347	100 (150) **	225 *	250 *	-
Alloy 800	100 (275) **	125 *	325 *	-
T310	50	50 *	125 (HR3C)	10 (250) **
T91 Chromised	75	50 (650) **	50-200	20 (250) **
Cr30A	50	50	75	10 (200) **
Cr35A	-	-	-	10 (10) **
In671	-	-	-	10

* includes pitting ** figure within parentheses is maximum pit depth

Table 8. Corrosion Probe Data from Philadelphia Electric's Eddystone Unit 1 [18]

Sample Position on Probe		Weight Loss , mg/cm^2		
	Material	4000 Hr. Probe	8000 Hr. Probe	Temp, °F
1	T-91	13.98	46.05	
2	T-91 Cr	3.37	19.80	
3	T-91 Cr+V	26.20	43.87	
4	347ss	7.93	9.25	
5	HR3C	5.76	5.64	890-950
6	Incoloy 800H	5.46	6.77	
7	Temp CR30A	2.46	4.63	
8	T-91 Cr+V	43.62	43.94	
9	347ss	9.82	10.83	1020-1120
10	HCM 12	56.49	47.10	
11	347ss Cr	2.81	5.84	
12	Incoloy 800H	3.44	6.82	
13	Inconel 617	0.97	2.55	
14	Esshete	8.81	10.23	1175-1180
15	T-91 Cr	-	-	
16	T-91 Cr+V	-	-	
17	347 ss	-	-	
18	FW 4C	6.32	7.14	
19	Incoloy 800H	-	-	1280-1310
20	T-91 MgZrO	47.98	100.09	
21	Temp CR30A	-	-	

superheater outlet conditions (1100°F metal temperature) showed alloy 304H to have a linear metal recession rate of about 0.04 mm/yr. Actual MHD plant conditions should be somewhere between the CFFF and lab test extremes, with the result that MHD superheater corrosion and corrosion in conventional superheaters delivering 1000°F steam are probably quite similar.

None of the tested alloys, with chromium contents to 25%, appeared to have sufficient corrosion resistance to meet a linear 0.5 mm/yr loss criterion for ITAH service at 1400°F, and it is doubtful that parabolic kinetics would be maintained in long term service, particularly in regard to localized pitting attack. Therefore, there is an indicated need for corrosion testing of alloys which might be expected to have superior performance, either owing to higher chromium content, or formation of alumina or silica scales, or better scale adhesion. Conventional coal ash corrosion testing has identified alloys with superior performance, and their relative performance would be expected to be much the same for MHD. Highest resistance would be expected of a 50Cr-50Ni alloy, which would be used as a clad over a less costly and stronger alloy. Superior resistance has also been shown by a Japanese 35% Cr alloy termed CR35A, which may be used either as a monolithic tube or as a cladding. Since alloy 310 has insufficient high temperature strength to be used in monolithic form and since bimetal tubes are more expensive, a modified alloy 310, termed HR3C, has been developed by Sumitomo with much superior strength and comparable if not slightly better corrosion resistance. These and a variety of other promising candidate alloys are presently in test in the CFFF LMF5 test series utilizing Montana Rosebud coal.

The large amount of uncertainty introduced by unknown amounts of scale loss point out the need for corrosion measurements based on the change in wall thickness rather than on remaining scale thickness. The approach to future tube corrosion evaluations will be to make pre-exposure ultrasonic wall thickness measurements at precisely defined locations and post-exposure remaining wall thickness, penetration, and steam-side scale thickness measurements from polished sections at the same locations. Gas-side scale thickness may be used as a secondary measurement. Scale, subsurface, and deposit examinations would be make as well from the polished sections.

SUMMARY AND CONCLUSIONS

Austenitic stainless steels, low and medium chromium steels, and carbon steel were tested as tubes for steam and intermediate temperature air heating in MHD power plants. Testing was conducted in a 20 MW_t facility with the firing of high sulfur Illinois #6 coal seeded with potassium carbonate. Tubes were located in three gas temperature zones and with tube metal temperatures ranging from 700°F to 1400°F. Corrosion occurred beneath deposits containing 75% or more K_2SO_4. Test exposures consisted of twelve different test runs over a period of three years. Tube samples were taken for evaluation at 500, 1500, and 2000 hour intervals. These evaluations included

measurement of scale thickness and depth of internal penetration, comparison of remaining wall thickness with initial ultrasonic thickness measurements, and examination of scale, penetration, and deposit morphologies by means of optical and scanning electron microscopy and by energy dispersive x-ray spectroscopy. The following conclusions were made from the evaluations:

1. **Corrosion resulted from solid state interaction of tube metals and their scales with K_2SO_4 in the deposits.**

2. **Complex alkali trisulfates such as $K_2Fe(SO_4)_3$, responsible for potentially severe conventional coal ash corrosion, have been detected on rare instances in trace amounts in MHD tube deposits, but are not normally present, probably as a result of low SO_2 and SO_3 concentrations in the flue gas.**

3. **Many of the corrosion characteristics were similar to those occurring in liquid phase coal ash corrosion. These included having the same corrosion precursor (K_2SO_4), the same type of scales, and the same migration of iron into the deposit to produce $FeSO_4$, and precipitation of iron oxide near the outer boundary of the $FeSO_4$ as a result of decreasing sulfur partial pressure and increasing oxygen partial pressure.**

4. **Corrosion resulted in oxide scales containing sulfur either in solution or as discrete sulfides. Sulfur penetration of the scale resulted in enhanced outward metal ion migration and production of Cr-Fe scales often having multiple layers. Much separation of these scale layers and scale fracturing occurred, augmented by the relative large number and intensity of thermal cycling which occurred. $FeSO_4$ between the scale and the deposit appeared to be a brittle phase prone to spalling and to contributing to scale spalling. This scale damage resulted in further corrosion, and this process would eventually reach a break-away stage wherein scales could no longer be repaired due to subsurface chromium depletion and rapid attack would occur. However, cyclic conditions were far more severe in these tests than would be expected in actual service.**

5. **Internal penetration of all the austenitic stainless steels occurred as a result of inward migration of oxygen and sulfur being faster than the outward migration of cations. This penetration resulted in subscale sulfides in some cases, in transgranular oxidation/sulfidation of the surface grains, and intergranular penetration to a depth of several grains, depending upon the chromium content.**

6. **Resistance to corrosion increased with increasing alloy chromium content. Alloy 310 was the most resistant of those tested.**

7. For the austenitic alloys, corrosion appeared to be more somewhat more intense within 30-35 degrees of the leading edge.

8. There were numerous cases in which 1500 hour corrosion was substantially more than 2000 hour corrosion, seeming to indicate some difference in initial exposure condition between the two sets of tubes.

9. Data was too scattered to determine the corrosion kinetics, i.e. whether parabolic or linear with time. From the observed severe disruption of the scales in these tests, accelerated breakaway corrosion would be predicted for all of the alloys. However, much of the scale disruption was due to highly cyclic exposure conditions not typical of service in an actual plant.

10. Monotonically increasing corrosion with temperature was expected but was not generally observed due to the large data scatter.

11. There was no discernable difference in corrosion between TS1 with a gas temperature of around 2250°F and hard, thick deposits, and TS2, with a gas temperature of about 1700°F and friable deposits. There was, however, evidence of more scale spalling at the higher gas temperature.

12. Of the alloys tested at superheater temperatures, only 310 had scale + penetration less than 0.5 mm/yr (for the first year) on a linear basis, and it appeared that none would meet that criterion at 1400°F for intermediate temperature airheater service. Both alloy 310 and 253MA data showed less that 0.5 mm/yr on a parabolic basis, at both temperatures, while data for the 18-8 stainless steels were variably above or below a parabolic 0.5 mm/yr rate.

13. For the stainless steels, little or no difference was found, at a given metal temperature, between corrosion at the the leading and trailing edges of tubes. But carbon and low chromium steels in TS3 showed less corrosion at the trailing edge.

14. None of the ferritic alloys had internal penetration, but all had thick scales. Linear scaling rates were above 0.5 mm/yr for all alloys. Corrosion of alloys T22 and P5 was generally below a parabolic 0.5 mm/yr, while T11 and carbon steel were believed to be above, considering suspected scale losses.

ACKNOWLEDGMENTS

This work was supported by the U. S. Department of Energy, under Contract DE-AC02-79ET10815. Mike Hodges did most of the sample preparations and Teresa Young performed the SEM/EDS examinations.

REFERENCES

1. Van Weele, S.. "Fireside Corrosion Testing of Candidate Superheater Tube Alloys, Coatings, and Claddings", Final Report,ORNL/Sub/89-SA187/02, prepared by Foster Wheeler Development Corp., Livingston, NJ. August 1991.

2. Bienstock, D., R. J. Demski, and R. C. Corey, "Corrosion of Heat-Exchange Tubes in a Simulated Coal-Fired MHD System," ASME Paper 70-WA/CD-3, July 1970.

3. Hals, F., L. Keefe, and A. El Bindari, "Studies of Seed Recovery and Corrosion h Coal Fired MHD Power ", Avco-Everett Research Laboratory, ASME Paper 64-WA/ENER-5, Sept. 1964.

4. Natesan, K., "Materials for Application in MHD Steam Bottoming Plant: Summary Report," Report No. ANL/MHD-84-5, November 1984.

5. Natesan, K., "An Evaluation of Corrosion Behavior of Materials for Application in an MHD Steam Bottoming Plant," Report No. ANL/MHD-88-1, August 1988.

6. White, M., S. F. Chou, and P. L. Daniel, "Gas-side Fouling and Corrosion in MHD combustion Systems," Proceedings of 23rd Symposium on Engineering Aspects of Magnetohydrodynamics, Somerset, PA. June 1985.

7. Foote, J. P. and M. K. White, "HRSR Component Testing at the CFFF During 1985," Proceedings of 24th Symposium on Engineering Aspects of Magnetohydrodynamics, Butte, MT. June 1986.

8. Attig, R. C., J. N. Chapman, N. R. Johanson, J. W. Muelhauser, and Y. C. L. Wu, "CFFF Status Report: Western Coal and Proof-of-Concept Testing," Proceedings of 25th Symposium on Engineering Aspects of Magnetohydrodynamics. June 1987.

9. White, M. K. and M. Li, "Results of 500-Hour Superheater/Intermediate Temperature Airheater Tube Corrosion Tests in the MHD Coal Fired Flow Facility," Report No. DOE/ET/10815-144, The University of Tennessee Space Institute, Tullahoma, TN. November 1990.

10. Daniel, P. L. and M. E. Scott, "Analysis of Tube Segments from the DOE/UTSI MHD Superheater Test Module," Final Report - DOE/CH/10018-15. Babcock & Wilcox Co., Alliance, OH. March 1990.

11. Rapp, R. A. "Chemistry and Electrochemistry of the Hot Corrosion of Metals," Corrosion-NACE, Volume 42, Number 10, October 1986.

12. Hendry, A. and D. J. Lees, "Corrosion of Austenitic Steels in Molten Sulfate Deposits," Corrosion Science, Volume 20, Permagon Press Ltd, England, 1980.

13. Lai, G. Y., High Temperature Corrosion of Engineering Alloys, ASM International, Materials Park, Ohio, 1990.

14. Tamura, M., et al. "High Temperature Performance of 35Cr-45Ni-Fe Alloy." Proceedings of Symposium, High Temperature Corrosion in Energy Systems, Metallurgical Society of AIME, 1985.

15. Nakagawa, K., et al. Ishikawajima-Hirima Heavy Industries Company, Ltd., Tokyo. "Electrochemical Evaluation of Superheater Materials in Coal Ash Corrosion Atmosphere." American Society fir Metals Conference on Coatings and Bimetallics for Energy System and Chemical Process Environments, Hilton Head Island, South Carolina, November12-14, 1984.

16. Steam, 39th Edition, Babcock & Wilcox Company. p.15.19, 1978.

17. Latham, E. P. and J. Chamberlain, "Superheater Corrosion in Plants Burning High-Chlorine Coals", EPRI TR-101729. December 1992.

18. Plumley, A. L. and W. R. Roczniak, "Coal Ash Corrosion Field Testing of Advanced Boiler Tube Materials - II", Combustion Engineering, Inc., Presented at Second Int. Conference on Improved Coal-Fired Power Plants, Palo Alto, CA. November 2-4, 1988.

END

DATE FILMED

1/21/94